

Dear Dr. Patrick Jöckel,

Thank you very much for handling our manuscript. Please find below our itemized responses to the reviewers' comments and a marked-up manuscript. We have addressed all the comments raised by both reviewers and incorporated them in the revised manuscript. We believe this work will be an important contribution to the community.

Thank you for your consideration.

Sincerely,

Xiao Lu et al.

Reviewer #1 Dr. Julia Marshall

Comment [1-1]: This paper presents an analysis of the global methane budget and trend from 2010-2017 by simultaneously optimizing the source distributions, the OH sink (through hemispheric scaling factors), and linear trends using an analytical inversion approach with the GEOS-Chem model. Overall it is clearly written and structured and the figures are sufficiently clear and complete. From the subject matter it fits well within the scope of ACP.

At first glance this paper seems extremely similar in approach and content to Maasakkers et al. (2019) who used a very similar setup with the same model over an overlapping period (2010-2015) to do basically the same thing. The main difference that I can see is that here surface measurements are also included as a data constraint in order to show their complementarity (and consistency).

Response [1-1]: We thank Dr. Julia Marshall for the positive and valuable comments. All of them have been implemented in the revised manuscript.

As mentioned by the reviewer, the main improvement in our work relative to Maasakkers et al. (2019) is adding the in situ observations in the analytical inversion framework, comparing their ability and result with the satellite-based inversion, and quantifying the maximum information from the joint inversion. Such information is extremely important for a better understanding of the methane budgets and for the design of methane observing systems, yet it has not been addressed in previous studies to the best of our knowledge. In addition, our analytical inversion as done here implements a number of improvements to the Maasakkers et al. (2019) methodology, including in particular (1) separate optimization of subcontinental wetland emissions from other emission sectors to resolve their seasonal and interannual variability; (2) optimization of annual hemispheric OH concentrations rather than mean value of the period. Achieving these improvements increases the number of state vectors (and therefore computational costs) by 60%. We believe this work delivers sufficiently novel and important knowledge to the community.

Comment [1-2]: There's something a bit worrying showing up in Figure 6. Figure 6 seems to show that the both the in-situ-only and GOSAT-only inversions overestimate concentrations in the southern hemisphere and underestimate them in the northern hemisphere (more in the mid-latitudes in NH than in the Arctic). Interestingly, this consistent latitude-dependent bias does not seem to be present in the priors, or at least not as strongly. (Note that the 60-90N and 60-90S curves are more

or less on top of each other when compared to the observations for the prior runs.) The fact that they then diverge so systematically after optimisation seems to imply that something is going wrong with the OH hemispheric optimisation - or is there another explanation?

Interestingly this pattern appears least distinct when considering the in-situ-only posterior sampled at GOSAT locations, whereas it is most pronounced in the GOSAT-only posterior. Can you explain this? Does this have something to do with the seasonal latitudinal coverage of the GOSAT measurements? In the comparison of the GOSAT-informed concentrations (both with and without the in-situ data) to the ObsPack measurements (panels 6c and 6d, less evident in 6b) there seems to be almost an temporal anti-correlation in the model-data mismatch between the 30-60N stations and the 60-90N stations.

It seems to represent a systematic error in the interhemispheric gradient, which can be explained through either the distribution of the sink, the distribution of the sources, or errors in the transport – or most likely a combination of all three. However as both the sink and the sources are being optimised, it seems surprising that such a zonally dependent offset is emerging. Even if there are transport errors (and there always are), I would expect a solution to emerge that was consistent with the interhemispheric gradient of the measurements. Of course the OH sink is only being optimised as a hemispheric scaling: might this reflect a problem in the spatial or temporal distribution that is being scaled? Still, usually the fluxes will adapt to compensate, provided they have sufficient flexibility. The fact that Zhang et al. (2018) found the inversion results to be not so sensitive to different OH fields suggests that this is not the case.

Some explanation of the source of this systematic error should be included. The only mention of transport errors is the claim that the regularisation factor γ should help account for error correlations in the observations due to transport and source aggregation errors. Interestingly this does not seem to appear in the very similar simulations from the same group with a similar set-up, as seen in Figure 3d of Maasackers et al. (2019).

Response [1-2]: Thank you very much for pointing this out. We figure out that the hemispheric bias as shown in the original Figure 6 is because the posterior hemispheric OH scaling factors were not correctly implemented in the posterior model simulation. We have corrected the implementation, rerun the posterior model simulation, and updated Figures 5-7 and Tables 1 and 3 in the text. As shown in the updated Figures 6b and 6g, the latitude-dependent bias between the observed and modeled methane concentration has been corrected for the ingested methane observations, indicating that there is no systematic error in the inversion. The updates do not influence the analyses or conclusions. We apologize for the confusion.

Figure 6f shows that the in-situ-only inversion biases low to GOSAT observations, and Figure 6c shows that the GOSAT-only inversion overestimates in-situ observations in the Southern Hemisphere while underestimates them in the Northern Hemisphere. These discrepancies, as already presented in the original texts and figure, do not reflect systematic error in the inversion, but rather provide insights on the consistency and complementarity between the two observations in the methane inversion, as analyzed in Section 3.5 and in [Response #1-3]. We have revised the text to clarify.

We now state in Section 3.1 “...The in-situ-only inversion effectively corrects this bias and its trend, and also significantly improves the correlations across all platforms. The GOSAT-only inversion performs comparably in correcting the 2010-2017 trend for the independent in-situ data (Fig.6c) and bias for background observations (e.g. aircraft

observations in the Southern Hemisphere (Fig.S2)), but there is a low bias at northern mid-latitudes reflecting surface and tower data in North America and Europe. As we will see, the in situ observations are important for optimizing emissions in these regions.

... The GOSAT-only inversion corrects the bias and trend in the prior simulation at all latitudes. The in-situ-only inversion corrects the trends, but biases low to the GOSAT observations by about 10 ppbv with larger bias in the Southern Hemisphere due to the sparsity of in situ observation there. The comparison suggests that in situ and GOSAT observations are largely consistent for informing the global methane change but also have some complementarity for the inversion....”

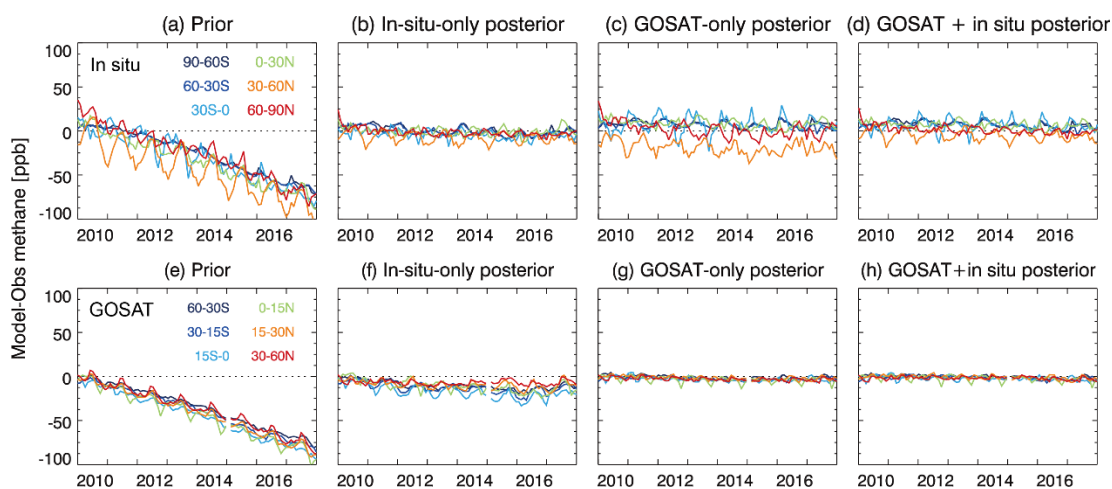


Figure 6. Ability of the inversions to fit the in situ methane observations and GOSAT satellite observations. Panels (a)-(d) show the monthly time series of the differences between observed and simulated in situ methane concentrations averaged over different latitude bands from 2010 to 2017. Panels (e)-(h) are the same as panels (a)-(d) but for GOSAT methane concentrations.

Comment [1-3]: Perhaps the most interesting (while also troubling) result is in Figure 13: the negative correlation between methane lifetime and estimated (anthropogenic) emissions is not in and of itself surprising. What is surprising is the fact that none of the three solutions are in any way consistent with each another. This can be explained by an underestimating of the posterior error covariances, as the authors do in L505-509. The fact that the GOSAT+in situ result does not lie somehow between the GOSAT-only and in-situ-only result is, however, worrying. The authors suggest that this is due to a correction of a bias in the GOSAT-only inversion by ingesting the in-situ measurements. This bias was diagnosed as being in both the OH (too low, because the methane in the SH was overestimated) and the fluxes (too low, because the methane in the NH mid-latitudes was underestimated). From this perspective it makes some sense that it would correct in the direction that it did, but why would it overshoot the in-situ-only solution? Is there some fundamental inconsistency in the two types of measurements (or an error in the model) that makes it impossible to match them both simultaneously?

This result seems to suggest that the measurements themselves are not really consistent with each other, which the paper claimed to set out to test (L91-94). Thus this result seems to contradict

the conclusion that "the GOSAT and in situ data are generally consistent and can fit each other independently through our inversions" (L535-536). Even if the concentrations in the different inversion come closer to each other, is the result really consistent if the emissions and the lifetime are so very divergent?

Response [1-3]: The fact that the GOSAT+in situ result does not lie between the GOSAT-only and in-situ-only result (Fig.13) can be inferred from Figures 6c and 6f. Figure 6c suggests that both emissions and OH concentrations are too low in the GOSAT-only inversion, as the reviewer understands, while Figure 6f indicates either underestimation of emissions or overestimation of OH concentrations in the in-situ-only inversion, and the former one is more likely as GOSAT measurements used here are over land which should be more sensitive to emissions than OH loss. The GOSAT + in situ joint inversion thus has to enhance both the methane emissions and OH concentrations compared to the In-situ-only and GOSAT-only inversions to correct these biases. We have revised the text accordingly in Section 3.5 to clarify this issue.

We agree with the reviewer that Figure 13 indicates that the measurements are not consistent with each other in optimizing the global methane budget, as stated in the original text (L505-506) "Comparison of the posterior PDFs between the GOSAT-only and In situ-only inversions implies that the two are inconsistent, since the 99% probability contour does not overlap (Fig.13)". We have removed "the GOSAT and in situ data are generally consistent and can fit each other independently through our inversions (L535-536)" which caused confusion. We have revised several places to clarify that the observations are consistent in correcting regional methane emissions in the inversion but are less consistent in terms of informing global methane budgets.

In the abstract, we now state "The in-situ-only and GOSAT-only inversions show consistent corrections to regional methane emissions but are less consistent in optimizing the global methane budget."

In Section 3.5, we now state "Comparison of the posterior PDFs between the GOSAT-only and In-situ-only inversions implies that the two are inconsistent in optimizing global methane budgets, since the 99% probability contours do not overlap (Fig.13a). ... Remarkably, the solution from the GOSAT + in situ joint inversion is more in agreement with in situ observations than GOSAT, and does not lie between these two solutions. Inspection of Figure 6c shows that the GOSAT-only inversion is biased low relative to in situ observations at northern mid-latitudes and biased high in the southern hemisphere, implying that both emissions and OH concentrations are too low. On the other hand, Figure 6f indicates either underestimation of emissions or overestimation of OH concentrations in the in-situ-only inversion, and the former one is more likely as GOSAT measurements used here are over land which should be more sensitive to emissions than OH loss. Ingestion of both observations in the GOSAT + in situ inversion thus enhances both the methane emissions and OH concentrations compared to the in-situ-only and GOSAT-only inversion to correct these biases. It also narrows the posterior error of mean anthropogenic emissions and methane lifetime against tropospheric OH by 20% and 50% compared to the GOSAT-only and in-situ-only inversions, respectively (Fig. 13a). Thus we find that the GOSAT and in situ observations are complementary in quantifying the global budget. "

In the conclusion, we now state "We find that the GOSAT-only inversion can generally

fit the in situ data and the in-situ-only inversion can generally fit the GOSAT data, indicating consistency between the two data sets. However, ...”, “The GOSAT-only and in-situ-only inversions also show consistent corrections to regional methane emissions in the US, Europe, and China.”, and “GOSAT and in situ observations have complementarity in constraining global emissions.”

Comments [1-4]: While trying to understand this rather surprising result I realised that I would like to see some more figures: OH was scaled per hemisphere per year (16 state vector values). A time series of these scaling factors (perhaps as an additional panel or two in Figure 7?) would be interesting to see, rather than just an average lifetime over the whole period (similar to Figure 7d in Maasakkers et al. (2019)). This might also help convince me that scaling OH based on surface-based methane measurements alone makes sense - do the OH scaling factors in this case stay close to one throughout?

Another plot that might help convince the reader of the adequacy of the transport model and the improvement of the sources and sinks would be geographical (zonal + altitude?) plot of the model-data mismatch for aircraft data presented in Figure 5d. Even if it has to go into a supplement, it would be a useful piece of information for the reader to assess if this very surprising result might make sense.

Once these concerns are addressed, I think the paper would be appropriate for publication in ACP.

Response [1-4]: Thank you for the advice, we have added the two figures (Fig.7b and Fig.S2) and revised the text accordingly.

1) We present the posterior methane lifetime (as an indicator of OH scaling factors) in Figure 7b. We now state in Section 3.5 **“We also find that the in-situ-only inversion yields a larger interannual variability of posterior OH concentrations and thus methane lifetime than the GOSAT-only inversion (Fig.7b), due to the heterogeneous spatial and temporal distribution of the in situ observations.”.**

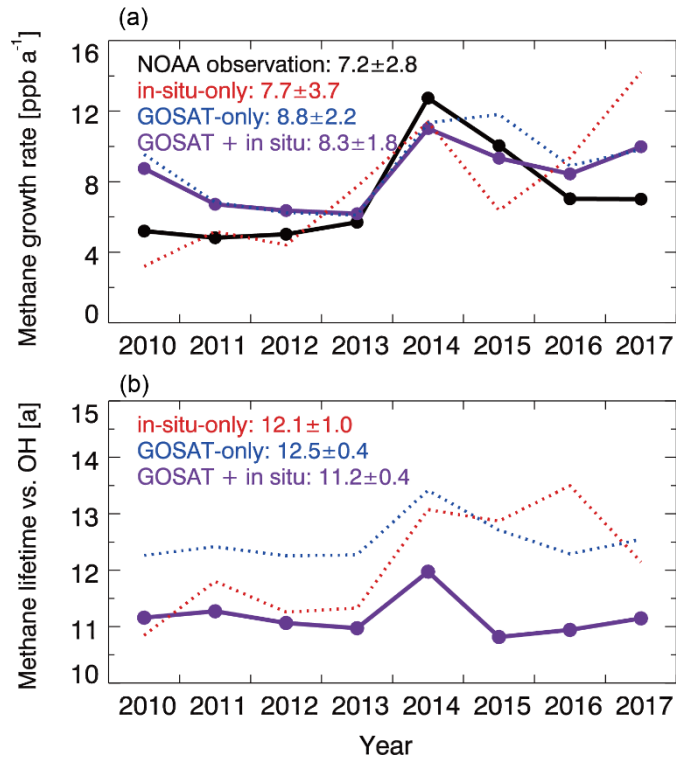


Figure 7. (a) Annual global growth rate of atmospheric methane, 2010-2017. Results from our three different inversions (In-situ-only, GOSAT-only, GOSAT + in situ) are compared to the observed growth rates inferred from the NOAA surface observational network (https://www.esrl.noaa.gov/gmd/ccgg/trends_ch4/, last access: 20 June, 2020). Mean annual growth rates and standard deviations from the different inversions are shown inset. (b). Methane lifetime against oxidation by tropospheric OH, 2010-2017, from the three different inversions. Mean lifetime and standard deviations are shown inset. The methane lifetime in the prior estimate is 10.6 years.

2) We present the model-observation bias for aircraft data for the prior and posterior simulation in Fig.S2, and state in Section 3.1 **“The GOSAT-only inversion performs comparably in correcting the 2010-2017 trend for the independent in-situ data (Fig.6c) and bias for background observations (e.g. aircraft observations in the Southern Hemisphere (Fig.S2))”**

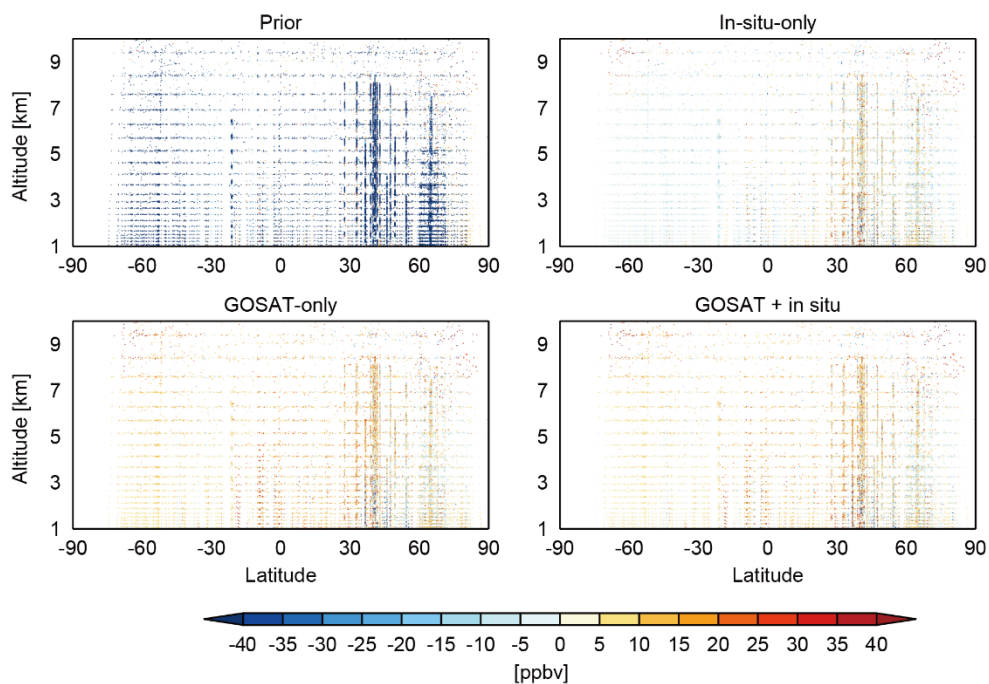


Figure S2. Differences between simulated and observed aircraft methane concentrations from the GLOBALVIEWplus ObsPack data product using GEOS-Chem with prior estimates and with posterior estimates from the in-situ-only, GOSAT-only, and GOSAT + in situ inversions.

Comments [1-5]: Minor comments: I would recommend adding how many independent pieces of information are contained in the GLOBALVIEW measurements alone to the abstract. This information is contained in the paper, but the way the numbers are presented in the abstract (which is as far as some readers get), it rather underplays the observation constraint brought about by the in-situ measurements alone.

Response [1-5]: We have revised accordingly in the abstract **“The in-situ-only and the GOSAT-only inversion alone, achieve respectively 113 and 212 independent pieces of information (DOFS) for quantifying mean 2010-2017 anthropogenic emissions on 1009 global model grid elements, and DOFS of 67 and 122 for 2010-2017 emission trends. The joint GOSAT + in situ inversion achieves DOFS of 262 and 161 respectively for mean emissions and trends. The in situ data thus increase the global information content from the GOSAT-only inversion by 20-30%.”**

Comments [1-6]: One point that should be added into the discussion: When looking at the ability of a measurement system to assess long-term trends it is critical to consider the length of time over which these measurements are available. In this case, the surface-based network still has an advantage, and does not suffer from the same comparability issues that can arise when new sensors/sampling are introduced. This is mentioned briefly in lines 567-568, but they are first mentioned as a method for satellite validation. Unless this measurements are being made across a profile (such as AirCore or aircraft), I cannot see how this could be the case.

Response [1-6]: We agree. We now rephrased in the Section 3.5 **“In situ observations will in any case continue to play a critical role for documenting long-term trends of methane with**

consistent calibration, ...”.

Comments [1-7]: In line 475-476 you mention in passing that your optimisation approach can only solve for constant linear trends over the whole inversions period, which may not be appropriate for China. I wonder if it is really appropriate for other regions either? This is a clear drawback to the choice of state vector in your analytical inversion setup, and should be more clearly stated as such. If you want to test if this lack of trend is consistent with the findings of Sheng et al. (2019), showing an increase to 2012 and a decrease afterwards, perhaps you could perform the same inversion but broken up into two chunks: 2010-2012 and 2013-2017. Yes, this would require new transport simulations, but it would be interesting to check the robustness of the other trends as well. However this might be beyond the scope of the current study. (Perhaps something to add to the discussion?)

Response [1-7]: We agree, and indeed separating the inversions into two or more chunks will increase significantly the computational costs. We have clarified this limitation in Section 2.2: **“The inclusion of linear trends in state vectors allows us to identify the direction of emission change for each 4° ×5° grid in the 8-year period, but it would not capture high-frequency interannual variability.”**

Comments [1-8]: I noticed that the panels labelled "China" and "Canada" in Figure 12 are identical. I suspect that they're both showing the results for Canada? In any case, this should be checked carefully and corrected.

Response [1-8]: Thanks for pointing it out. We had corrected the figure before it was posted on ACP Discussion.

Typographical/language remarks:

Comments [1-8]: Co-author Hartmut Boesch's last name is misspelled.

Response[1-8]: Corrected

Comments [1-9]:L127: with largest -> with the largest

Response[1-9]: Corrected

Comments [1-10]:L162: WETCHART -> WETCHARTS

Response[1-10]: Corrected

Comments [1-11]:L169: "full-chemistry" should not be hyphenated here (not a compound adjective before the noun)

Response[1-11]: Corrected

Comments [1-12]:L172: closed -> close

Response[1-12]: It has been rephrased.

Comments [1-13]:L218: challenged -> challenging

Response[1-13]: Corrected

Comments [1-14]:L225: Bayesian -> The Bayesian

Response[1-14]: Corrected

Comments [1-15]:L231: underestimate -> underestimation

Response[1-15]: Corrected

Comments [1-16]:L238: change -> changes

Response[1-16]: Corrected

Comments [1-17]:L266: be somewhat deviated -> deviate somewhat; overfit -> overfitting

Response[1-17]: It has been removed.

Comments [1-18]:L278: overfit -> overfitting

Response[1-18]: Corrected

Comments [1-19]:L284: Analytical solution -> The analytical solution

Response[1-19]: Corrected

Comments [1-20]:L288: I would suggest adding a colon after "analyses"

Response[1-20]: Corrected

Comments [1-21]:L290: capitalisation of "In situ-only" seems odd. Perhaps "in-situ-only" would be better as a compound adjective.

Response[1-21]: Corrected

Comments [1-22]:L339: year -> years

Response[1-22]: Corrected

Comments [1-23]:L345: by year -> by the year

Response[1-23]: Corrected

Comments [1-24]:L349: has insignificant -> has an insignificant

Response[1-24]: Corrected

Comments [1-25]:L364: higher information than in situ observations -> more information than do in situ observations

Response[1-25]: Corrected

Comments [1-26]:L375: I guess that ".," should just be ",,"?

Response[1-26]: Corrected

Comments [1-27]:L392: In situ observation is -> The in situ observations are

Response[1-27]: Corrected

Comments [1-28]:L418: Thompton -> Thompson

Response[1-28]: Corrected

Comments [1-29]:L453: US -> the US

Response[1-29]: Corrected

Comments [1-30]: Figure 11: I guess this percentage change is over the full period (rather than per year)? This should be clarified in the caption label. It also makes it a bit hard to compare to the text, where % trend per year is given. I assume that this is not a compounding percentage change, but rather the total percentage change divided by the number of years? In any case, this should be clarified.

Response [1-30]: **Figure 11 shows the percentage change per year that derive directly from the inversions. We now state in the figure caption “Figure 11. Same as Figure 8 but for optimization of non-wetland (mainly anthropogenic) emission trends (% a⁻¹) in 2010-2017.”.**

Comments [1-31]:L501-502: This might seem like a small thing, but this is one of the most interesting findings of the paper, and as such should be perfectly clear. I would suggest the following change in phrasing: "are more effective than the satellite observations in independently constraining methane emissions from the sink by OH." -> "are more effective than the satellite observations in constraining methane emissions independently from the OH sink."

Response [1-31]: We have rephrased as suggested.

Comments [1-32]:L553: weak -> a weak

Response[1-32]: Corrected

Comments [1-33]:L560: remove "the"

Response[1-33]: Corrected

Comments [1-34]:L561: and methane lifetime -> and a methane lifetime

Response[1-34]: Corrected

Reviewer #2

Comments [2-1]: "Global methane budget and trend, 2010–2017: complementarity of inverse analyses using in situ (GLOBALVIEWplus CH4 ObsPack) and satellite (GOSAT) observations" presents long-term global inversions based on different available observation datasets. The authors present an inversion system based on the analytical solution of the Bayesian Gaussian problem which allow to better understand the weight of each piece in the system. The authors analyze the outputs thoroughly and use relevant comprehensive metrics to assess the usefulness of each type of observations.

The manuscript is well written, well structured and of significant importance for the community to be published in ACP after some weaknesses are properly addressed. Main problems are detailed in dedicated sections below and technical revisions are listed in Sect. 5. Overall, the manuscript is of high quality but falls short of properly exploiting the full potential of the system presented here. Sensitivity tests and additional inversions should be added to the manuscript (without computing additional response functions) to prove fully relevant to the community and to stand out of more regular inversion papers. It can be done with relatively little efforts considering all the material and the quality of the background work done to reach the present submitted manuscript.

Response [2-1]: We thank the reviewer for the positive and valuable comments. All of them have been implemented in the revised manuscript. In particular, we have performed a number of additional inversions to test the sensitivity of our results to the choices in cost-function construction (e.g. usage of observations, error assumption of the observations and state). Please see our itemized responses below.

Comments [2-2]: 1 Bias correction: p.7 l.191: Bias correction is mentioned. This is a critical point. It may have a huge impact on the inversions. Putting it under the carpet in one line is a little bit short. Please add details on this aspect and possibly some quantification of the impact of such a bias correction. Is the bias correction put in the constant c in eq. (2)? Or is it use on-line in the computation of GEOS-Chem? Or posterior to it? What is the impact on the response functions? If it is the constant c , please include (at least in supplement) your results with/without/with another bias correction to really see how sensitive your results are to that aspect.

Response [2-2]: Thanks for pointing it out. The bias correction is done off-line before the inversion. We have added the text briefly describing the procedures for bias correction, and a **Figure S1 to show the influence of bias correction. We now state in Section 2.3 “GEOS-Chem has excessive methane in the high-latitudes stratosphere, a flaw common to many models (Patra et al., 2011) especially at coarse model resolution. Following Zhang et al. (2020), we compute correction factors to GEOS-Chem stratospheric methane subcolumns as a function of season and equivalent latitude to match the measurements from the solar occultation ACE-FTS v3.6 instrument (Waymark et al., 2014; Koo et al., 2017). As shown in Zhang et al. (2020), the correction can be up to 10% at high latitudes during winter and spring. We apply the correction factors before the inversion to avoid wrongly attributing this model transport bias to methane emissions and loss. Figure S1 shows that the systematic differences in the posterior scaling factors of non-wetland emissions with vs. without bias correction are more prominent at the northern high latitudes, as also shown in Stanevich et al. (2020), but the global total emissions only differ by 1%.”**

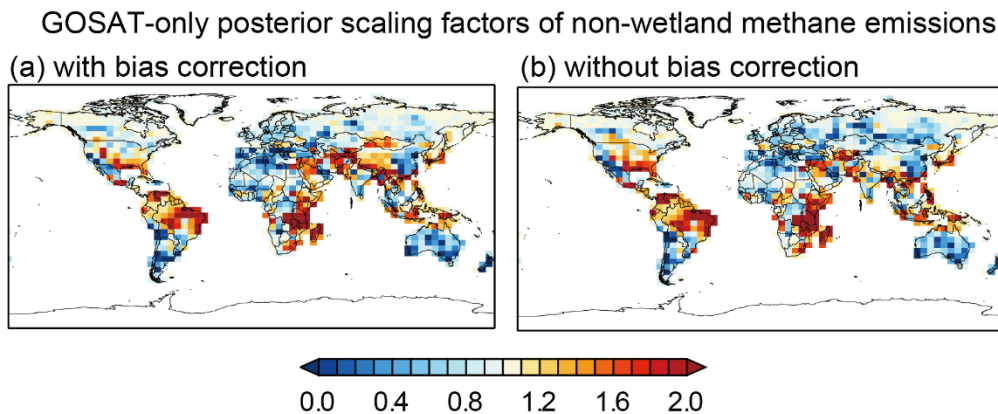


Figure S1. Posterior scaling factors of non-wetland methane emissions from GOSAT-only inversion (a) with GOSAT stratospheric bias corrections and (b) without GOSAT stratospheric bias corrections.

Reference:

Stanevich, I., Jones, D. B. A., Strong, K., Parker, R. J., Boesch, H., Wunch, D., Notholt, J., Petri, C., Warneke, T., Sussmann, R., Schneider, M., Hase, F., Kivi, R., Deutscher, N. M., Velasco, V. A., Walker, K. A., and Deng, F.: Characterizing model errors in chemical transport modeling of methane: impact of model resolution in versions v9-02 of GEOS-Chem and v35j of its adjoint model, *Geosci. Model Dev.*, 13, 3839–3862, <https://doi.org/10.5194/gmd-13-3839-2020>, 2020.

Zhang, Y., Jacob, D. J., Lu, X., Maasakkers, J. D., Scarpelli, T. R., Sheng, J.-X., Shen, L., Qu, Z., Sulprizio, M. P., Chang, J., Bloom, A. A., Ma, S., Worden, J., Parker, R. J., and Boesch, H.: Attribution of the accelerating increase in atmospheric methane during 2010–2018 by inverse analysis of GOSAT observations, *Atmos. Chem. Phys. Discuss.*, <https://doi.org/10.5194/acp-2020-964>, in review, 2020.

Comments [2-3]: 2 Non-linearity of GEOS-Chem and OH chemistry. This is a little bit harsh to neglect it straight away. Could you run forward runs with your different posterior states and compare with what you get with the matrices Kx to have an idea of how negligible it is?

Response [2-3]: The GEOS-Chem methane simulation used prescribed monthly 3-D fields of global tropospheric OH concentrations taken from a GEOS-Chem simulation with full chemistry. With this regard the optimization of methane emissions is strictly linear. The only non-linearity emerges regarding the optimization of OH, because the sensitivity of the methane concentration to changes in OH concentrations depends on the methane concentration through first-order loss, but the variability of methane concentration is sufficiently small so that this non-linearity is negligible. We have tested that the $K\hat{x}$ and posterior simulation of y has a small mean difference of 2 ± 3 ppbv. We now state in Section 2.4 “The optimization of methane emission and its trends is strictly linear by design because we use prescribed monthly 3-D OH fields as described in Section 2.2. There is some non-linearity regarding the optimization of OH, because the sensitivity of the methane concentration to changes in OH concentrations depends on the methane concentration through first-order loss,

but we assume that the variability of methane concentration is sufficiently small that this non-linearity is negligible (we verify this assumption below)... Comparison of the resulting Jacobian matrix to GEOS-Chem as $F(x) - Kx - c$ shows a negligible residual difference of 2+3 ppb, verifying the assumption of linearity.”

Comments [2-4]: 3 Regularization term: The authors use a regularization term to correct for ill-specified observation errors. However, their estimation is based on approximate matrices. Why not using the rigorous Chi-square criterion? such as in Desroziers et Ivanov (2001, <https://rmets.onlinelibrary.wiley.com/doi/10.1002/qj.49712757417>)

Response [2-4]: Thanks for pointing it out. We have made the revision to estimate the optimal value of the regularization parameter in the context of the Chi-square distribution. We have also tested the impact of using different regularization parameters on the global methane budget as discussed in [Response #2-5].

We now state in Section 2.4 “... For a given state vector element i , the expected value of $(x_i - x_{Ai})^2$ is the prior error variance σ_{Ai}^2 . For an n -dimensional state vector with a diagonal prior error covariance matrix, the state component J_A of the cost function is the sum of n random normal elements

$$J_A(x) = (x - x_A)^T S_A^{-1} (x - x_A) = \sum_n \frac{(x_i - x_{Ai})^2}{\sigma_{Ai}^2} \quad (6),$$

and its pdf is given by the Chi-square distribution with n degrees of freedom ($n=3378$ in this case), with an expected value of n and a standard deviation of $\sqrt{2n}$. One can apply the same reasoning to the observation component J_O of the posterior cost function,

$$J_O(x) = (y - Kx)^T S_O^{-1} (y - Kx) = \sum_m \frac{(y_i - Kx_i)^2}{\sigma_{oi}^2} \quad (7),$$

whose pdf follows a chi-square distribution with m degrees of freedom. However, this component is less sensitive to the choice of γ because of the large random error component for individual observations.

Figure 4 shows the dependences of $J_A(\hat{x})$ and $J_O(\hat{x})$ on the choice of the regularization parameter γ , for the in situ and GOSAT observations. The in situ observations are sufficiently sparse that $\gamma = 1$ (no regularization) is expected. In the case of GOSAT, however, $\gamma = 1$ would yield $J_A(\hat{x}) = 6n \gg n + \sqrt{2n}$ which indicates overfitting, while $\gamma = 0.1$ yields $J_A(\hat{x}) \approx n$ which is the expected value and is used here....”

Comments [2-5]: 4 Computation cost and sensitivity tests. It is nowhere stated what is the computation cost of the system (computing response functions on the one hand, solving the matrix products on the other hand). Once the response functions are computed it is in principle quite straightforward to change parameters in the R/B matrices to see the impact.

I think the main strength of the system presented here comes from this very fact (otherwise, a variational inversion would give posterior fluxes at reduced cost, even if DOFS can be retrieved easily). This is a critical limitation of the present paper.

Different horizontal and temporal correlations should be tested in the prior matrix, as well as standard deviation of errors, to see the impact of such modifications, given that we never really know how good are our prior/obs errors.

More critically are observation errors. Even though the observation data set is very large, it should be possible to imagine a matrix that is diagonal only by block, allowing to consider correlations between GOSAT neighbour observations, while keeping it possible to compute the inverse easily. As stated by the authors, the inversions are not consistent with each others (Fig. 13). This comes probably from ill-specified error matrices, which the authors have the tools to inquire into.

Response [2-5]: Thank you for pointing it out.

1) We have added the following text in Section 2.4 (Analytical Inversion) to clarify the computation cost of the system “A requirement of the analytical approach is that the Jacobian matrix be explicitly constructed, requiring $n + 1$ forward model runs. Building the Jacobian matrix for the 3378 state vectors in this 8-year period study requires about one million core hours (8 cores \times 36 hours per simulation \times 3378 simulations). However, this construction is readily done in parallel on high-performance computing clusters.”.

2) We have also conducted a number of additional inversions to examine the results with different error assumption and ingestion of observations. For the prior standard deviation of state vectors (non-wetland emission trends and OH), we test their different magnitude (decrease by 50%) but not their distributions (correlations) due to the lack of objective information on the later. For the observation error, the ability to test off-diagonal assumption is also limited by the calculation of S_o^{-1} which involves inverting a matrix with $\sim 10^{12}$ elements. Therefore we test the unknown observation error correlations by changing the regularization parameter γ .

We have added a new Figure 13b, and now state in Section 2.4 “We will make use of these advantages in comparing the ability of the in-situ-only, GOSAT-only, and GOSAT + in situ inversions, and to test how choices in cost-function construction affect our conclusions including changing the regularization parameter γ , changing the prior error estimates, and using different types of in-situ observations. Our analysis will focus on results from the base inversions with the default settings, but we will use results from the sensitivity inversions to address specific issues.”.

And in Section 3.5 we state “We examine in Figure 13b the sensitivity of the global methane budget optimization to the choice of different regularization parameter γ (and therefore observation error S_o) and prior error of methane emission trends and OH concentrations. We find that reducing γ or prior errors of trend and OH by 50% yields consistent estimates of anthropogenic emissions and OH concentrations as compared to the default inversion, with differences within 3%. Decreasing the weighting of observations in the inversion (i.e. assuming larger observation error) enlarges the posterior error and pushes the posterior estimates closer to the prior estimates. Assuming a lower prior error for OH concentration from 10% to 5% results in lower methane lifetime (closer to the prior) and higher emissions, and also reduces the error correlation between the optimization of methane emissions and OH, while assuming a lower prior error for non-wetland emission trends leads to an opposite effect. Our results are consistent with Maasakkers et al. (2019), which shows that different assumptions of error distribution and magnitude in their analyses have relatively small results. We also find that having the shipboard and aircraft measurements in the in-situ-only inversion pushes the estimate to be more consistent with the GOSAT-only

inversion (Fig.13b), implying that the shipboard and aircraft measurements by emphasizing the methane in the remote atmosphere play a similar role as satellite measurements in global methane budget optimization.”

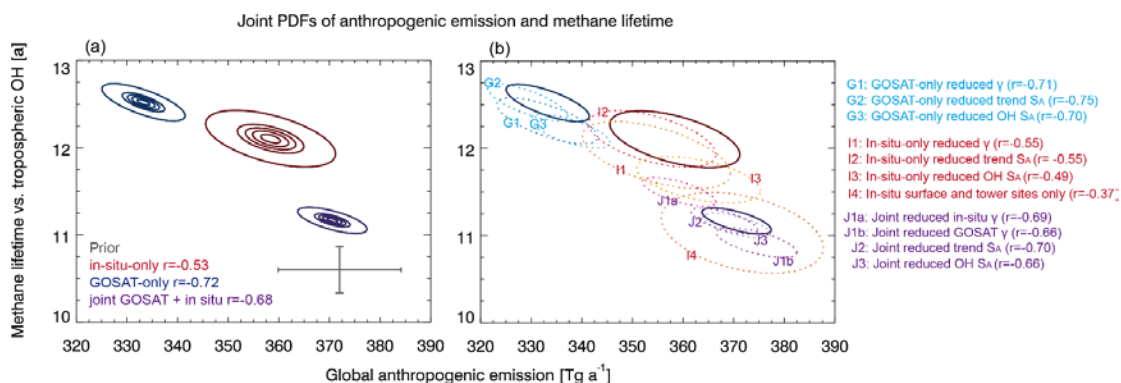


Figure 13. Joint probability density functions (PDFs) of global mean anthropogenic methane emission and methane lifetime against oxidation by tropospheric OH optimized by different inversions. Panel (a) shows the results from the prior and the three base inversions. The prior estimates are shown in grey with bars representing the prior error standard deviation. The thick contours show probabilities of 0.99 (outermost), 0.7, 0.5, 0.3, and 0.1 (innermost). The error correlation coefficients are given inset. Panel (b) shows the 0.99 probability contours from the three base inversions along with the same contours for ten additional sensitivity inversions using reduced values of the regularization parameter γ (0.05 instead of 0.1 for GOSAT, 0.5 instead of 1 for in situ); reduced errors for the methane emission trends on the $4^\circ \times 5^\circ$ grid ($5\% \text{ a}^{-1}$ instead of $10\% \text{ a}^{-1}$); reduced errors on annual hemispheric mean OH concentrations (5% instead of 10%); or surface and tower data only in the in-situ-only inversion.

Comments [2-6]: 5 Technical comments. p.4 l.89: aircraft measurements: those can be particularly challenging to ingest inversion systems as CTMs never really excel in representing the vertical distribution of CH₄ concentrations. Plus it is never clearly stated whether or not they are really used in the inversion or only in the posterior evaluation. Please discuss more about the aircraft measurements and justify better their use (is it only vertical profiles, very hard to assimilate? or transects, easier to use?)

Response [2-6]: Thank you for pointing it out.

1) The aircraft measurements are used in the inversions, as stated in the original text (L122-124) **“We obtain in this manner 157054 observation data points for the inversion including 81119 from 103 surface sites, 27433 from 13 towers, 827 from 3 ship cruises, and 47675 from 29 aircraft campaigns.”** We have added a Figure S2 to also address [Comment #1-4], which shows that the posterior model can well fit the aircraft methane measurements measuring the background (e.g. in the Southern Hemisphere), but indeed some discrepancies emerge in the northern mid-latitudes, reflecting the difficulty in modeling methane vertical distributions or optimizing emissions near source.

2) We have also added an additional inversion using only surface and tower observations in the inversion and compared the results with the In-situ-only inversion (which ingest all in situ observations) in Fig.S3 and Fig.13b. Comparison of Figure S3 to Figure 8a-b shows that

adding the aircraft and shipboard observations to the surface and tower observations increases the DOFS for constraining non-wetland methane emissions from 96 to 113 (18%), and reflects the upward correction in the South America which is consistent with the GOSAT-only inversion (Fig.8d). We also find in the Figure 13b that adding the aircraft and shipboard measurements pushes the inversed global methane and OH levels more consistent with the GOSAT-only inversion, however, it makes the inversion less effective in optimizing the global methane budget and OH. These results thus illustrate the ability of aircraft and shipboard measurements in the inversion.

We now state in Section 3.2 “We find that the DOFS from the in-situ-only inversion observations are mostly (85%) from the surface and tower measurements (Fig.S3).”

We also state in Section 3.5 “...A sensitivity inversion using only the surface and tower measurements in the In-situ-only inversion yields $r=-0.37$ (Fig.13b). It indicates that in situ observations, in particular surface and tower measurements, are more effective than the satellite observations in constraining methane emissions independently from the sink by OH.”, and “We also find that having the shipboard and aircraft measurements in the in-situ-only inversion pushes the estimate to be more consistent with the GOSAT-only inversion (Fig.13b), implying that the shipboard and aircraft measurements by emphasizing the methane in the remote atmosphere play a similar role as satellite measurements in global methane budget optimization.”

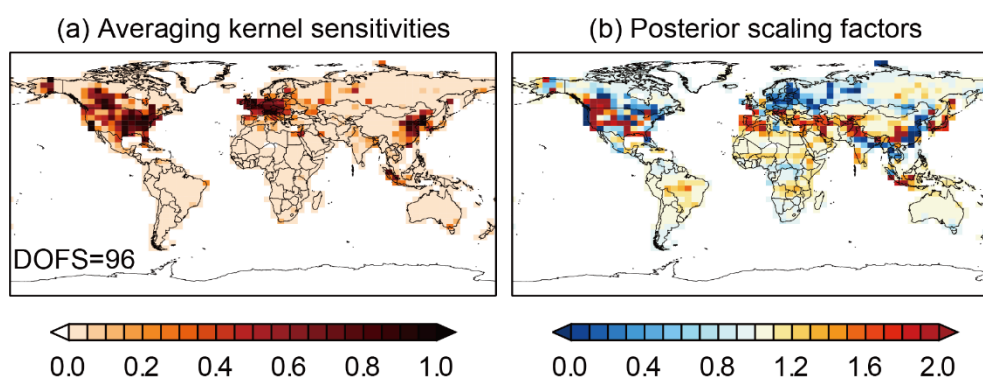


Figure S3. Same as Figure 8a and 8b but from a sensitivity inversion using only surface and tower methane observations.

Comments [2-7]: p.4 1.104: how exactly the linear trend are computed as response functions? same for OH? A start of explanation is given p.8, but additional information would be welcome.

Response [2-7]: We now state in the text to introduce the construction of response functions (Jacobian matrix K) in Section 2.4: “We construct the Jacobian matrix K explicitly by conducting GEOS-Chem simulations with each element of the state vector perturbed separately. For the linear emission trend elements, this is done by perturbing the 2010-2017 emission trend in each grid cell from 0% (the best prior estimate) to 10% a^{-1} ; for OH, this is done by perturbing yearly hemispheric OH fields by 20% without modifying the spatial or seasonal distribution.”

Comments [2-8]: p.7 1.163: What is the corresponding total error on the prior budget when using your prior distributed errors? Please represent it on Fig. 13

Response [2-8]: We have revised Fig.13 accordingly.

Comments [2-9]: p.8 l.208-213: observation error: it is not clear what ensembles are taken. Do you separate each station? Some regions for GOSAT? etc.

Response [2-9]: We now state in Section 2.3: “For in-situ observations, we derive ϵ_0 separately for the ensemble of background surface sites (Dlugokencky et al., 1994), non-background sites, tower sites, shipboard measurements, and aircraft measurements, while for GOSAT observations ϵ_0 is calculated for each $4^\circ \times 5^\circ$ grid cell.”

Reference

Dlugokencky, E. J., Steele, L. P., Lang, P. M., and Masarie, K. A.: The growth rate and distribution of atmospheric methane, J. Geophys. Res., 99, 17021, <http://doi.org/10.1029/94jd01245>, 1994.

Comments [2-10]: p.9 l.284: not correct. The other way around. the analytical solution is the solution of the Bayesian Gaussian problem. The cost function is derived from the formulation of the Gaussian problem when the analytical solution cannot be computed explicitly. Actually, writing the cost function in Eq. (1) in a paper using analytical inversions is superfluous; the factor gamma can be introduced differently.

Response [2-10]: We have rephrased as **“The analytical solution to the Bayesian optimization problem, as done here, has several advantages relative to the more commonly used variational (numerical) solution.”**

Comments [2-11]: p.11 l.376: This warning should also be repeated in the method section. Actually as response functions are computed for each pixels individually, why not duplicating the corresponding time series to separate sectors in the target vector? This would not add new response functions to compute and allow you to assess how good is the distribution in sectors. You could even imagine specifying different correlation lengths to different sectors.

Response [2-11]: We cannot separate sectors at the level of individual grid cells because they will all have the same response function. We can separate sectors for ensembles of grid cells and this is precisely what we do with the matrix W . We have added the following text in Section 2.4 “We cannot separate individual sectors within a $4^\circ \times 5^\circ$ grid cell because they will all have the same response function (Jacobian column). However, we can aggregate results spatially and by sector...”

Comments [2-12]: p.11 l.382: Is GEOS-Chem really suitable with very coarse resolution to constrain US emissions? the resolution is fine for background sites, but what about sites nearby emission hotspots. Representation errors will likely bias your results at such stations, making it very important to filter properly data prior to the inversion.

Response [2-12]: Thanks for pointing it out. We agree that representation errors will likely bias results at stations near source regions, and it is important to filter properly data prior to the inversion. As already mentioned in Section 2.1, we address this problem by “For surface and tower measurements, we use only daytime (10-16 local time) observations and average them to the corresponding daytime mean values. We exclude outliers at individual sites that depart by more than three standard deviations from the mean.”. Still this might be insufficient

to properly interpret sites nearby emission hotspots. A high-resolution inversion (e.g. Turner et al., 2015; Sheng et al., 2018) would be preferable to better interpret the in-situ observations near emission hotspots and to understand the spatial pattern of US anthropogenic methane emissions.

Reference:

Sheng, J.-X., Jacob, D. J., Turner, A. J., Maasakkers, J. D., Sulprizio, M. P., Bloom, A. A., Andrews, A. E., and Wunch, D.: High-resolution inversion of methane emissions in the Southeast US using SEAC⁴ aircraft observations of atmospheric methane: anthropogenic and wetland sources, *Atmos. Chem. Phys.*, 18, 6483-6491, <http://doi.org/10.5194/acp-18-6483-2018>, 2018.

Turner, A. J., Jacob, D. J., Wecht, K. J., Maasakkers, J. D., Lundgren, E., Andrews, A. E., Biraud, S. C., Boesch, H., Bowman, K. W., Deutscher, N. M., Dubey, M. K., Griffith, D. W. T., Hase, F., Kuze, A., Notholt, J., Ohyama, H., Parker, R., Payne, V. H., Sussmann, R., Sweeney, C., Velazco, V. A., Warneke, T., Wennberg, P. O., and Wunch, D.: Estimating global and North American methane emissions with high spatial resolution using GOSAT satellite data, *Atmos. Chem. Phys.*, 15, 7049-7069, <http://doi.org/10.5194/acp-15-7049-2015>, 2015.

1 **Global methane budget and trend, 2010-2017: complementarity of inverse analyses**
2 **using in situ (GLOBALVIEWplus CH₄ ObsPack) and satellite (GOSAT) observations**

3
4 Xiao Lu¹, Daniel J. Jacob¹, Yuzhong Zhang^{1,2,3}, Joannes D. Maasakkers⁴, Melissa P. Sulprizio¹, Lu Shen¹,
5 Zhen Qu¹, Tia R. Scarpelli¹, Hannah Nesser¹, Robert M. Yantosca¹, Jianxiong Sheng⁵, Arlyn Andrews⁶,
6 Robert J. Parker^{7,8}, Hartmut Boesch^{7,8}, A. Anthony Bloom⁹, Shuang Ma⁹

7
8 ¹[Harvard](#) John A. Paulson School of Engineering and Applied Sciences, Harvard University, Cambridge,
9 MA, USA

10 ²School of Engineering, Westlake University, Hangzhou, Zhejiang Province, China

11 ³Institute of Advanced Technology, Westlake Institute for Advanced Study, Hangzhou, Zhejiang Province,
12 China

13 ⁴SRON Netherlands Institute for Space Research, Utrecht, The Netherlands.

14 ⁵Center for Global Change Science, Massachusetts Institute of Technology, Cambridge, MA, USA

15 ⁶National Oceanic and Atmospheric Administration, Earth System Research Laboratory, Boulder, CO,
16 USA

17 ⁷National Centre for Earth Observation, University of Leicester, UK

18 ⁸Earth Observation Science, Department of Physics and Astronomy, University of Leicester, UK

19 ⁹Jet Propulsion Laboratory, California Institute of Technology, Pasadena, CA, USA

20
21 *Correspondence to:* Xiao Lu (xiaolu@g.harvard.edu) and Yuzhong Zhang
22 (zhangyuzhong@westlake.edu.cn)

24 **Abstract**

25 We use satellite (GOSAT) and in situ (GLOBALVIEWplus CH4 ObsPack) observations of atmospheric
26 methane in a joint global inversion of methane sources, sinks, and trends for the 2010-2017 period. The
27 inversion is done by analytical solution to the Bayesian optimization problem, yielding closed-form
28 estimates of information content to assess the consistency and complementarity (or redundancy) of the
29 satellite and in situ datasets. We find that GOSAT and in situ observations are to a large extent
30 complementary, with GOSAT providing a stronger overall constraint on the global methane distributions,
31 but in situ observations being more important for northern mid-latitudes and for relaxing global error
32 correlations between methane emissions and the main methane sink (oxidation by OH radicals). The in-
33 situ-only and the GOSAT-only observations inversion alone, achieve respectively 113 and 212
34 independent pieces of information (DOFS) for quantifying mean 2010-2017 anthropogenic emissions on
35 1009 global model grid elements, and ~~a~~ DOFS of 67 and 122 for 2010-2017 emission trends. ~~Adding the~~
36 ~~in situ data increases the DOFS by about 20-30%,~~ The joint GOSAT + in situ inversion achieves DOFS
37 of ~~to~~ 262 and 161 respectively for mean emissions and trends. The in situ data thus increase the global
38 information content from the GOSAT-only inversion by 20-30%. The in-situ-only and GOSAT-only
39 inversions show consistent corrections to regional methane emissions but are less consistent in optimizing
40 the global methane budget. ~~Our~~The joint inversion finds that oil/gas emissions in the US and Canada are
41 underestimated relative to the values reported by these countries to the United Nations Framework
42 Convention on Climate Change (UNFCCC) and used here as prior estimates, while coal emissions in
43 China are overestimated. Wetland emissions in North America are much lower than in the mean
44 WetCHARTs inventory used as prior estimate. Oil/gas emissions in the US increase over the 2010-2017
45 period but decrease in Canada and Europe. ~~Our~~The joint GOSAT+in situ inversion yields a global
46 methane emission of 551 Tg a⁻¹ averaged over 2010-2017 and a methane lifetime of 11.2 years against
47 oxidation by tropospheric OH (86% of the methane sink).

48

49 **1 Introduction**

50 Methane (CH₄) is the second most important anthropogenic greenhouse gas, and plays a central role in
51 atmospheric chemistry as a precursor of tropospheric ozone and a sink of hydroxyl radicals (OH). It is
52 emitted from many natural and anthropogenic sources that are difficult to quantify (Saunois et al., 2020).
53 Atmospheric methane observations from satellites and in situ (surface, tower, shipboard, and aircraft)
54 platforms have been used extensively to infer methane emissions and their trends through inverse analyses
55 (Houweling et al., 2017). But the information from satellite and in situ observations does not always agree
56 (Monteil et al., 2013; Bruhwiler et al., 2017) and is hard to compare because of large differences in
57 observational density, precision, and the actual quantity being measured (Cressot et al., 2014). Here we
58 use an analytical solution to the Bayesian inverse problem to quantitatively compare and combine the
59 information from satellite (GOSAT) and in situ (GLOBALVIEWplus CH₄ ObsPack) observations for
60 estimating global methane sources and their trends over the 2010-2017 period, including contributions
61 from different source sectors and from the methane sink (oxidation by tropospheric OH).

62
63 Inverse analyses of atmospheric methane observations using chemical transport models (CTM) provide a
64 formal method for inferring methane emissions and their trends (Brasseur and Jacob, 2017). Global
65 satellite observations of atmospheric methane columns from the shortwave infrared SCIAMACHY and
66 GOSAT instruments have been widely used for this purpose (Bergamaschi et al., 2013; Wecht et al., 2014;
67 Turner et al., 2015; Maasakkers et al., 2019; Miller et al., 2019; Lunt et al., 2019). Other inverse analyses
68 have relied on in situ methane observations that have much higher precision, are more sensitive to surface
69 emissions, and may include isotopic information, but are much sparser (Pison et al, 2009; Bousquet et al.,
70 2011; Miller et al., 2013; Patra et al., 2016; McNorton et al., 2018).

71
72 A number of inverse analyses have combined in situ and satellite observations (Bergamaschi et al., 2007,
73 2009, 2013; Fraser et al., 2013; Monteil et al, 2013; Cressot et al., 2014; Houweling et al., 2014; Alexe et
74 al., 2015; Ganesan et al., 2017; Janardanan et al., 2020), but few of them have compared the information
75 from the two data streams and then mostly qualitatively. Bergamaschi et al. (2009, 2013), Fraser et al.
76 (2014), and Alexe et al. (2015) found that surface and satellite methane observations provided consistent
77 constraints on global methane emissions, but that satellite observations achieved stronger regional
78 constraints in the tropics. No study to our knowledge has compared the ability of satellite and in situ
79 observations to attribute long-term methane trends.

80
81 Analytical solution to the inverse problem, as used here, provides closed-form error characterization as
82 part of the solution, and from there allows derivation of the information content from different
83 components of the observing system (Rodgers, 2000). Application to satellite observations has been used
84 to determine where the observations can actually constrain the inverse solution (Turner et al., 2015). The
85 major obstacle to this analytical solution in the past has been the need to construct the Jacobian matrix
86 for the CTM forward model, but this is now readily done using massively parallel computing clusters
87 (Maasakkers et al., 2019). Such a method provides a means to quantify the differences in information

88 content between different data streams (e.g., satellite vs. in situ) and from there to contribute to the design
89 of a better observing system.

90

91 Here we apply satellite observations of atmospheric methane columns from the GOSAT instrument
92 together with an extensive global compilation of in situ observations (including surface, tower, shipboard,
93 and aircraft methane measurements) from the GLOBALVIEWplus CH₄ ObsPack v1.0 data product
94 (Cooperative Global Atmospheric Data Integration Project, 2019), to quantify the global distribution of
95 methane emissions, loss from reaction with OH, and related trends for the 2010-2017 period. We use for
96 this purpose an analytical inversion method that formally characterizes the information content from the
97 two data streams, whether that information is consistent, and whether it is complementary or redundant
98 (Rodgers, 2000; Jacob et al., 2016). Our work provides a comprehensive global perspective on the sources
99 contributing to 2010-2017 methane emissions and trends, as well as a general framework for synthesizing
100 the information from satellite and in situ observations.

101

102 **2 Methods**

103 Figure 1 summarizes the components of our analytical inversion system, which builds on previous
104 inversions of GOSAT satellite data by Maasackers et al. (2019) and Zhang et al. (2020a,2019) but adds
105 the in situ observations. We apply observations y from GLOBALVIEWplus observations and/or GOSAT
106 (Section 2.1), with the GEOS-Chem CTM as forward model (Section 2.3), to optimize the state vector x
107 of our inverse problem. The state vector has dimension $n = 3378$ including mean 2010-2017 non-wetland
108 methane emissions on the GEOS-Chem $4^\circ \times 5^\circ$ global grid ($n_1 = 1009$), 2010-2017 linear trends for these
109 emissions on that grid ($n_2 = 1009$), monthly mean wetland methane emissions for individual years in 14
110 subcontinental regions ($n_3 = 12 \times 8 \times 14 = 1344$), and tropospheric OH concentrations in each hemisphere
111 for individual years ($n_4 = 2 \times 8 = 16$). Section 2.2 describes the prior state vector estimates (x_A) and the
112 prior error covariance matrix (S_A). We derive posterior estimates \hat{x} of the state vector and the associated
113 error covariance matrix \hat{S} by analytical solution to the Bayesian optimization problem (Section 2.4). We
114 present results from three inversions using in situ observations only (~~in~~-in-situ-only inversion), GOSAT
115 observations only (GOSAT-only inversion), and both GOSAT and in situ observations (GOSAT + in situ
116 inversion).

117

118 **2.1 Methane observations**

119 The GLOBALVIEWplus CH₄ ObsPack v1.0 data product compiled by the National Oceanic and
120 Atmospheric Administration (NOAA) Global Monitoring Laboratory includes worldwide high-accuracy
121 measurements of atmospheric methane concentrations from different observational platforms (surface,
122 tower, shipboard, and aircraft) (Cooperative Global Atmospheric Data Integration Project, 2019). Here
123 we use the ensemble of GLOBALVIEWplus observations for 2010-2017. For surface and tower
124 measurements, we use only daytime (10-16 local time) observations and average them to the
125 corresponding daytime mean values. We exclude outliers at individual sites that depart by more than three
126 standard deviations from the mean. We obtain in this manner 157054 observation data points for the

127 inversion including 81119 from 103 surface sites, 27433 from 13 towers, 827 from 3 ship cruises, and
128 47675 from 29 aircraft campaigns. Figure 2a shows the mean methane concentrations in 2010-2017 from
129 the in situ data. The data are relatively dense in North America and western Europe, with also a few sites
130 in China, but otherwise mainly measure background concentrations. The number of available surface and
131 tower observations increases from 10493 in 2010 to 19657 in 2017 with the largest changes in Europe
132 and Canada.

133
134 GOSAT is a nadir-viewing satellite instrument ~~launched in in space since~~ 2009 that measures the
135 backscattered solar radiation from a sun-synchronous orbit at around 13:00 local time (Butz et al., 2011;
136 Kuze et al, 2016). Observing pixels are 10-km in diameter and separated by about 250 km along-track
137 and cross-track in normal observation mode, with higher-density data collected in targeted observation
138 modes. Methane is retrieved at the 1.65 μm absorption band. We use dry column methane mixing ratios
139 from the University of Leicester version 9.0 Proxy XCH₄ retrieval (Parker et al., 2020). The retrieval has
140 a single-observation precision of 13 ppb and a regional bias of 2 ppb (Buchwitz et al., 2015). We use
141 GOSAT data for 2010-2017 including 1.6 million retrievals over land as shown in Figure 2b. We do not
142 use glint data over the oceans and data poleward of 60°N because of seasonal bias and the potential for
143 large errors (Maasakkers et al., 2019).

144 **2.2 Prior estimates**

146 Table 1 summarizes the prior estimates of the mean 2010-2017 methane emissions used for the state vector,
147 and Figure 3 shows the spatial patterns. Natural sources include the ensemble mean of the WetCHARTs_S
148 inventory version 1.2.1 (Bloom et al., 2017) for wetlands, open fires from the Global Fire Emissions
149 Database version 4s with seasonal and interannual variability (van der Werf et al., 2017), termites from
150 Fung et al. (1991), and seeps from Etiope et al. (2019) with global scaling to 2 Tg a⁻¹ from Hmiel et al.
151 (2020). The default anthropogenic emissions are from EDGAR v4.3.2 (Janssens-Maenhout et al., 2019),
152 and are superseded for fugitive fuel emissions (oil, gas, coal) by the Scarpelli et al. (2020) inventory
153 which spatially allocates national emissions reported by countries to the United Nations Framework
154 Convention of Climate Change (UNFCCC). US anthropogenic emissions are further superseded by the
155 gridded version of Inventory of U.S. Greenhouse Gas Emissions and Sinks from the Environmental
156 Protection Agency (EPA GHGI) (Maasakkers et al., 2016). The WetCHARTs_S wetlands inventory
157 includes seasonal and interannual variability that is optimized in the inversion through correction to the
158 monthly emissions. Seasonality from Zhang et al. (2016) is imposed for rice emissions, and temperature-
159 dependent seasonality is applied to manure emissions (Maasakkers et al., 2016). Other emissions are
160 aseasonal.

161
162 We assume a 50% error standard deviation for all anthropogenic and non-wetland natural emissions on
163 the 4° latitude \times 5° longitude grid, with no spatial error covariance so that their prior error covariance
164 matrix is diagonal, which is a reasonable assumption for anthropogenic emissions (Maasakkers et al.,
165 2016). We assume $0 \pm 10\%$ a⁻¹ as prior estimate for the linear 2010-2017 emission trends on the 4° \times 5°

166 grid; a sensitivity test using $0 \pm 5\%$ a^{-1} is also performed. The inclusion of linear trends in state vectors
167 allows us to identify the direction of emission change for each $4^\circ \times 5^\circ$ grid in the 8-year period, but it
168 would not capture high-frequency interannual variability. Prior estimates of monthly mean wetland
169 methane emissions for individual years in 14 subcontinental regions, along with their error covariance
170 matrix, are from the WetCHARTs v1.2.1 inventory ensemble (Bloom et al., 2017). The prior methane
171 emissions total 533 Tg a^{-1} , at the low end of the current top-down estimates (~~538-593~~550-594 Tg a^{-1}) for
172 2008-2017 (Saunio et al., 2020), and this largely reflects the downward revision of global seep emissions
173 by Hmiel et al. (2020).

174
175 Prior monthly 3-D fields of global tropospheric OH concentrations are taken from a GEOS-Chem
176 simulation with full-chemistry (Wecht et al., 2014) that yields a methane lifetime $\tau_{\text{CH}_4}^{\text{OH}}$ due to oxidation
177 by tropospheric OH of ~~10.6±1.1~~ years and an inter-hemispheric OH ratio (North to South) of 1.16. The
178 methane lifetime is consistent with the value of 11.2 ± 1.3 years inferred from methylchloroform
179 observations (Prather et al., 2012), while the inter-hemispheric OH ratio ~~is slightly higher than the lies~~
180 between the observed range of 0.97 ± 0.12 (Patra et al., 2014) ~~and the but closed to~~ recent multi-model
181 estimates of 1.3 ± 0.1 (Zhao et al., 2019). We assume no interannual variability in this prior OH field. We
182 ~~assume~~ use 10% as prior error standard deviation for the hemispheric OH concentrations in individual
183 years, based on Holmes et al. (2013), and also conduct a sensitivity test assuming 5%. Corrections to OH
184 in the inversion are applied as a hemispheric scaling factor for individual years, without changing the
185 spatial or temporal pattern of the original fields. Zhang et al. (2018) conducted methane inversions with
186 twelve different OH fields from the ACCMIP model ensemble (Naik et al., 2013) and found no significant
187 difference in results with the GEOS-Chem OH fields used here except for two outlier models.

188 189 **2.3 Forward Model**

190 We use the GEOS-Chem 12.5.0 (<http://geos-chem.org>) global CTM (Bey et al., 2001; Wecht et al., 2014;
191 Maasakkers et al., 2019) as forward model to simulate atmospheric methane concentrations and their
192 sensitivity to the state vector elements. The model is driven by MERRA-2 reanalysis meteorological fields
193 from the NASA Global Modeling and Assimilation Office (GMAO) (Gelaro et al., 2017). The methane
194 sink is computed within the model from 3-D tropospheric oxidant fields including OH (optimized in the
195 inversion), Cl atoms (Wang et al., 2019), 2-D stratospheric oxidant fields (Murray et al., 2012), and soil
196 uptake (Murguia-Flores et al., 2018). We conduct GEOS-Chem model simulations for 2010-2017 at
197 global $4^\circ \times 5^\circ$ resolution with 47 vertical layers extending to the mesosphere.

198
199 GEOS-Chem has excessive methane in the high-latitudes stratosphere, a flaw common to many models
200 (Patra et al., 2011) especially at coarse model resolution. Following Zhang et al. (2020), we compute
201 correction factors to GEOS-Chem stratospheric methane subcolumns as a function of season and
202 equivalent latitude to match the measurements from the solar occultation ACE-FTS v3.6 instrument
203 (Waymark et al., 2014; Koo et al., 2017). As shown in Zhang et al. (2020), the correction can be up to 10%
204 at high latitudes during winter and spring. We apply the correction factors before the inversion to avoid

205 wrongly attributing this model transport bias to methane emissions and loss. Figure S1 shows that the
206 systematic differences in the posterior scaling factors of non-wetland emissions with vs. without bias
207 correction are more prominent at the northern high latitudes, as also shown in Stanevich et al. (2020), but
208 the global total emissions only differ by 1%, and we correct for this bias, with stratospheric methane
209 profiles measured by the solar occultation ACE-FTS v3.6 instrument (Waymark et al., 2014; Koo et al.,
210 2017) following Zhang et al. (2019).

211
212 Initial ~~model conditions~~ GEOS-Chem methane concentrations on January 1, 2010 are ~~set to be adjusted to~~
213 have unbiased ~~in~~ zonal mean relative to GOSAT observations for January 2010, and we find that ~~they the~~
214 resulting model values are also unbiased relative to the GLOBALVIEWplus in situ observations in
215 January 2010. In this manner, model discrepancies with observations over the 2010-2017 period can be
216 attributed to model errors in emissions or OH over that period, instead of error in initial conditions. We
217 archive model methane dry mixing ratios at each location and time of the in situ and GOSAT datasets for
218 2010-2017.

219
220 As forward model F for the inversion, GEOS-Chem relates the state vector \mathbf{x} to the atmospheric
221 concentrations \mathbf{y} as $\mathbf{y} = F(\mathbf{x})$ (Fig.1). The simulation of observations with the prior estimates of state
222 vectors (\mathbf{x}_A) in 2010-2017 diagnoses systematic errors in comparison to observations that enable
223 improved estimate of the state vector through the inversion. In addition, the random component of the
224 discrepancy can be used to estimate the observation error (sum of instrument error, representation error,
225 and forward model error) in the Bayesian optimization problem using the residual error method (Heald et
226 al., 2004). The method assumes that the systematic component of the model bias ($\overline{\mathbf{y} - F(\mathbf{x}_A)}$) for
227 individual years, where the overbar denotes the temporal average in a $4^\circ \times 5^\circ$ grid cell (for GOSAT) or for
228 an observation platform (for in situ observations), is to be corrected in the inversion, while the residual
229 term ($\epsilon_0 = \mathbf{y} - F(\mathbf{x}_A) - \overline{\mathbf{y} - F(\mathbf{x}_A)}$) represents the random observation error. Here we applied this
230 method to construct the observation error covariance matrix \mathbf{S}_o from the statistics of ϵ_0 . For in-situ
231 observations, we derive ϵ_0 separately for the ensemble of background surface sites (Dlugokencky et al.,
232 1994), non-background sites, tower sites, shipboard measurements, and aircraft measurements, while for
233 GOSAT observations ϵ_0 is calculated for each $4^\circ \times 5^\circ$ grid cell.

234
235 We find that the mean standard deviation of the random observation error (ϵ_0) for the GLOBALVIEWplus
236 in situ data averages 36 ppbv (20 and 45 ppbv for background and non-background surface observations,
237 68 ppbv for tower observations, 10 ppbv for shipboard observations, 24 ppbv for aircraft observations),
238 compared to 13 ppbv for GOSAT. The observation error for in situ observations is dominated by the
239 forward model error while for GOSAT it is dominated by the instrument error. The forward model error
240 is higher for surface concentrations near source regions than for columns or other in situ observations
241 measuring background, because the amplitude of methane variability is much higher (Cusworth et al.,
242 2018) and more challenging for a model at $4^\circ \times 5^\circ$ resolution to capture. We assume that \mathbf{S}_o is diagonal
243 in the absence of better objective information, but in fact some error correlation between different

244 observations could be expected to arise from transport and source aggregation errors in the forward model.
 245 This is considered by introducing a regularization factor γ in the minimization of the cost function for
 246 the inversion (Section 2.4).

248 2.4 Analytical Inversion

249 The Bayesian solution to the state vector optimization problem assuming Gaussian prior and observation
 250 errors involves minimizing the cost function $J(\mathbf{x})$:

$$251 \quad J(\mathbf{x}) = (\mathbf{x} - \mathbf{x}_A)^T \mathbf{S}_A^{-1} (\mathbf{x} - \mathbf{x}_A) + \gamma (\mathbf{y} - \mathbf{F}(\mathbf{x}))^T \mathbf{S}_O^{-1} (\mathbf{y} - \mathbf{F}(\mathbf{x})) \quad (1),$$

252 where \mathbf{x} is the state vector, \mathbf{x}_A denotes the prior estimate of \mathbf{x} , \mathbf{S}_A is the prior error covariance matrix,
 253 \mathbf{y} is the observation vector, $\mathbf{F}(\mathbf{x})$ represents the GEOS-Chem simulation of \mathbf{y} , \mathbf{S}_O is the observation
 254 error covariance matrix, and γ is a regularization factor. The need for γ in $J(\mathbf{x})$ is to avoid giving
 255 excessive weighting to observations, due to the likely underestimation of \mathbf{S}_O when unknown error
 256 correlations are not included in its construction (Zhang et al., 2018; Maasakkers et al., 2019). γ here plays
 257 the same role as the regularization parameter in Tikhonov methods (Brasseur and Jacob, 2017) and reflects
 258 our inability to properly quantify the magnitude of errors.

259
 260 Minimization of the cost function in equation (1) has an analytical solution if the forward model is linear
 261 (Rodgers, 2000). ~~The inverse problem here is not strictly linear.~~ The optimization of methane emission
 262 and its trends is strictly linear by design because we use prescribed monthly 3-D OH fields as described
 263 in Section 2.2. There is some non-linearity regarding the optimization of OH, because the sensitivity of
 264 the methane concentration to changes in OH concentrations depends on the methane concentration
 265 through first-order loss. ~~The~~ but we assume that the variability of methane concentration is sufficiently
 266 small that this non-linearity is negligible (we verify this assumption below). We thus express the GEOS-
 267 Chem forward model as $\mathbf{y} = \mathbf{K}\mathbf{x} + \mathbf{c}$, where $\mathbf{K} = \partial\mathbf{y}/\partial\mathbf{x}$ represents the Jacobian matrix and \mathbf{c} is an
 268 initialization constant. We construct the Jacobian matrix \mathbf{K} explicitly by conducting GEOS-Chem
 269 simulations with each element of the state vector perturbed separately. For the linear emission trend
 270 elements, this is done by perturbing the 2010-2017 emission trend in each grid cell from 0% (the best
 271 prior estimate) to 10% a⁻¹; for OH, this is done by perturbing yearly hemispheric OH fields by 20%
 272 without modifying the spatial or seasonal distribution. Comparison of the resulting Jacobian matrix to
 273 GEOS-Chem as $\mathbf{F}(\mathbf{x}) - \mathbf{K}\mathbf{x} - \mathbf{c}$ shows a negligible residual difference of 2±3 ppb, verifying the assumption
 274 of linearity.

275
 276
 277 Minimizing the Bayesian cost function by solving $dJ(\mathbf{x})/d\mathbf{x} = \mathbf{0}$ yields closed-form expressions for the
 278 posterior estimate of the state vector $\hat{\mathbf{x}}$ ~~and its~~ with error covariance matrix $\hat{\mathbf{S}}$:

$$279 \quad \hat{\mathbf{x}} = \mathbf{x}_A + \mathbf{G}(\mathbf{y} - \mathbf{K}\mathbf{x}_A) \quad (2),$$

$$280 \quad \hat{\mathbf{S}} = (\gamma \mathbf{K}^T \mathbf{S}_O^{-1} \mathbf{K} + \mathbf{S}_A^{-1})^{-1} \quad (3),$$

281
 282 where \mathbf{G} is the gain matrix,

$$\mathbf{G} = \frac{\partial \hat{\mathbf{x}}}{\partial \mathbf{y}} = (\gamma \mathbf{K}^T \mathbf{S}_O^{-1} \mathbf{K} + \mathbf{S}_A^{-1})^{-1} \gamma \mathbf{K}^T \mathbf{S}_O^{-1} \quad (4).$$

From the posterior error covariance matrix one can derive the averaging kernel matrix describing the sensitivity of the posterior estimate to the true state:

$$\mathbf{A} = \frac{\partial \hat{\mathbf{x}}}{\partial \mathbf{x}} = \mathbf{I}_n - \hat{\mathbf{S}} \mathbf{S}_A^{-1} \quad (5).$$

The trace of \mathbf{A} quantifies the degrees of freedom for signal (DOFS), which represents the number of pieces of independent information gained from the observing system for constraining the state vector (Rodgers, 2000).

We choose the value of the regularization parameter γ in order to avoid overfitting to the observations when the number m of observations is much larger than the number n of state vector elements, and the error covariance of the observations cannot be properly quantified. Overfitting would be implied by a highly unlikely departure of the posterior solution from the prior estimate, which can be indicated from the posterior cost function. For a given state vector element i , the expected value of $(x_i - x_{Ai})^2$ is the prior error variance σ_{Ai}^2 . For an n -dimensional state vector with a diagonal prior error covariance matrix, the state component J_A of the cost function is the sum of n random normal elements

$$J_A(\mathbf{x}) = (\mathbf{x} - \mathbf{x}_A)^T \mathbf{S}_A^{-1} (\mathbf{x} - \mathbf{x}_A) = \sum_n \frac{(x_i - x_{Ai})^2}{\sigma_{Ai}^2} \quad (6),$$

and its pdf is given by the Chi-square distribution with n degrees of freedom ($n=3378$ in this case), with an expected value of n and a standard deviation of $\sqrt{2n}$. One can apply the same reasoning to the observation component J_O of the posterior cost function,

$$J_O(\mathbf{x}) = (\mathbf{y} - \mathbf{K}\mathbf{x})^T \mathbf{S}_O^{-1} (\mathbf{y} - \mathbf{K}\mathbf{x}) = \sum_m \frac{(y_i - Kx_i)^2}{\sigma_{oi}^2} \quad (7),$$

whose pdf follows a chi-square distribution with m degrees of freedom. However, this component is less sensitive to the choice of γ because of the large random error component for individual observations.

~~We choose the value for the regularization parameter γ in order to achieve a solution most consistent with the estimated error on the prior estimates. For a given state vector element i , the expected value of $(\hat{x}_i - x_{Ai})^2$ is the prior error variance σ_{Ai}^2 . For a diagonal prior error covariance matrix, the state component J_A of the posterior cost function is~~

$$J_A(\hat{\mathbf{x}}) = (\hat{\mathbf{x}} - \mathbf{x}_A)^T \mathbf{S}_A^{-1} (\hat{\mathbf{x}} - \mathbf{x}_A) = \sum_n \frac{(\hat{x}_i - x_{Ai})^2}{\sigma_{Ai}^2} \approx n \quad (6),$$

~~where n is the number of state vector elements. In our case the prior error covariance matrix is not strictly diagonal because of covariance for the wetland terms (Bloom et al., 2017), so one may expect $J_A(\hat{\mathbf{x}})$ to be somewhat deviated from n . Nevertheless, $J_A(\hat{\mathbf{x}}) \gg n$ implies overfit to the observations because the posterior state vector estimates are far outside the estimated errors on the prior estimates.~~

318
319 One can apply the same reasoning to the observation component J_o of the posterior cost function,

$$320 J_o(\hat{\mathbf{x}}) = (\mathbf{y} - \mathbf{K}\hat{\mathbf{x}})^T \mathbf{S}_o^{-1} (\mathbf{y} - \mathbf{K}\hat{\mathbf{x}}) \approx m \quad (7),$$

321
322 where m is the number of observations. However, this component is less sensitive to the choice of γ
323 because of the large random error component for individual observations.

324
325 Figure 4 shows the dependences of $J_A(\hat{\mathbf{x}})$ and $J_o(\hat{\mathbf{x}})$ on the choice of the regularization parameter γ , for
326 the in situ and GOSAT observations. The in situ observations are sufficiently sparse that $\gamma = 1$ (no
327 regularization) is expected provides the best solution. In the case of GOSAT, however, $\gamma = 1$ would yield
328 $J_A(\hat{\mathbf{x}}) = 6n \gg n \pm \sqrt{2n}$ which indicates overfitting, while $\gamma = 0.1$ yields $J_A(\hat{\mathbf{x}}) \approx n$ which is the
329 expected value and is used here. This can be explained by the high observation density of GOSAT, such
330 that error correlation between individual observations through the forward model may be expected and
331 would have a large effect on the solution. Maasackers et al. (2019) found that $\gamma = 0.05$ and $\gamma = 0.1$
332 gave similar solutions in their global inversions of GOSAT data. We also conduct sensitivity tests using
333 $\gamma = 0.5$ for in situ observations and $\gamma = 0.05$ for GOSAT observations.

334
335 The Analytical solution to the cost function minimization Bayesian optimization problem, as done here,
336 has several advantages relative to the more commonly used variational (numerical) solution approach for
337 finding the minimum. (1) It finds the true minimum in the cost function, rather than an approximation
338 that may be sensitive to the choice of initial estimate. (2) It identifies the information content of the
339 inversion and the ability to constrain each state vector element. (3) It enables a range of sensitivity
340 analyses, modifying the prior estimates, modifying the error covariance matrices, adding/subtracting
341 observations, etc. at minimal computational cost. We will make use of these advantages in comparing the
342 ability of the in-situ-only, GOSAT-only, and GOSAT + in situ inversions, and to test how choices in
343 cost-function construction affect our conclusions including changing the regularization parameter γ ,
344 changing the prior error estimates, and using different types of in-situ observations. Our analysis will
345 focus on results from the base inversions with the default settings, but we will use results from the
346 sensitivity inversions to address specific issues.

347
348 A requirement of the analytical approach is that the Jacobian matrix be explicitly constructed, requiring
349 $n + 1$ forward model runs. Building the Jacobian matrix for the 3378 state vectors in this 8-year period
350 study requires about one million core hours (8 cores \times 36 hours per simulation \times 3378 simulations).
351 However, this construction is readily done in parallel on high-performance computing clusters.

352
353 Our inversion returns posterior emission estimates and their temporal trends on a $4^\circ \times 5^\circ$ grid for non-
354 wetland emissions, and monthly mean wetland emissions for individual years in 14 subcontinental regions.
355 We cannot separate individual sectors within a $4^\circ \times 5^\circ$ grid cell because they will all have the same response
356 function (Jacobian column). However, we can aggregate these results spatially and by sector in a way

357 that retains the error covariance of the solution (Maasakkers et al., 2019). Consider a reduced state vector
358 \mathbf{x}_{red} representing a linear combination of the original state vector elements that may be a sum over a
359 particular region or the globe, and may be weighted by the contributions from individual sectors following
360 the prior distribution. The linear transformation from the posterior full-dimension state vector $\hat{\mathbf{x}}$ to the
361 reduced state vector $\hat{\mathbf{x}}_{red}$ is defined by a summation matrix \mathbf{W}

$$\hat{\mathbf{x}}_{red} = \mathbf{W}\hat{\mathbf{x}} \quad (8).$$

362
363
364 The posterior error covariance and averaging kernel matrices for the reduced state vector can then be
365 calculated as:

$$\hat{\mathbf{S}}_{red} = \mathbf{W}\hat{\mathbf{S}}\mathbf{W}^T \quad (9),$$

$$\mathbf{A}_{red} = \mathbf{W}\mathbf{A}\mathbf{W}^* \quad (10),$$

366
367 where $\mathbf{W}^* = \mathbf{W}^T(\mathbf{W}\mathbf{W}^T)^{-1}$ (Calisesi et al., 2005). $\hat{\mathbf{S}}_{red}$ provides a means to determine error
368 correlations between aggregates of quantities optimized by the inversion, e.g., between global methane
369 emissions and global OH concentrations. \mathbf{A}_{red} provides a means to determine the ability of the inversion
370 to constrain an aggregated term (e.g., emissions from a particular sector).
371

372 373 **3. Results and discussion**

374 **3.1 Ability to fit the in situ and GOSAT data**

375 We will present results from three different inversions for 2010-2017: (1) using only in situ observations
376 (~~In~~-situ-only inversion), (2) using only GOSAT observations (GOSAT-only inversion), and (3) using
377 both GOSAT and in situ observations (GOSAT + in situ inversion). Here we first evaluate the ability of
378 these different inversions to fit the in situ and GOSAT observations, including when the data are not used
379 in the inversion (consistency check). This is done by conducting GEOS-Chem simulations with posterior
380 values for the state vectors and comparing to observations.
381

382 Figures 5 and 6 show the resulting comparisons for the in situ observations, arranged by type of platform
383 (Fig.5), and by latitude bands and months (panels (a)-(d) in Fig.6). The model simulation with prior
384 estimates shows a 30-60 ppb low bias for all in situ platforms growing with time. The ~~In~~-situ-only
385 inversion effectively corrects this bias and its trend, and also significantly improves the correlations across
386 all platforms. ~~The GOSAT-only inversion performs comparably in correcting the bias for the independent
387 aircraft data measuring the background, and also corrects the 2010-2017 trend, but still shows notable
388 low bias at northern mid-latitudes because of difficulty in fitting the surface and tower data in the US and
389 Europe that are adjacent to methane sources. The GOSAT-only inversion performs comparably in
390 correcting the 2010-2017 trend for the independent in-situ data (Fig.6c) and bias for background
391 observations (e.g. aircraft observations in the Southern Hemisphere (Fig.S2)), but there is a low bias at
392 northern mid-latitudes reflecting surface and tower data in North America and Europe. As we will see,
393 the in situ observations are important for optimizing emissions in these regions.~~

394
395 Figure 6 also compares the fits to the GOSAT observations (panels (e)-(h)). ~~Both the In situ only and~~

~~GOSAT-only inversions correct the bias and trend in the prior simulation at all latitudes. The in-situ-only inversion corrects the trends, but biases low to the GOSAT observations by about 10 ppbv with larger bias in the Southern Hemisphere due to the sparsity of in situ observation there. The comparison suggests that in situ and GOSAT observations are largely consistent for informing the global methane change but also have some complementarity for the inversion. An important implication is that the in situ observations, even though sparse and mostly at northern mid-latitudes, can still inform the global methane levels.~~ The GOSAT + in situ joint inversion shows good agreement with both the in situ and GOSAT observations.

Figure 7a further evaluates the global methane growth rate as determined by the methane budget imbalance for individual years in 2010-2017 from the three inversions. The observed methane growth rate inferred from the NOAA sites (https://www.esrl.noaa.gov/gmd/ccgg/trends_ch4/, last access: 20 June 2020) averages 7.2 ± 2.8 ppb a^{-1} over the period, peaking in 2014, and overall accelerating with higher growth in 2015-2017 than in 2010-2013. We find that all posterior simulations show comparable mean methane growth rate (7.7 ± 3.7 ppb a^{-1} for in-situ-only inversion, 8.8 ± 2.2 ppb a^{-1} for GOSAT-only inversion, and 8.3 ± 1.8 ppb a^{-1} for the GOSAT + in situ inversion). However, the in-situ-only inversion overestimates the increasing trend in the methane growth rate, largely driven by the year 2017, and fails to fit its interannual variability. This may reflect the heavy weighting of the in situ observations toward northern mid-latitudes. GOSAT observations in the inversion do much better in capturing the observed methane interannual variability and trend. Adding in situ observations to GOSAT observations provides a better fit in 2015 than GOSAT-only inversion but has an insignificant effect in other years. Zhang et al. (2020a,2019) interpreted the trend and interannual variability in the GOSAT-only inversion as due to a combination of anthropogenic emissions, wetlands, and OH concentrations.

3.2 Anthropogenic methane emissions

Figure 8 shows the averaging kernel sensitivities (diagonal elements of the averaging kernel matrix) and posterior scaling factors for the non-wetland emissions (dominated by anthropogenic emissions) in the in-situ-only, GOSAT-only, and GOSAT + in situ joint inversions. The DOFS (trace of the averaging kernel matrix) quantify the number of independent pieces of information from the inversion, starting from 1009 unknowns for anthropogenic emissions (Figure 1). The DOFS are 113 for the in-situ-only inversion, 212 for the GOSAT-only inversion, and 262 for the GOSAT + in situ joint inversion. The higher DOFS from the joint inversion indicate that the satellite and in situ observations have complementarity but also some redundancy. Strict complementarity would imply a DOFS of $325 = 113 + 212$. We find that 75% of the in situ information is at northern mid-latitudes ($30-60^{\circ}N$, DOFS=82, calculated as the sum of averaging kernel sensitivities in that latitude band) where the observations are densest, with another 9% (DOFS=10) at $60-90^{\circ}N$. GOSAT provides higher-more information than do in situ observations at northern mid-latitudes (DOFS=96) and dominates in the tropics (DOFS=105). This dominance of satellites for informing methane sources in the tropics has been pointed out in previous studies (Bergamaschi et al., 2013; Monteil et al., 2013; Fraser et al., 2013; Alexe et al., 2015). We find that the

435 DOFS from the in-situ-only inversion observations are mostly (85%) from the surface and tower
436 measurements (Fig.S3).

437
438 We investigate further the inversion results for northern mid-latitudes where most of the information of
439 in situ observations is contained including for the US, Canada, Europe, and China. Table 2 gives the
440 optimization of anthropogenic methane emissions (calculated as the difference between total non-wetland
441 emissions and the non-wetland natural emissions) in these regions. Figure 9 shows the optimization by
442 source sectors, assuming that (1) the partitioning between sectors of non-wetland emissions in individual
443 grid cells is correct in the prior inventory (this does not assume that the prior distribution of sectoral
444 emissions is correct)-, (2) the scaling factors are to be applied equally to all sectors in a grid cell. These
445 assumptions are adequate when the sectors are spatially separated but are more prone to error when they
446 spatially overlap. Figure 9 also shows the averaging kernel sensitivities of emission sectors (diagonal
447 terms of A_{red} derived from Equations (8) and (10)), measuring the ability of the inversion to optimize
448 different emissions sectors, and the DOFS for each inversion summed over the region. Wetland methane
449 emissions are optimized separately as will be discussed in Section 3.3.

450
451 Inspection of the DOFS shows that the in situ observations are more effective than GOSAT for optimizing
452 US anthropogenic methane emissions (DOFS=41 vs. DOFS=22) and this applies to all sectors (Figure 9).
453 The averaging kernel sensitivities panel in Figure 9 shows that US results from the joint GOSAT + in situ
454 inversion are mostly determined by the in situ observations. The joint GOSAT + in situ inversion increases
455 anthropogenic US emissions from 28 Tg a⁻¹ in the prior EPA GHGI to 36 Tg a⁻¹, with most of the increase
456 driven by ~~livestock and~~ oil/gas sources in the central US. Averaging kernel sensitivity for major sectors
457 is large (0.63-0.93), indicating that the posterior estimates are mostly determined by the observations
458 rather than by the prior estimates. The underestimate of oil/gas emissions in the EPA GHGI has been
459 reported before in local observations and higher-resolution inversions (Miller et al., 2013; Turner et al.,
460 2015; (Alvarez et al., 2018; Cui et al., 2019; Maasakkers et al., 2020).

461
462 The in situ observations are also more effective than GOSAT in optimizing anthropogenic methane
463 emissions in Canada (DOFS=21 vs. DOFS=6), particularly in Alberta where oil/gas emissions are high
464 (Fig.8). This reflects in part our exclusion of GOSAT data poleward of 60°N. Oil/gas emissions in Canada
465 increase by a factor of 2 in the GOSAT + in situ inversion to 4.5 Tg a⁻¹ compared to UNFCCC the ICF
466 (2015)-prior estimate, with an averaging kernel sensitivity of 0.57 (Fig.9). Total anthropogenic emissions
467 increase from 5 Tg a⁻¹ to 8 Tg a⁻¹.

468
469 In situ and GOSAT observations show comparable ability in optimizing the total anthropogenic emissions
470 in Europe (DOFS=16~18). They agree that prior anthropogenic methane emissions are too high in
471 northern Europe but disagree in southern Europe. Averaging kernel sensitivities from the in-situ-only
472 inversion are slightly weaker than for the US and Canada because of the lower density of in situ sites. The
473 Integrated Carbon Observation system (ICOS) network (<https://www.icos-cp.eu/>, last access: 17 July

2020) has increased substantially the number of available methane observations in Europe since 2017 so that future inversions should expect a stronger constraint from in situ observations. Total European anthropogenic emissions decrease from 27 Tg a⁻¹ to 23 Tg a⁻¹ in the GOSAT + in situ joint inversion, with decreases for all sectors but this may reflect the inability of our 4°× 5° resolution to effectively separate emission sectors.

The only other region where in situ observations provides significant information is China, though the corresponding DOFS=13 is less than for GOSAT (DOFS=22). Both inversions agree that emissions must be greatly decreased from the prior estimate, and the joint inversion (DOFS=28) has stronger power in doing so. The posterior 2010-2017 Chinese anthropogenic emission is 43 Tg a⁻¹ in the joint inversion, compared to 63 Tg a⁻¹ in the prior estimate. Our results agree with a recent study by Janardanan et al. (2020), which also used GOSAT and surface observations to estimate a mean 2011-2017 anthropogenic methane emission in China of 46±9 Tg a⁻¹. The downward correction is mainly driven by a 40% decrease in coal emissions from 19 Tg a⁻¹ to 11 Tg a⁻¹ (Fig. 9). Previous inversions using the EDGAR inventory (>20 Tg a⁻¹) as prior estimate found a similar correction (Alexe et al., 2015; Thompson et al., 2015; Turner et al., 2015; Maasakkers et al., 2019; Miller et al., 2019). In our case, the prior estimate of coal emissions (19 Tg a⁻¹) is the value reported by China to the UNFCCC and we find that it is still too high. A recent inventory by Sheng et al. (2019) gives a coal emission estimate of 15 Tg a⁻¹ for China in 2010-2016.

3.3 Wetland methane emissions

The inversion optimizes wetland emissions for the 14 regions of Figure 3 and for 96 individual months covering 2010-2017, amounting to 1344 state vector elements. Results from the in-situ-only, GOSAT-only, and GOSAT + in situ inversions yield DOFS of 221, 183, and 301 respectively. In situ observations provide more information for boreal wetlands while GOSAT dominates for tropical wetlands.

Zhang et al. (2020a) give a detailed analysis of GOSAT-only inversion results for tropical wetlands. ~~Where~~ we analyzed further the boreal/temperate North America wetlands, where in situ observations provide significant added information (Figure 10). Both in situ and GOSAT observations agree that the prior WetCHARTs emissions are too high. The posterior estimates from the GOSAT + in situ inversion are 4.5 and 2.0 Tg a⁻¹ for boreal and temperate North America, respectively, compared to 12.8 and 6.9 Tg a⁻¹ in WetCHARTs. Posterior boreal wetland CH₄ emissions for North America are on the lower end but within the WetCHARTs estimates (WetCHARTs models range 3~33 Tg a⁻¹); however, posterior temperate CH₄ emissions for North America are ~~lower and~~ outside the WetCHARTs range (3~12 Tg a⁻¹). The correction for boreal North America is particularly large in May-June, which can potentially be attributed to suppression of wetland emissions by either snow cover (Pickett-Heaps et al., 2011) or ~~by~~ frozen soils (Zona et al., 2016). The WetCHARTs emission overestimate for temperate North America (mainly coastal wetlands in the eastern US) has been reported before from inversions using aircraft data (Sheng et al., 2018) and GOSAT data (Maasakkers et al., 2020).

513

514 **3.4 Anthropogenic methane emission trends**

515 Figure 11 presents the 2010-2017 trends ($\% \text{ a}^{-1}$) of anthropogenic methane emissions from the three
516 inversions, and the corresponding averaging kernel sensitivities. The GOSAT + in situ inversion has a
517 DOFS = 161 for quantifying the spatial distribution of the trends. Most of that information is from GOSAT
518 (DOFS = 122) but in situ observations add significant information. Information from in situ observations
519 is concentrated in the US, Canada, Europe, and China. Table 2 summarizes the trends for the four regions.
520 Figure 12 shows the trends disaggregated by sectors, using the same procedure as for Figure 9.

521

522 In situ observations provide stronger constraints than GOSAT on anthropogenic emission trends in the
523 US (DOFS=29 vs. DOFS=12). They agree on the upward trend in the eastern US as also found in
524 Maasakkers et al. (2020) which used GOSAT in a high resolution inversion to interpret methane trends in
525 the US in 2010-2015. However, they show opposite trends (positive trend from in-situ-only inversion
526 but negative from GOSAT-only inversion) in total emissions and in the central south US (Table 2, Fig.
527 11). The GOSAT + in situ joint inversion (DOFS=31) estimates that US anthropogenic methane emissions
528 increased by $0.4 \text{ Tg a}^{-1} \text{ a}^{-1}$ ($1.1\% \text{ a}^{-1}$) from 2010 to 2017, with the largest contribution from oil/gas
529 emissions ($0.3 \text{ Tg a}^{-1} \text{ a}^{-1}$, $2.5\% \text{ a}^{-1}$). This posterior trend is much smaller than previous studies showing
530 large increases in US oil/gas emissions ($2.1\text{--}4.4 \text{ Tg a}^{-1} \text{ a}^{-1}$) inferred from ethane/propane levels (Franco
531 et al., 2016; Hausmann et al., 2016; Helmig et al., 2016), but is more consistent with a recent study by
532 Lan et al. (2019) of $0.3\pm 0.1 \text{ Tg a}^{-1} \text{ a}^{-1}$ in 2006-2015 based on long-term in situ measurements. The
533 inversion also reveals rising emissions from oil/gas in the central south US, including the Permian Basin
534 which is currently the largest oil-producing basin in the US (Zhang et al., 2020b).

535

536 We find that anthropogenic emissions in Canada decrease over the 2010-2017 period by $0.2 \text{ Tg a}^{-1} \text{ a}^{-1}$
537 ($2.5\% \text{ a}^{-1}$) in the GOSAT + in situ joint inversion, mostly driven by oil/gas emissions in Alberta and
538 livestock emissions (Figs. 11-12). Anthropogenic emissions in Europe decrease by $0.4 \text{ Tg a}^{-1} \text{ a}^{-1}$ ($1.7\% \text{ a}^{-1}$).
539

540

541 All three inversions show increases of Chinese anthropogenic methane emissions over 2010-2017 by 0.1-
542 $0.4 \text{ Tg a}^{-1} \text{ a}^{-1}$ ($0.3\text{--}0.9\% \text{ a}^{-1}$), but the spatial patterns and source attributions are different. The largest
543 difference is for coal mining emissions in the North China Plain, where in situ observations indicate a
544 decrease of $-0.8 \text{ Tg a}^{-1} \text{ a}^{-1}$ while GOSAT shows an increase of $0.1 \text{ Tg a}^{-1} \text{ a}^{-1}$. A previous GOSAT
545 inversion study found a large increase of coal mining emissions in China over 2010-2015 (Miller et al.,
546 2019). However, a recent bottom-up inventory estimates that Chinese coal emission peaked in 2012 and
547 decreased afterward, leading to no significant overall trend for 2010-2016 (Sheng et al., 2019). Our
548 inversion assumes linear trends in emissions over 2010-2017 but that may not be appropriate for China.

549

550 **3.5 Global methane budget for 2010-2017**

551 Table 1 shows the optimized global anthropogenic emissions from different sectors as determined by the

552 joint GOSAT + in situ inversion. Corrections to the global prior estimates are mostly determined by
553 GOSAT (Fig. 8). They include upward corrections to livestock and rice methane emissions, and
554 downward correction to the coal mining emissions driven by overestimation in China. The joint inversion
555 also estimates a global increase in anthropogenic emissions by $1.7 \pm 0.6 \text{ Tg a}^{-1} \text{ a}^{-1}$ ($0.5\% \text{ a}^{-1}$) in 2010-2017,
556 dominantly driven by trends in the tropics (Fig. 11).

557
558 A number of previous studies have analyzed surface observations to interpret global methane budgets and
559 trends (Dlugokencky et al., 2009; Bruhwiler et al., 2014; Houweling et al., 2017). As shown in Figure 6,
560 our ~~in~~-situ-only inversion can fit the GOSAT observations of global methane distribution and trend,
561 indicating that the in situ data provide useful information on the global budget. Here we examine whether
562 this information adds to that from GOSAT. For this purpose and following Maasackers et al. (2019), we
563 collapse the full state vector to a reduced state vector ($\hat{\mathbf{x}}_{red}$) that contains global mean methane emissions
564 and OH as elements, and derive the associated error covariance matrix ($\hat{\mathbf{S}}_{red}$) as introduced in Section
565 2.4.

566
567 Figure 13 shows the joint probability density functions (PDFs) of the mean anthropogenic methane
568 emissions and methane lifetime against oxidation by tropospheric OH from the three inversions. There is
569 strong negative correlation ($r=-0.72$) between the optimization of methane emissions and OH in the
570 GOSAT-only inversion, and somewhat less in the ~~in~~-situ-only inversion ($r=-0.53$), although the posterior
571 error variance is larger due to the lower data density as indicated by the axes of the ellipses. A sensitivity
572 inversion using only the surface and tower measurements in the ~~in~~-situ-only inversion yields $r=-0.37$
573 ~~(Fig.13b)~~. It indicates that in situ observations, in particular surface and tower measurements, are more
574 effective than the satellite observations in ~~independently~~-constraining methane emissions independently
575 from the sink by OH. A likely reason is that surface measurements in source regions are more sensitive
576 to methane emissions than are column measurements. We also find that the in-situ-only inversion yields
577 a larger interannual variability of posterior OH concentrations and thus methane lifetime than the GOSAT-
578 only inversion (Fig.7b), due to the heterogeneous spatial and temporal distribution of the in situ
579 observations.

580
581 Comparison of the posterior PDFs between the GOSAT-only and ~~in~~-situ-only inversions implies that the
582 two are inconsistent in optimizing global methane budgets, since the 99% probability contours ~~does~~ not
583 overlap (Fig.13a). ~~But this is likely because possible cause is that~~ the posterior error covariance matrix
584 underestimates the actual error variance ~~in particular for global budget errors~~ due to its assumption of
585 independent identically distributed (IID) observational errors (Brasseur and Jacob, 2017), and this would
586 particularly affect the global budget which sums emission results for individual grid cells. Remarkably,
587 the solution from the GOSAT + in situ joint inversion is more in agreement with in situ observations than
588 GOSAT, and does not lie between these two solutions. Inspection of Figure 6c shows that the GOSAT-
589 only inversion is biased low relative to in situ observations at northern mid-latitudes and biased high in
590 the southern hemisphere, implying that both emissions and OH concentrations are too low. On the other

591 hand, Figure 6f indicates either underestimation of emissions or overestimation of OH concentrations in
592 the in-situ-only inversion, and the former one is more likely as GOSAT measurements used here are over
593 land which should be more sensitive to emissions than OH loss. Ingestion of both observations in the
594 GOSAT + in situ inversion thus enhances both the methane emissions and OH concentrations compared
595 to the in-situ-only and GOSAT-only inversion to correct these biases. It also narrows the posterior error
596 of mean anthropogenic emissions and methane lifetime against tropospheric OH by 20% and 50%
597 compared to the GOSAT-only and in-situ-only inversions, respectively (Fig. 13a). Ingestion of the in situ
598 observations in the inversion corrects that bias, and narrows the posterior error of mean anthropogenic
599 emissions and methane lifetime against tropospheric OH by 30% (Fig. 13), compared to the GOSAT only
600 inversion.— Thus we find that the GOSAT and in situ observations are complementary in quantifying the
601 global budget.

602
603 Table 3 summarizes the global mean methane budget in 2010-2017. The GOSAT + in situ joint inversion
604 estimates a total methane emission of 551 ± 2 Tg a⁻¹, of which 371 Tg a⁻¹ are anthropogenic, and a total
605 sink of 528 ± 2 Tg a⁻¹. The total emission is at the low end of within the 538-593-550-594 Tg a⁻¹ range
606 of top-down estimates but lower than the 594-881 Tg a⁻¹ range of bottom-up estimates reported for the
607 2008-2017 decade by the Global Carbon Project (Saunio et al., 2020). Our joint inversion yields a
608 methane lifetime against OH oxidation of 11.2 ± 0.1 years, compared to consistent with the observationally-
609 based estimate of 11.2 ± 1.3 years (Prather et al., 2012), and pushes the northern to southern hemispheric
610 OH ratio (1.060-98 in GOSAT + in situ inversion versus 1.16 in prior estimate) closer to observed the
611 values of (0.97±0.12) inferred from methyl chloroform observations (Patra et al., 2014).

612
613 We examine in Figure 13b the sensitivity of the global methane budget optimization to the choice of
614 different regularization parameter γ (and therefore observation error S_0) and prior error of methane
615 emission trends and OH concentrations. We find that reducing γ or prior errors of trend and OH by 50%
616 yields consistent estimates of anthropogenic emissions and OH concentrations as compared to the default
617 inversion, with differences within 3%. Decreasing the weighting of observations in the inversion (i.e.
618 assuming larger observation error) enlarges the posterior error and pushes the posterior estimates closer
619 to the prior estimates. Assuming a lower prior error for OH concentration from 10% to 5% results in lower
620 methane lifetime (closer to the prior) and higher emissions, and also reduces the error correlation between
621 the optimization of methane emissions and OH, while assuming a lower prior error for non-wetland
622 emission trends leads to an opposite effect. Our results are consistent with Maasakkers et al. (2019), which
623 shows that different assumptions of error distribution and magnitude in their analyses have relatively
624 small results. We also find that having the shipboard and aircraft measurements in the in-situ-only
625 inversion pushes the estimate to be more consistent with the GOSAT-only inversion (Fig.13b), implying
626 that the shipboard and aircraft measurements by emphasizing the methane in the remote atmosphere play
627 a similar role as satellite measurements in global methane budget optimization.

628 629 **4 Conclusions**

630 We quantified and attributed global sources, sinks, and trends of atmospheric methane for 2010-2017 by
631 inversions of GOSAT satellite data and the GLOBALVIEWplus in situ methane observations from surface
632 sites, towers, ships, and aircraft. The inversions use an analytical solution to Bayesian optimization
633 problem including closed-form error covariance matrices from which the detailed information content of
634 the inversion can be derived. We conduct inversions using GOSAT and in situ data separately and
635 combined. In this manner we are able to quantify the consistency and complementarity (or redundancy)
636 of the satellite and in situ observations.

637
638 ~~We find that the GOSAT and in situ data are generally consistent and can fit each other independently~~
639 ~~through our inversions. Nevertheless, We find that the GOSAT-only inversion can generally fit the in situ~~
640 ~~data and the in-situ-only inversion can generally fit the GOSAT data, indicating consistency between the~~
641 ~~two data sets. However,~~ the GOSAT-only inversion has difficulty ~~fitting to fit~~ the in situ observations in
642 source regions (US and Europe), while ~~In the in-situ-only inversion s could not~~ cannot reproduce the
643 interannual variability of ~~the~~ methane growth rate due to ~~its the~~ heavy weighting ~~of in situ data to the~~
644 northern mid-latitudes. The GOSAT + in situ inversion shows the best ~~agreement with fit to the ensemble~~
645 ~~of~~ observations.

646
647 GOSAT and in situ observations ~~are to a large extent complementary in terms of~~ have complementarity
648 in constraining global emissions. GOSAT provides stronger constraints than in situ observations for the
649 tropics, while in situ observations are more important in the US, Canada, Europe, and northern China
650 where observations are most dense. The GOSAT-only and in-situ-only inversions also show consistent
651 corrections to regional methane emissions in the US, Europe, and China. The joint GOSAT + in situ
652 inversion ~~indicates~~ reveals large underestimates of oil/gas emissions in the US and Canada, and large
653 overestimates of coal emissions in China, relative to the national inventories reported to the United
654 Nations Framework Convention on Climate Change (UNFCCC) and used here as prior estimates for our
655 inversions. Emissions from boreal wetlands are overestimated in the mean WetCHARTs inventory used
656 as prior estimate, particularly in May-June when snow cover and frozen soils inhibit methane emission.

657
658 Our inversions ~~estimate~~ indicate increasing trends in US anthropogenic emissions driven by oil/gas
659 production but decreasing trends in Canada (oil/gas) and Europe. Joint inversion of GOSAT ~~and~~ + in situ
660 data shows a weak decreasing trend in Chinese coal emissions for 2010-2017, consistent with a recent
661 bottom-up inventory (Sheng et al., 2019).

662
663 We find that GOSAT and in situ observations are also complementary in constraining the global methane
664 budget. While the global budget information relies more on GOSAT observations, information from the
665 in situ observations at northern mid-latitudes avoids the large error correlations between methane
666 emissions and sink from OH and also corrects the underestimation of both emission and OH in the
667 GOSAT-only inversion. Our joint GOSAT + in situ inversion yields ~~the~~ global methane emissions and
668 loss of 551 ± 2 and 5298 ± 2 Tg a⁻¹ a⁻¹ averaged over 2010-2017, and a methane lifetime of 11.2 ± 0.1 years.

669

670 Our study presents a framework to integrate satellite and in situ data in analytical inversions. We conclude
671 that on the basis of the present observation system, in situ and satellite observations are complementary
672 for constraining global methane budgets and regional emissions. Satellite observations of atmospheric
673 methane are presently expanding with the new availability of global daily data from the TROPOMI
674 instrument launched in October 2017~~8~~ (Hu et al., 2018). ~~This will call for re-evaluating the role of in situ
675 observations for constraining regional and global methane budgets, as can be done with the methods
676 presented here. In situ observations will in any case continue to play a critical role for documenting long-
677 term trends of methane with consistent calibration, for observation of oceanic and polar regions where
678 satellites have limited capability, for high-frequency measurements in source regions giving insight into
679 the magnitude and intermittency of local emissions, and for independent validation of satellite-based
680 inversions. In situ observations as presented in this paper will continue to play a critical role for satellite
681 validation and for quantification of long-term trends. Their role for source characterization in supplement
682 to satellite data will need to be re-evaluated as satellite observations expand, and the framework presented
683 in this paper provides a means for doing so.~~

684

685 **Data availability**

686 The GLOBALVIEWplus CH₄ ObsPack v1.0 data product is available at
687 https://www.esrl.noaa.gov/gmd/ccgg/obspack/data.php?id=obspack_ch4_1_GLOBALVIEWplus_v1.0_2019-01-08
688 (last access: July 17, 2020). The GOSAT proxy satellite methane observations are available
689 at <https://doi.org/10.5285/18ef8247f52a4cb6a14013f8235cc1eb> (last access: July 17, 2020). Modeling
690 data can be accessed by contacting the corresponding authors Xiao Lu (xiaolu@g.harvard.edu) and
691 Yuzhong Zhang (zhangyuzhong@westlake.edu.cn).

692

693 **Author contributions**

694 XL and DJJ designed the study. XL and YZZ conducted the modeling and data analyses with contributions
695 from JDM, MPS, LS, ZQ, TRS, HON, RMY, and JXS. AA contributed to the GLOBALVIEWplus CH₄
696 ObsPack v1.0 data product. RJP and HB contributed to the GOSAT satellite methane retrievals. AAB and
697 SM contributed to the WetCHARTs wetland emission inventory and its interpretation. XL and DJJ wrote
698 the paper with input from all authors.

699

700 **Competing interests**

701 The authors declare that they have no conflict of interest.

702

703 **Acknowledgement**

704 This work was supported by the NOAA AC4 program. RJP and HB are funded via the UK National Centre
705 for Earth Observation (NCEO grant numbers: NE/R016518/1 and NE/N018079/1). RJP and HB
706 acknowledge funding from the ESA GHG-CCI and Copernicus C3S projects. We thank the Japanese
707 Aerospace Exploration Agency, National Institute for Environmental Studies, and the Ministry of

708 Environment for the GOSAT data and their continuous support as part of the Joint Research Agreement.
709 This research used the ALICE High Performance Computing Facility at the University of Leicester for
710 the GOSAT retrievals. Part of this research was carried out at the Jet Propulsion Laboratory, California
711 Institute of Technology, under a contract with the National Aeronautics and Space Administration.

712
713 We acknowledge all data providers/laboratories (<https://search.datacite.org/works/10.25925/20190108>)
714 contributed to the GLOBALVIEWplus CH₄ ObsPack v1.0 data product compiled by NOAA Global
715 Monitoring Laboratory. We acknowledge methane observations collected from the CONTRAIL
716 (Comprehensive Observation Network for TRace gases by AIrLiner) project (Machida et al., 2019). Data
717 collected at WLEF Park Falls towers were supported by the NSF DEB-0845166 and DOE Ameriflux
718 Network Management Project. Data collected at the Southern Great Plains were supported by the Office
719 of Biological and Environmental Research of the US Department of Energy under contract no. DE-AC02-
720 05CH11231 as part of the Atmospheric Radiation Measurement (ARM) Program, ARM Aerial Facility
721 (AAF), and Terrestrial Ecosystem Science (TES) Program.

722

723 Reference

- 724 Alexe, M., Bergamaschi, P., Segers, A., Detmers, R., Butz, A., Hasekamp, O., Guerlet, S., Parker, R., Boesch, H., Frankenberg,
725 C., Scheepmaker, R. A., Dlugokencky, E., Sweeney, C., Wofsy, S. C., and Kort, E. A.: Inverse modelling of CH₄ emissions
726 for 2010–2011 using different satellite retrieval products from GOSAT and SCIAMACHY, *Atmos. Chem. Phys.*, 15, 113-
727 133, <http://doi.org/10.5194/acp-15-113-2015>, 2015.
- 728 Alvarez, R. A., Zavala-Araiza, D., Lyon, D. R., Allen, D. T., Barkley, Z. R., Brandt, A. R., Davis, K. J., Herndon, S. C., Jacob,
729 D. J., Karion, A., Kort, E. A., Lamb, B. K., Lauvaux, T., Maasackers, J. D., Marchese, A. J., Omara, M., Pacala, S. W.,
730 Peischl, J., Robinson, A. L., Shepson, P. B., Sweeney, C., Townsend-Small, A., Wofsy, S. C., and Hamburg, S. P.:
731 Assessment of methane emissions from the U.S. oil and gas supply chain, *Science*, 361, 186-188,
732 <http://doi.org/10.1126/science.aar7204>, 2018.
- 733 Bergamaschi, P., Frankenberg, C., Meirink, J. F., Krol, M., Dentener, F., Wagner, T., Platt, U., Kaplan, J. O., Körner, S.,
734 Heimann, M., Dlugokencky, E. J., and Goede, A.: Satellite cartography of atmospheric methane from SCIAMACHY on
735 board ENVISAT: 2. Evaluation based on inverse model simulations, *J. Geophys. Res.*, 112,
736 <http://doi.org/10.1029/2006jd007268>, 2007.
- 737 Bergamaschi, P., Frankenberg, C., Meirink, J. F., Krol, M., Villani, M. G., Houweling, S., Dentener, F., Dlugokencky, E. J.,
738 Miller, J. B., Gatti, L. V., Engel, A., and Levin, I.: Inverse modeling of global and regional CH₄ emissions using
739 SCIAMACHY satellite retrievals, *J. Geophys. Res.*, 114, <http://doi.org/10.1029/2009jd012287>, 2009.
- 740 Bergamaschi, P., Houweling, S., Segers, A., Krol, M., Frankenberg, C., Scheepmaker, R. A., Dlugokencky, E., Wofsy, S. C.,
741 Kort, E. A., Sweeney, C., Schuck, T., Brenninkmeijer, C., Chen, H., Beck, V., and Gerbig, C.: Atmospheric CH₄ in the
742 first decade of the 21st century: Inverse modeling analysis using SCIAMACHY satellite retrievals and NOAA surface
743 measurements, *J. Geophys. Res.*, 118, 7350-7369, <http://doi.org/10.1002/jgrd.50480>, 2013.
- 744 Bey, I., Jacob, D. J., Yantosca, R. M., Logan, J. A., Field, B. D., Fiore, A. M., Li, Q., Liu, H. Y., Mickley, L. J., and Schultz,
745 M. G.: Global modeling of tropospheric chemistry with assimilated meteorology: Model description and evaluation, *J.*
746 *Geophys. Res.*, 106, 23073-23095, <http://doi.org/10.1029/2001jd000807>, 2001.
- 747 Bloom, A. A., Bowman, K. W., Lee, M., Turner, A. J., Schroeder, R., Worden, J. R., Weidner, R., McDonald, K. C., and Jacob,
748 D. J.: A global wetland methane emissions and uncertainty dataset for atmospheric chemical transport models
749 (WetCHARTs version 1.0), *Geoscientific Model Development*, 10, 2141-2156, <http://doi.org/10.5194/gmd-10-2141-2017>,
750 2017.

751 Bousquet, P., Ringeval, B., Pison, I., Dlugokencky, E. J., Brunke, E. G., Carouge, C., Chevallier, F., Fortems-Cheiney, A.,
752 Frankenberg, C., Hauglustaine, D. A., Krummel, P. B., Langenfelds, R. L., Ramonet, M., Schmidt, M., Steele, L. P., Szopa,
753 S., Yver, C., Viovy, N., and Ciais, P.: Source attribution of the changes in atmospheric methane for 2006–2008, *Atmos.*
754 *Chem. Phys.*, 11, 3689-3700, <http://doi.org/10.5194/acp-11-3689-2011>, 2011.

755 Brasseur, G. P., and Jacob, D. J.: *Modeling of Atmospheric Chemistry*, Cambridge University Press,
756 <http://doi.org/10.1017/9781316544754>, 2017.

757 Bruhwiler, L., Dlugokencky, E., Masarie, K., Ishizawa, M., Andrews, A., Miller, J., Sweeney, C., Tans, P., and Worthy, D.:
758 CarbonTracker-CH4: an assimilation system for estimating emissions of atmospheric methane, *Atmos. Chem. Phys.*, 14,
759 8269-8293, <http://doi.org/10.5194/acp-14-8269-2014>, 2014.

760 Bruhwiler, L. M., Basu, S., Bergamaschi, P., Bousquet, P., Dlugokencky, E., Houweling, S., Ishizawa, M., Kim, H. S., Locatelli,
761 R., Maksyutov, S., Montzka, S., Pandey, S., Patra, P. K., Petron, G., Saunio, M., Sweeney, C., Schwietzke, S., Tans, P.,
762 and Weatherhead, E. C.: U.S. CH₄ emissions from oil and gas production: Have recent large increases been detected?, *J.*
763 *Geophys. Res.*, 122, 4070-4083, <http://doi.org/10.1002/2016jd026157>, 2017.

764 Buchwitz, M., Reuter, M., Schneising, O., Boesch, H., Guerlet, S., Dils, B., Aben, I., Armante, R., Bergamaschi, P.,
765 Blumenstock, T., Bovensmann, H., Brunner, D., Buchmann, B., Burrows, J. P., Butz, A., Chédin, A., Chevallier, F.,
766 Crevoisier, C. D., Deutscher, N. M., Frankenberg, C., Hase, F., Hasekamp, O. P., Heymann, J., Kaminski, T., Laeng, A.,
767 Lichtenberg, G., De Mazière, M., Noël, S., Notholt, J., Orphal, J., Popp, C., Parker, R., Scholze, M., Sussmann, R., Stiller,
768 G. P., Warneke, T., Zehner, C., Bril, A., Crisp, D., Griffith, D. W. T., Kuze, A., O'Dell, C., Oshchepkov, S., Sherlock, V.,
769 Suto, H., Wennberg, P., Wunch, D., Yokota, T., and Yoshida, Y.: The Greenhouse Gas Climate Change Initiative (GHG-
770 CCI): Comparison and quality assessment of near-surface-sensitive satellite-derived CO₂ and CH₄ global data sets,
771 *Remote Sens. Environ.*, 162, 344-362, <http://doi.org/10.1016/j.rse.2013.04.024>, 2015.

772 Butz, A., Guerlet, S., Hasekamp, O., Schepers, D., Galli, A., Aben, I., Frankenberg, C., Hartmann, J. M., Tran, H., Kuze, A.,
773 Keppel-Aleks, G., Toon, G., Wunch, D., Wennberg, P., Deutscher, N., Griffith, D., Macatangay, R., Messerschmidt, J.,
774 Notholt, J., and Warneke, T.: Toward accurate CO₂ and CH₄ observations from GOSAT, *Geophys. Res. Lett.*, 38, n/a-n/a,
775 <http://doi.org/10.1029/2011gl047888>, 2011.

776 Calisesi, Y., Soebijanta, V. T., and van Oss, R.: Regridding of remote soundings: Formulation and application to ozone profile
777 comparison, *J. Geophys. Res.*, 110, <http://doi.org/10.1029/2005jd006122>, 2005.

778 Cooperative Global Atmospheric Data Integration Project: Multi-laboratory compilation of atmospheric methane data for the
779 period 1957-2017; `obspack_ch4_1_GLOBALVIEWplus_v1.0_2019_01_08`; NOAA Earth System Research Laboratory,
780 Global Monitoring Laboratory. <http://dx.doi.org/10.25925/20190108>, 2019

781 Cressot, C., Chevallier, F., Bousquet, P., Crevoisier, C., Dlugokencky, E. J., Fortems-Cheiney, A., Frankenberg, C., Parker, R.,
782 Pison, I., Scheepmaker, R. A., Montzka, S. A., Krummel, P. B., Steele, L. P., and Langenfelds, R. L.: On the consistency
783 between global and regional methane emissions inferred from SCIAMACHY, TANSO-FTS, IASI and surface
784 measurements, *Atmos. Chem. Phys.*, 14, 577-592, <http://doi.org/10.5194/acp-14-577-2014>, 2014.

785 Cui, Y. Y., Henze, D. K., Brioude, J., Angevine, W. M., Liu, Z., Bousserez, N., Guerrette, J., McKeen, S. A., Peischl, J., Yuan,
786 B., Ryerson, T., Frost, G., and Trainer, M.: Inversion Estimates of Lognormally Distributed Methane Emission Rates
787 From the Haynesville-Bossier Oil and Gas Production Region Using Airborne Measurements, *J. Geophys. Res.*, 124,
788 3520-3531, <http://doi.org/10.1029/2018jd029489>, 2019.

789 Cusworth, D. H., Jacob, D. J., Sheng, J.-X., Benmergui, J., Turner, A. J., Brandman, J., White, L., and Randles, C. A.: Detecting
790 high-emitting methane sources in oil/gas fields using satellite observations, *Atmos. Chem. Phys.*, 18, 16885-16896,
791 <http://doi.org/10.5194/acp-18-16885-2018>, 2018.

792 [Dlugokencky, E. J., Steele, L. P., Lang, P. M., and Masarie, K. A.: The growth rate and distribution of atmospheric](http://doi.org/10.1029/94jd01245)
793 [methane, *J. Geophys. Res.*, 99, 17021, <http://doi.org/10.1029/94jd01245>, 1994.](http://doi.org/10.1029/94jd01245)

794 Dlugokencky, E. J., Bruhwiler, L., White, J. W. C., Emmons, L. K., Novelli, P. C., Montzka, S. A., Masarie, K. A., Lang, P. M.,
795 Crotwell, A. M., Miller, J. B., and Gatti, L. V.: Observational constraints on recent increases in the atmospheric

796 CH₄burden, *Geophys. Res. Lett.*, 36, <http://doi.org/10.1029/2009gl039780>, 2009.

797 Etiopio, G., Ciotoli, G., Schwietzke, S., and Schoell, M.: Gridded maps of geological methane emissions and their isotopic
798 signature, *Earth System Science Data*, 11, 1-22, <http://doi.org/10.5194/essd-11-1-2019>, 2019.

799 Franco, B., Mahieu, E., Emmons, L. K., Tzompa-Sosa, Z. A., Fischer, E. V., Sudo, K., Bovy, B., Conway, S., Griffin, D.,
800 Hannigan, J. W., Strong, K., and Walker, K. A.: Evaluating ethane and methane emissions associated with the development
801 of oil and natural gas extraction in North America, *Environmental Research Letters*, 11, 044010,
802 <http://doi.org/10.1088/1748-9326/11/4/044010>, 2016.

803 Fraser, A., Palmer, P. I., Feng, L., Boesch, H., Cogan, A., Parker, R., Dlugokencky, E. J., Fraser, P. J., Krummel, P. B.,
804 Langenfelds, R. L., amp, apos, Doherty, S., Prinn, R. G., Steele, L. P., van der Schoot, M., and Weiss, R. F.: Estimating
805 regional methane surface fluxes: the relative importance of surface and GOSAT mole fraction measurements, *Atmos.*
806 *Chem. Phys.*, 13, 5697-5713, <http://doi.org/10.5194/acp-13-5697-2013>, 2013.

807 Fung, I., John, J., Lerner, J., Matthews, E., Prather, M., Steele, L. P., and Fraser, P. J.: Three-dimensional model synthesis of
808 the global methane cycle, *J. Geophys. Res.*, 96, 13033, <http://doi.org/10.1029/91jd01247>, 1991.

809 Ganesan, A. L., Rigby, M., Lunt, M. F., Parker, R. J., Boesch, H., Goulding, N., Umezawa, T., Zahn, A., Chatterjee, A., Prinn,
810 R. G., Tiwari, Y. K., van der Schoot, M., and Krummel, P. B.: Atmospheric observations show accurate reporting and little
811 growth in India's methane emissions, *Nat Commun*, 8, 836, <http://doi.org/10.1038/s41467-017-00994-7>, 2017.

812 Gelaro, R., McCarty, W., Suárez, M. J., Todling, R., Molod, A., Takacs, L., Randles, C. A., Darmenov, A., Bosilovich, M. G.,
813 Reichle, R., Wargan, K., Coy, L., Cullather, R., Draper, C., Akella, S., Buchard, V., Conaty, A., da Silva, A. M., Gu, W.,
814 Kim, G.-K., Koster, R., Lucchesi, R., Merkova, D., Nielsen, J. E., Partyka, G., Pawson, S., Putman, W., Rienecker, M.,
815 Schubert, S. D., Sienkiewicz, M., and Zhao, B.: The Modern-Era Retrospective Analysis for Research and Applications,
816 Version 2 (MERRA-2), *J. Clim.*, 30, 5419-5454, <http://doi.org/10.1175/jcli-d-16-0758.1>, 2017.

817 Hausmann, P., Sussmann, R., and Smale, D.: Contribution of oil and natural gas production to renewed increase in atmospheric
818 methane (2007–2014): top–down estimate from ethane and methane column observations, *Atmos. Chem. Phys.*, 16, 3227-
819 3244, <http://doi.org/10.5194/acp-16-3227-2016>, 2016.

820 Heald, C. L., Jacob, D. J., Jones, D. B. A., Palmer, P. I., Logan, J. A., Streets, D. G., Sachse, G. W., Gille, J. C., Hoffman, R.
821 N., and Nehr Korn, T.: Comparative inverse analysis of satellite (MOPITT) and aircraft (TRACE-P) observations to
822 estimate Asian sources of carbon monoxide, *J. Geophys. Res.*, 109, <http://doi.org/10.1029/2004jd005185>, 2004.

823 Helmig, D., Rossabi, S., Hueber, J., Tans, P., Montzka, S. A., Masarie, K., Thoning, K., Plass-Duelmer, C., Claude, A.,
824 Carpenter, L. J., Lewis, A. C., Punjabi, S., Reimann, S., Vollmer, M. K., Steinbrecher, R., Hannigan, J. W., Emmons, L.
825 K., Mahieu, E., Franco, B., Smale, D., and Pozzer, A.: Reversal of global atmospheric ethane and propane trends largely
826 due to US oil and natural gas production, *Nature Geosci.*, 9, 490-495, <http://doi.org/10.1038/ngeo2721>, 2016.

827 Hmiel, B., Petrenko, V. V., Dyonisius, M. N., Buizert, C., Smith, A. M., Place, P. F., Harth, C., Beaudette, R., Hua, Q., Yang,
828 B., Vimont, I., Michel, S. E., Severinghaus, J. P., Etheridge, D., Bromley, T., Schmitt, J., Fäin, X., Weiss, R. F., and
829 Dlugokencky, E.: Preindustrial 14CH₄ indicates greater anthropogenic fossil CH₄ emissions, *Nature*, 578, 409-412,
830 <http://doi.org/10.1038/s41586-020-1991-8>, 2020.

831 Holmes, C. D., Prather, M. J., Søvde, O. A., and Myhre, G.: Future methane, hydroxyl, and their uncertainties: key climate and
832 emission parameters for future predictions, *Atmos. Chem. Phys.*, 13, 285-302, <http://doi.org/10.5194/acp-13-285-2013>,
833 2013.

834 Houweling, S., Krol, M., Bergamaschi, P., Frankenberg, C., Dlugokencky, E. J., Morino, I., Notholt, J., Sherlock, V., Wunch,
835 D., Beck, V., Gerbig, C., Chen, H., Kort, E. A., Röckmann, T., and Aben, I.: A multi-year methane inversion using
836 SCIAMACHY, accounting for systematic errors using TCCON measurements, *Atmos. Chem. Phys.*, 14, 3991-4012,
837 <http://doi.org/10.5194/acp-14-3991-2014>, 2014.

838 Houweling, S., Bergamaschi, P., Chevallier, F., Heimann, M., Kaminski, T., Krol, M., Michalak, A. M., and Patra, P.: Global
839 inverse modeling of CH₄ sources and sinks: an overview of methods, *Atmos. Chem. Phys.*, 17, 235-256,
840 <http://doi.org/10.5194/acp-17-235-2017>, 2017.

841 Hu, H., Landgraf, J., Detmers, R., Borsdorff, T., Aan de Brugh, J., Aben, I., Butz, A., and Hasekamp, O.: Toward Global
842 Mapping of Methane With TROPOMI: First Results and Intersatellite Comparison to GOSAT, *Geophys. Res. Lett.*, 45,
843 3682-3689, <http://doi.org/10.1002/2018gl077259>, 2018.

844 Jacob, D. J., Turner, A. J., Maasakkers, J. D., Sheng, J., Sun, K., Liu, X., Chance, K., Aben, I., McKeever, J., and Frankenberg,
845 C.: Satellite observations of atmospheric methane and their value for quantifying methane emissions, *Atmos. Chem. Phys.*,
846 16, 14371-14396, <http://doi.org/10.5194/acp-16-14371-2016>, 2016.

847 Janardanan, R., Maksyutov, S., Tsuruta, A., Wang, F., Tiwari, Y. K., Valsala, V., Ito, A., Yoshida, Y., Kaiser, J. W., Janssens-
848 Maenhout, G., Arshinov, M., Sasakawa, M., Tohjima, Y., Worthy, D. E. J., Dlugokencky, E. J., Ramonet, M., Arduini, J.,
849 Lavric, J. V., Piacentino, S., Krummel, P. B., Langenfelds, R. L., Mammarella, I., and Matsunaga, T.: Country-Scale
850 Analysis of Methane Emissions with a High-Resolution Inverse Model Using GOSAT and Surface Observations, *Remote
851 Sensing*, 12, 375, <http://doi.org/10.3390/rs12030375>, 2020.

852 Janssens-Maenhout, G., Crippa, M., Guizzardi, D., Muntean, M., Schaaf, E., Dentener, F., Bergamaschi, P., Pagliari, V., Olivier,
853 J. G. J., Peters, J. A. H. W., van Aardenne, J. A., Monni, S., Doering, U., Petrescu, A. M. R., Solazzo, E., and Oreggioni,
854 G. D.: EDGAR v4.3.2 Global Atlas of the three major greenhouse gas emissions for the period 1970–2012, *Earth System
855 Science Data*, 11, 959-1002, <http://doi.org/10.5194/essd-11-959-2019>, 2019.

856 Koo, J.-H., Walker, K. A., Jones, A., Sheese, P. E., Boone, C. D., Bernath, P. F., and Manney, G. L.: Global climatology based
857 on the ACE-FTS version 3.5 dataset: Addition of mesospheric levels and carbon-containing species in the UTLS, *J. Quant.
858 Spectrosc. Radiat. Transfer*, 186, 52-62, <http://doi.org/10.1016/j.jqsrt.2016.07.003>, 2017.

859 Kuze, A., Suto, H., Shiomi, K., Kawakami, S., Tanaka, M., Ueda, Y., Deguchi, A., Yoshida, J., Yamamoto, Y., Kataoka, F.,
860 Taylor, T. E., and Buijs, H. L.: Update on GOSAT TANSO-FTS performance, operations, and data products after more
861 than 6 years in space, *Atmospheric Measurement Techniques*, 9, 2445-2461, <http://doi.org/10.5194/amt-9-2445-2016>,
862 2016.

863 Lan, X., Tans, P., Sweeney, C., Andrews, A., Dlugokencky, E., Schwietzke, S., Kofler, J., McKain, K., Thoning, K., Crotwell,
864 M., Montzka, S., Miller, B. R., and Biraud, S. C.: Long-Term Measurements Show Little Evidence for Large Increases in
865 Total U.S. Methane Emissions Over the Past Decade, *Geophys. Res. Lett.*, 46, 4991-4999,
866 <http://doi.org/10.1029/2018gl081731>, 2019.

867 Lunt, M. F., Palmer, P. I., Feng, L., Taylor, C. M., Boesch, H., and Parker, R. J.: An increase in methane emissions from tropical
868 Africa between 2010 and 2016 inferred from satellite data, *Atmos. Chem. Phys.*, 19, 14721-14740,
869 <http://doi.org/10.5194/acp-19-14721-2019>, 2019.

870 Maasakkers, J. D., Jacob, D. J., Sulprizio, M. P., Turner, A. J., Weitz, M., Wirth, T., Hight, C., DeFigueiredo, M., Desai, M.,
871 Schmeltz, R., Hockstad, L., Bloom, A. A., Bowman, K. W., Jeong, S., and Fischer, M. L.: Gridded National Inventory of
872 U.S. Methane Emissions, *Environ. Sci. Technol.*, 50, 13123-13133, <http://doi.org/10.1021/acs.est.6b02878>, 2016.

873 Maasakkers, J. D., Jacob, D. J., Sulprizio, M. P., Scarpelli, T. R., Nesser, H., Sheng, J.-X., Zhang, Y., Hersher, M., Bloom, A.
874 A., Bowman, K. W., Worden, J. R., Janssens-Maenhout, G., and Parker, R. J.: Global distribution of methane emissions,
875 emission trends, and OH concentrations and trends inferred from an inversion of GOSAT satellite data for 2010–2015,
876 *Atmos. Chem. Phys.*, 19, 7859-7881, <http://doi.org/10.5194/acp-19-7859-2019>, 2019.

877 ~~Maasakkers, J. D., Jacob, D. J., Sulprizio, M. P., Scarpelli, T. R., Nesser, H., Sheng, J.-X., Zhang, Y., Lu, X., Bloom, A. A.,
878 Bowman, K. W., Worden, J. R., and Parker, R. J.: 2010–2015 North American methane emissions, sectoral contributions,
879 and trends: a high resolution inversion of GOSAT satellite observations of atmospheric methane, submitted to *Atmos.
880 Chem. Phys.*, file available at <http://acmg.seas.harvard.edu/publications/2020/maasakkers2020.pdf>.~~

881 ~~Maasakkers, J. D., Jacob, D. J., Sulprizio, M. P., Scarpelli, T. R., Nesser, H., Sheng, J., Zhang, Y., Lu, X., Bloom, A. A.,
882 Bowman, K. W., Worden, J. R., and Parker, R. J.: 2010–2015 North American methane emissions, sectoral contributions,
883 and trends: a high-resolution inversion of GOSAT satellite observations of atmospheric methane, *Atmos. Chem. Phys.
884 Discuss.*, <https://doi.org/10.5194/acp-2020-915>, in review, 2020.~~

885 Machida T., H. Matsueda, Y. Sawa and Y. Niwa, Atmospheric trace gas data from the CONTRAIL flask air sampling over the

886 Pacific Ocean, Center for Global Environmental Research, NIES, DOI:10.17595/20190828.001., 2019

887 McNorton, J., Wilson, C., Gloor, M., Parker, R. J., Boesch, H., Feng, W., Hossaini, R., and Chipperfield, M. P.: Attribution of
888 recent increases in atmospheric methane through 3-D inverse modelling, *Atmos. Chem. Phys.*, 18, 18149-18168,
889 <http://doi.org/10.5194/acp-18-18149-2018>, 2018.

890 Miller, S. M., Wofsy, S. C., Michalak, A. M., Kort, E. A., Andrews, A. E., Biraud, S. C., Dlugokencky, E. J., Eluszkiewicz, J.,
891 Fischer, M. L., Janssens-Maenhout, G., Miller, B. R., Miller, J. B., Montzka, S. A., Nehrkorn, T., and Sweeney, C.:
892 Anthropogenic emissions of methane in the United States, *Proc. Natl. Acad. Sci. U. S. A.*, 110, 20018-20022,
893 <http://doi.org/10.1073/pnas.1314392110>, 2013.

894 Miller, S. M., Michalak, A. M., Detmers, R. G., Hasekamp, O. P., Bruhwiler, L. M. P., and Schwietzke, S.: China's coal mine
895 methane regulations have not curbed growing emissions, *Nat Commun*, 10, 303, <http://doi.org/10.1038/s41467-018-07891-7>, 2019.

897 Monteil, G., Houweling, S., Butz, A., Guerlet, S., Schepers, D., Hasekamp, O., Frankenberg, C., Scheepmaker, R., Aben, I.,
898 and Röckmann, T.: Comparison of CH₄ inversions based on 15 months of GOSAT and SCIAMACHY observations, *J.*
899 *Geophys. Res.*, 118, 11,807-811,823, <http://doi.org/10.1002/2013jd019760>, 2013.

900 Murguia-Flores, F., Arndt, S., Ganesan, A. L., Murray-Tortarolo, G., and Hornibrook, E. R. C.: Soil Methanotrophy Model
901 (MeMo v1.0): a process-based model to quantify global uptake of atmospheric methane by soil, *Geoscientific Model*
902 *Development*, 11, 2009-2032, <http://doi.org/10.5194/gmd-11-2009-2018>, 2018.

903 Murray, L. T., Jacob, D. J., Logan, J. A., Hudman, R. C., and Koshak, W. J.: Optimized regional and interannual variability of
904 lightning in a global chemical transport model constrained by LIS/OTD satellite data, *J. Geophys. Res.*, 117, D20307,
905 <http://doi.org/10.1029/2012jd017934>, 2012.

906 Naik, V., Voulgarakis, A., Fiore, A. M., Horowitz, L. W., Lamarque, J. F., Lin, M., Prather, M. J., Young, P. J., Bergmann, D.,
907 Cameron-Smith, P. J., Cionni, I., Collins, W. J., Dalsøren, S. B., Doherty, R., Eyring, V., Faluvegi, G., Folberth, G. A.,
908 Josse, B., Lee, Y. H., MacKenzie, I. A., Nagashima, T., van Noije, T. P. C., Plummer, D. A., Righi, M., Rumbold, S. T.,
909 Skeie, R., Shindell, D. T., Stevenson, D. S., Strode, S., Sudo, K., Szopa, S., and Zeng, G.: Preindustrial to present-day
910 changes in tropospheric hydroxyl radical and methane lifetime from the Atmospheric Chemistry and Climate Model
911 Intercomparison Project (ACCMIP), *Atmos. Chem. Phys.*, 13, 5277-5298, <http://doi.org/10.5194/acp-13-5277-2013>,
912 2013.

913 ~~Parker, R. J., Webb, A., Boesch, H., Somkuti, P., Barrio Guillo, R., Di Noia, A., Kalaitzi, N., Anand, J., Bergamaschi, P.,
914 Chevallier, F., Palmer, P. I., Feng, L., Deutscher, N. M., Feist, D. G., Griffith, D. W. T., Hase, F., Kivi, R., Morino, I.,
915 Notholt, J., Oh, Y. S., Ohyama, H., Petri, C., Pollard, D. F., Roehl, C., Sha, M. K., Shiomi, K., Strong, K., Sussmann, R.,
916 Té, Y., Velazco, V. A., Warneke, T., Wennberg, P. O., and Wunch, D.: A Decade of GOSAT Proxy Satellite
917 CH₄ Observations, *Earth Syst. Sci. Data Discuss.*, <https://doi.org/10.5194/essd-2020-114>, in review, 2020.~~

918 ~~Parker, R. J., Webb, A., Boesch, H., Somkuti, P., Barrio Guillo, R., Di Noia, A., Kalaitzi, N., Anand, J. S., Bergamaschi, P.,
919 Chevallier, F., Palmer, P. I., Feng, L., Deutscher, N. M., Feist, D. G., Griffith, D. W. T., Hase, F., Kivi, R., Morino, I.,
920 Notholt, J., Oh, Y.-S., Ohyama, H., Petri, C., Pollard, D. F., Roehl, C., Sha, M. K., Shiomi, K., Strong, K., Sussmann, R.,
921 Té, Y., Velazco, V. A., Warneke, T., Wennberg, P. O., and Wunch, D.: A decade of GOSAT Proxy satellite CH₄ observations,
922 *Earth Syst. Sci. Data*, 12, 3383–3412, <https://doi.org/10.5194/essd-12-3383-2020>, 2020.~~

923 Patra, P. K., Houweling, S., Krol, M., Bousquet, P., Belikov, D., Bergmann, D., Bian, H., Cameron-Smith, P., Chipperfield, M.
924 P., Corbin, K., Fortems-Cheiney, A., Fraser, A., Gloor, E., Hess, P., Ito, A., Kawa, S. R., Law, R. M., Loh, Z., Maksyutov,
925 S., Meng, L., Palmer, P. I., Prinn, R. G., Rigby, M., Saito, R., and Wilson, C.: TransCom model simulations of CH₄ and
926 related species: linking transport, surface flux and chemical loss with CH₄ variability in the troposphere and lower
927 stratosphere, *Atmos. Chem. Phys.*, 11, 12813-12837, <http://doi.org/10.5194/acp-11-12813-2011>, 2011.

928 Patra, P. K., Krol, M. C., Montzka, S. A., Arnold, T., Atlas, E. L., Lintner, B. R., Stephens, B. B., Xiang, B., Elkins, J. W.,
929 Fraser, P. J., Ghosh, A., Hints, E. J., Hurst, D. F., Ishijima, K., Krummel, P. B., Miller, B. R., Miyazaki, K., Moore, F. L.,
930 Muhle, J., O'Doherty, S., Prinn, R. G., Steele, L. P., Takigawa, M., Wang, H. J., Weiss, R. F., Wofsy, S. C., and Young, D.:

931 Observational evidence for interhemispheric hydroxyl-radical parity, *Nature*, 513, 219-223,
932 <http://doi.org/10.1038/nature13721>, 2014.

933 Patra, P. K., Saeki, T., Dlugokencky, E. J., Ishijima, K., Umezawa, T., Ito, A., Aoki, S., Morimoto, S., Kort, E. A., Crotwell,
934 A., Ravi Kumar, K., and Nakazawa, T.: Regional Methane Emission Estimation Based on Observed Atmospheric
935 Concentrations (2002-2012), *Journal of the Meteorological Society of Japan. Ser. II*, 94, 91-113,
936 <http://doi.org/10.2151/jmsj.2016-006>, 2016.

937 Pickett-Heaps, C. A., Jacob, D. J., Wecht, K. J., Kort, E. A., Wofsy, S. C., Diskin, G. S., Worthy, D. E. J., Kaplan, J. O., Bey,
938 I., and Drevet, J.: Magnitude and seasonality of wetland methane emissions from the Hudson Bay Lowlands (Canada),
939 *Atmos. Chem. Phys.*, 11, 3773-3779, <http://doi.org/10.5194/acp-11-3773-2011>, 2011.

940 Pison, I., Bousquet, P., Chevallier, F., Szopa, S., and Hauglustaine, D.: Multi-species inversion of CH₄, CO and H₂ emissions
941 from surface measurements, *Atmos. Chem. Phys.*, 9, 5281-5297, <http://doi.org/10.5194/acp-9-5281-2009>, 2009.

942 Prather, M. J., Holmes, C. D., and Hsu, J.: Reactive greenhouse gas scenarios: Systematic exploration of uncertainties and the
943 role of atmospheric chemistry, *Geophys. Res. Lett.*, 39, n/a-n/a, <http://doi.org/10.1029/2012gl051440>, 2012.

944 Rodgers, C. D.: *Inverse Methods for Atmospheric Sounding: Theory and Practice*, 2000.

945 Saunio, M., Stavert, A. R., Poulter, B., Bousquet, P., Canadell, J. G., Jackson, R. B., Raymond, P. A., Dlugokencky, E. J.,
946 Houweling, S., Patra, P. K., Ciais, P., Arora, V. K., Bastviken, D., Bergamaschi, P., Blake, D. R., Brailsford, G., Bruhwiler,
947 L., Carlson, K. M., Carrol, M., Castaldi, S., Chandra, N., Crevoisier, C., Crill, P. M., Covey, K., Curry, C. L., Etiope, G.,
948 Frankenberg, C., Gedney, N., Hegglin, M. I., Höglund-Isaksson, L., Hugelius, G., Ishizawa, M., Ito, A., Janssens-
949 Maenhout, G., Jensen, K. M., Joos, F., Kleinen, T., Krummel, P. B., Langenfelds, R. L., Laruelle, G. G., Liu, L., Machida,
950 T., Maksyutov, S., McDonald, K. C., McNorton, J., Miller, P. A., Melton, J. R., Morino, I., Müller, J., Murguia-Flores, F.,
951 Naik, V., Niwa, Y., Noce, S., O'Doherty, S., Parker, R. J., Peng, C., Peng, S., Peters, G. P., Prigent, C., Prinn, R., Ramonet,
952 M., Regnier, P., Riley, W. J., Rosentreter, J. A., Segers, A., Simpson, I. J., Shi, H., Smith, S. J., Steele, L. P., Thornton, B.
953 F., Tian, H., Tohjima, Y., Tubiello, F. N., Tsuruta, A., Viovy, N., Voulgarakis, A., Weber, T. S., van Weele, M., van der
954 Werf, G. R., Weiss, R. F., Worthy, D., Wunch, D., Yin, Y., Yoshida, Y., Zhang, W., Zhang, Z., Zhao, Y., Zheng, B., Zhu,
955 Q., Zhu, Q., and Zhuang, Q.: The Global Methane Budget 2000–2017, *Earth System Science Data*, 12, 1561-1623,
956 <http://doi.org/10.5194/essd-12-1561-2020>, 2020.

957 Scarpelli, T. R., Jacob, D. J., Maasakkers, J. D., Sulprizio, M. P., Sheng, J.-X., Rose, K., Romeo, L., Worden, J. R., and
958 Janssens-Maenhout, G.: A global gridded (0.1° x 0.1°) inventory of methane emissions from oil, gas, and coal
959 exploitation based on national reports to the United Nations Framework Convention on Climate Change, *Earth System*
960 *Science Data*, 12, 563-575, <http://doi.org/10.5194/essd-12-563-2020>, 2020.

961 Sheng, J.-X., Jacob, D. J., Turner, A. J., Maasakkers, J. D., Sulprizio, M. P., Bloom, A. A., Andrews, A. E., and Wunch, D.:
962 High-resolution inversion of methane emissions in the Southeast US using SEAC<sup>4</sup></sup>RS aircraft
963 observations of atmospheric methane: anthropogenic and wetland sources, *Atmos. Chem. Phys.*, 18, 6483-6491,
964 <http://doi.org/10.5194/acp-18-6483-2018>, 2018.

965 Sheng, J., Song, S., Zhang, Y., Prinn, R. G., and Janssens-Maenhout, G.: Bottom-Up Estimates of Coal Mine Methane
966 Emissions in China: A Gridded Inventory, Emission Factors, and Trends, *Environmental Science & Technology Letters*,
967 6, 473-478, <http://doi.org/10.1021/acs.estlett.9b00294>, 2019.

968 [Stanevich, I., Jones, D. B. A., Strong, K., Parker, R. J., Boesch, H., Wunch, D., Notholt, J., Petri, C., Warneke, T., Sussmann,](#)
969 [R., Schneider, M., Hase, F., Kivi, R., Deutscher, N. M., Velazco, V. A., Walker, K. A., and Deng, F.: Characterizing model](#)
970 [errors in chemical transport modeling of methane: impact of model resolution in versions v9-02 of GEOS-Chem and v35j](#)
971 [of its adjoint model, *Geosci. Model Dev.*, 13, 3839–3862, <https://doi.org/10.5194/gmd-13-3839-2020>, 2020.](#)

972 Thompson, R. L., Stohl, A., Zhou, L. X., Dlugokencky, E., Fukuyama, Y., Tohjima, Y., Kim, S. Y., Lee, H., Nisbet, E. G.,
973 Fisher, R. E., Lowry, D., Weiss, R. F., Prinn, R. G., O'Doherty, S., Young, D., and White, J. W. C.: Methane emissions in
974 East Asia for 2000-2011 estimated using an atmospheric Bayesian inversion, *J. Geophys. Res.*, 120, 4352-4369,
975 <http://doi.org/10.1002/2014jd022394>, 2015.

- 976 Turner, A. J., Jacob, D. J., Wecht, K. J., Maasakkers, J. D., Lundgren, E., Andrews, A. E., Biraud, S. C., Boesch, H., Bowman,
977 K. W., Deutscher, N. M., Dubey, M. K., Griffith, D. W. T., Hase, F., Kuze, A., Notholt, J., Ohyama, H., Parker, R., Payne,
978 V. H., Sussmann, R., Sweeney, C., Velasco, V. A., Warneke, T., Wennberg, P. O., and Wunch, D.: Estimating global and
979 North American methane emissions with high spatial resolution using GOSAT satellite data, *Atmos. Chem. Phys.*, 15,
980 7049-7069, <http://doi.org/10.5194/acp-15-7049-2015>, 2015.
- 981 van der Werf, G. R., Randerson, J. T., Giglio, L., van Leeuwen, T. T., Chen, Y., Rogers, B. M., Mu, M., van Marle, M. J. E.,
982 Morton, D. C., Collatz, G. J., Yokelson, R. J., and Kasibhatla, P. S.: Global fire emissions estimates during 1997–2016,
983 *Earth System Science Data*, 9, 697-720, <http://doi.org/10.5194/essd-9-697-2017>, 2017.
- 984 Wang, X., Jacob, D. J., Eastham, S. D., Sulprizio, M. P., Zhu, L., Chen, Q., Alexander, B., Sherwen, T., Evans, M. J., Lee, B.
985 H., Haskins, J. D., Lopez-Hilfiker, F. D., Thornton, J. A., Huey, G. L., and Liao, H.: The role of chlorine in global
986 tropospheric chemistry, *Atmos. Chem. Phys.*, 19, 3981-4003, <http://doi.org/10.5194/acp-19-3981-2019>, 2019.
- 987 Waymark, C., Walker, K., Boone, C. D., and Bernath, P. F.: ACE-FTS version 3.0 data set: validation and data processing
988 update, *ANNALS OF GEOPHYSICS*, 56, <http://doi.org/10.4401/ag-6339>, 2013.
- 989 Wecht, K. J., Jacob, D. J., Frankenberg, C., Jiang, Z., and Blake, D. R.: Mapping of North American methane emissions with
990 high spatial resolution by inversion of SCIAMACHY satellite data, *J. Geophys. Res.*, 119, 7741-7756,
991 <http://doi.org/10.1002/2014jd021551>, 2014.
- 992 Zhang, B., Tian, H., Ren, W., Tao, B., Lu, C., Yang, J., Banger, K., and Pan, S.: Methane emissions from global rice fields:
993 Magnitude, spatiotemporal patterns, and environmental controls, *Global Biogeochem. Cycles*, 30, 1246-1263,
994 <http://doi.org/10.1002/2016gb005381>, 2016.
- 995 Zhang, Y., Jacob, D. J., Maasakkers, J. D., Sulprizio, M. P., Sheng, J.-X., Gautam, R., and Worden, J.: Monitoring global
996 tropospheric OH concentrations using satellite observations of atmospheric methane, *Atmos. Chem. Phys.*, 18, 15959-
997 15973, <http://doi.org/10.5194/acp-18-15959-2018>, 2018.
- 998 Zhang, Y., Jacob, D. J., Lu, X., Maasakkers, J. D., Scarpelli, T. R., Sheng, J.-X., Shen, L., Qu, Z., Sulprizio, M. P., Chang, J.,
999 Bloom, A. A., Ma, S., Worden, J., Parker, R. J., and Boesch, H.: Attribution of the accelerating increase in atmospheric
1000 methane during 2010–2018 by inverse analysis of GOSAT observations, *Atmos. Chem. Phys. Discuss.*,
1001 <https://doi.org/10.5194/acp-2020-964>, in review, 2020.
- 1002 ~~Zhang, Y., Jacob, D., Scarpelli, T., Maasakkers, J. D., Sulprizio, M., Penn, E., Sheng, J. X., Bloom, A. A., and Worden, J.:~~
1003 ~~Attribution of the 2010–2017 trend in atmospheric methane by improved inverse analysis of GOSAT satellite observations,~~
1004 ~~AGU Fall meeting, 2019 (submitted to *Atmos. Chem. Phys.*, file available at~~
1005 ~~http://acmg.seas.harvard.edu/publications/2020/zhang_yuzhong2020ACP.pdf)~~
- 1006 Zhang, Y., Gautam, R., Pandey, S., Omara, M., Maasakkers, J. D., Sadavarte, P., Lyon, D., Nesser, H., Sulprizio, M. P., Varon,
1007 D. J., Zhang, R., Houweling, S., Zavala-Araiza, D., Alvarez, R. A., Lorente, A., Hamburg, S. P., Aben, I., and Jacob, D.
1008 J.: Quantifying methane emissions from the largest oil-producing basin in the United States from space, *Science Advances*,
1009 6, eaaz5120, <http://doi.org/10.1126/sciadv.aaz5120>, 2020.
- 1010 Zhao, Y., Saunio, M., Bousquet, P., Lin, X., Berchet, A., Hegglin, M. I., Canadell, J. G., Jackson, R. B., Hauglustaine, D. A.,
1011 Szopa, S., Stavert, A. R., Abraham, N. L., Archibald, A. T., Bekki, S., Deushi, M., Jöckel, P., Josse, B., Kinnison, D.,
1012 Kirner, O., Marécal, V., and Connor, F. M., Plummer, D. A., Revell, L. E., Rozanov, E., Stenke, A., Strode, S.,
1013 Tilmes, S., Dlugokencky, E. J., and Zheng, B.: Inter-model comparison of global hydroxyl radical (OH) distributions and
1014 their impact on atmospheric methane over the 2000–2016 period, *Atmos. Chem. Phys.*, 19, 13701-13723,
1015 <http://doi.org/10.5194/acp-19-13701-2019>, 2019.
- 1016 Zona, D., Gioli, B., Commane, R., Lindaas, J., Wofsy, S. C., Miller, C. E., Dinardo, S. J., Dengel, S., Sweeney, C., Karion, A.,
1017 Chang, R. Y., Henderson, J. M., Murphy, P. C., Goodrich, J. P., Moreaux, V., Liljedahl, A., Watts, J. D., Kimball, J. S.,
1018 Lipson, D. A., and Oechel, W. C.: Cold season emissions dominate the Arctic tundra methane budget, *Proc. Natl. Acad.*
1019 *Sci. U. S. A.*, 113, 40-45, <http://doi.org/10.1073/pnas.1516017113>, 2016.

1021

Table 1. Global sources and sinks of atmospheric methane, 2010-2017^a.

	Prior ^b	Posterior ^c
Total sources [Tg a⁻¹]	533	551
Natural Sources		
Wetlands	161	148
Open fires	14	16
Termites	12	14
Seeps	2	2
Anthropogenic sources		
Livestock	117	136
Oil	42	40
Natural gas	25	30
Coal mining	31	23
Rice cultivation	38	44
Wastewater	37	42
Landfills	30	31
Other Anthropogenic	25	25
Total Sinks [Tg a⁻¹]	540	528 <u>529</u>
Tropospheric OH	468	455 <u>456</u>
Stratospheric loss ^d	33	33
Soil uptake ^d	34	34
Tropospheric Cl ^d	5	5

1022

^a 8-year mean values for 2010-2017.

1023

^b Prior natural source estimates (2000-2017 means) are from Bloom et al. (2017) for wetlands, Etiope et al. (2019) and Hmiel et al. (2020) for seeps, Fung et al. (1991) for termite emissions, van der Werf et al. (2017) for open fire emissions. Prior anthropogenic source estimates for 2012 are from EDGAR v4.3.2 (Janssens-Maenhout et al., 2017) except from Scarpelli et al. (2020) for fuel exploitation (oil, gas, coal), and are overwritten for the US with the gridded EPA inventory of Maasakkers et al. (2016). The prior tropospheric OH concentration field is from Wecht et al. (2014) and yields a methane lifetime against oxidation by tropospheric OH of 10.6 years.

1024

1025

1026

1027

1028

1029

^c From the joint inversion of GOSAT and in situ data

1030

^d These minor sinks are not optimized by the inversion.

1031

1032

Table 2. Anthropogenic methane emissions and trends, 2010-2017 ^a

Inversions	In-situ-only inversion	GOSAT-only inversion	GOSAT+in situ inversion
US ^b (prior: 28 Tg a ⁻¹)			
Posterior (Tg a ⁻¹)	35	31	36
2010-2017 trend (Tg a ⁻¹ a ⁻¹)	0.5	-0.1	0.4
Canada (prior: 5 Tg a ⁻¹)			
Posterior (Tg a ⁻¹)	8	5	8
2010-2017 trend (Tg a ⁻¹ a ⁻¹)	-0.2	-0.0	-0.2
Europe ^c (prior: 27 Tg a ⁻¹)			
Posterior (Tg a ⁻¹)	28	17	23
2010-2017 trend (Tg a ⁻¹ a ⁻¹)	0.1	-0.6	-0.4
China (prior: 63 Tg a ⁻¹)			
Posterior (Tg a ⁻¹)	45	46	43
2010-2017 trend (Tg a ⁻¹ a ⁻¹)	0.3	0.4	0.1

1033

^a Posterior estimates of mean 2010-2017 emissions and trends for the In-situ-only, GOSAT-only, and GOSAT + in situ joint inversions.

1034

1035

^b Including contiguous US and Alaska.

1036

^c Europe is defined as west of 30°E, excluding Russia.

1037

1038

1039

Table 3. Optimized global methane budget, 2010-2017.

Inversions	<u>In-situ-only</u> <u>inversion</u>	<u>GOSAT-only</u> <u>inversion</u>	<u>GOSAT+in situ</u> <u>inversion</u>
Total sources [Tg a⁻¹]	515±4 ^d	504±3 ^d	551±2 ^d
Anthropogenic ^a	359	333	371
Seeps, termites	15	15	16
Open fires	15	16	16
Wetlands	126	140	148
Total sinks [Tg a⁻¹]	<u>496494±4^e</u>	<u>480478±3^e</u>	<u>529528±2^e</u>
Tropospheric OH ^b	<u>421423</u>	<u>406408</u>	<u>456455</u>
Other losses ^c	73	72	73
Mean imbalance [Tg a⁻¹]	<u>2119</u>	<u>2624</u>	<u>2322</u>

^a See Table 1 for sectoral breakdown from the joint inversion.

^b Methane lifetime against oxidation by tropospheric OH is 11.2±0.1 years in the GOSAT + in situ inversion.

^c Soils, stratosphere, and oxidation by tropospheric Cl.

^d ~~Error standard deviation estimated from the quadrature of error variance of non-wetland emissions and wetland emissions.~~

^e ~~Error standard deviation only accounts for the uncertainty in oxidation by tropospheric OH.~~

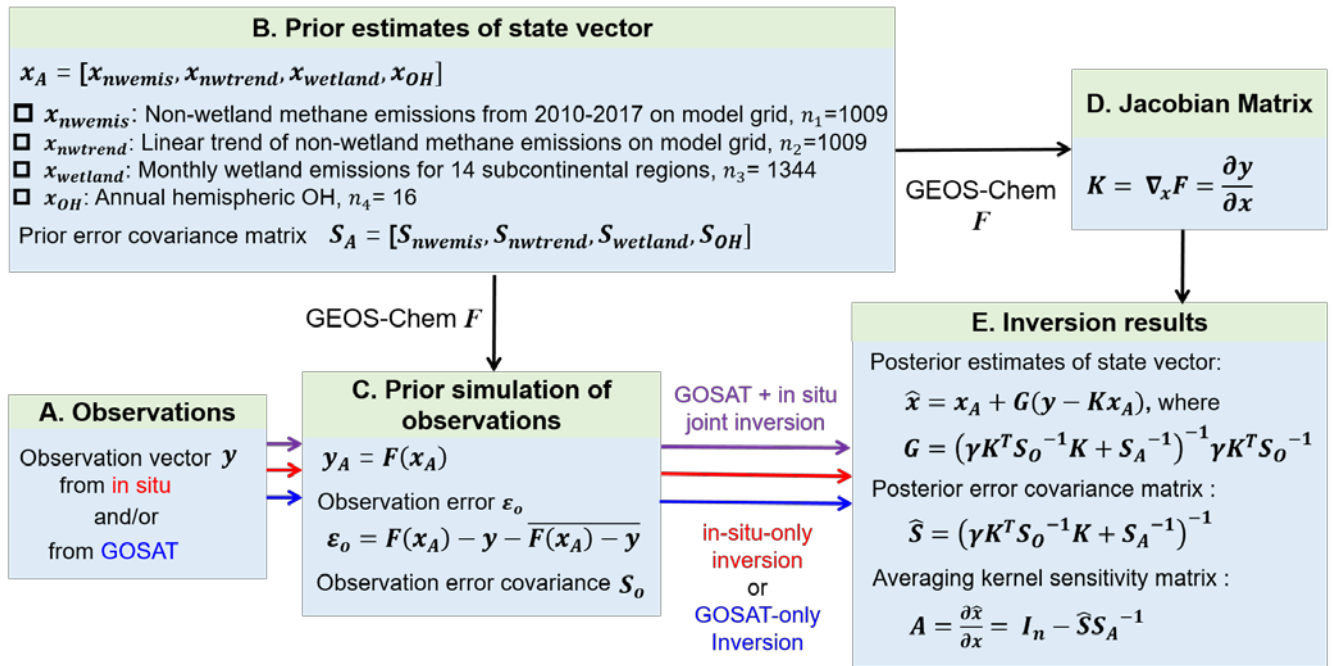


Figure 1. Analytical inversion framework. The inversion is applied to GOSAT and GLOBALVIEWplus in situ observations for 2010-2017. GEOS-Chem is the chemical transport model (CTM) used as forward model for the inversion. γ is a regularization factor in the Bayesian cost function (see text).

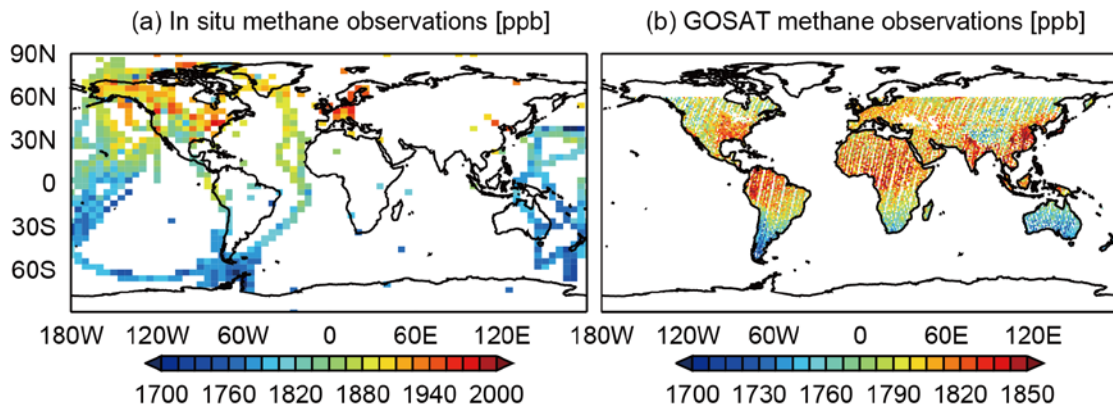
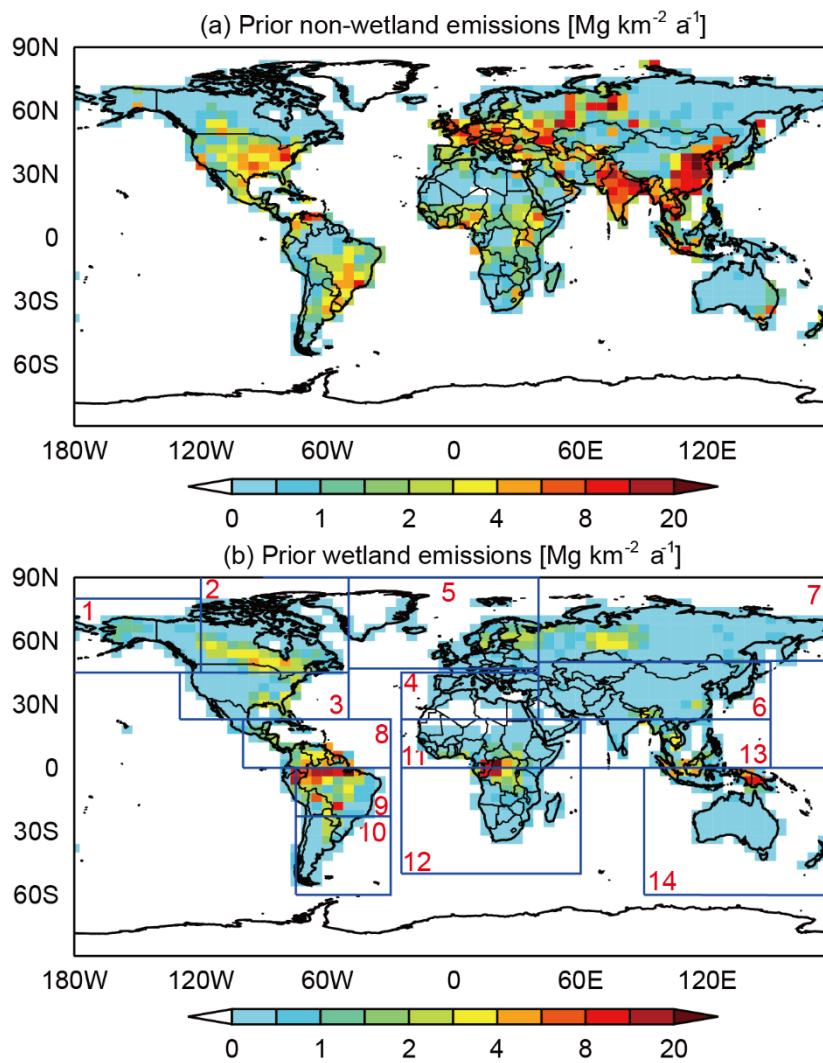


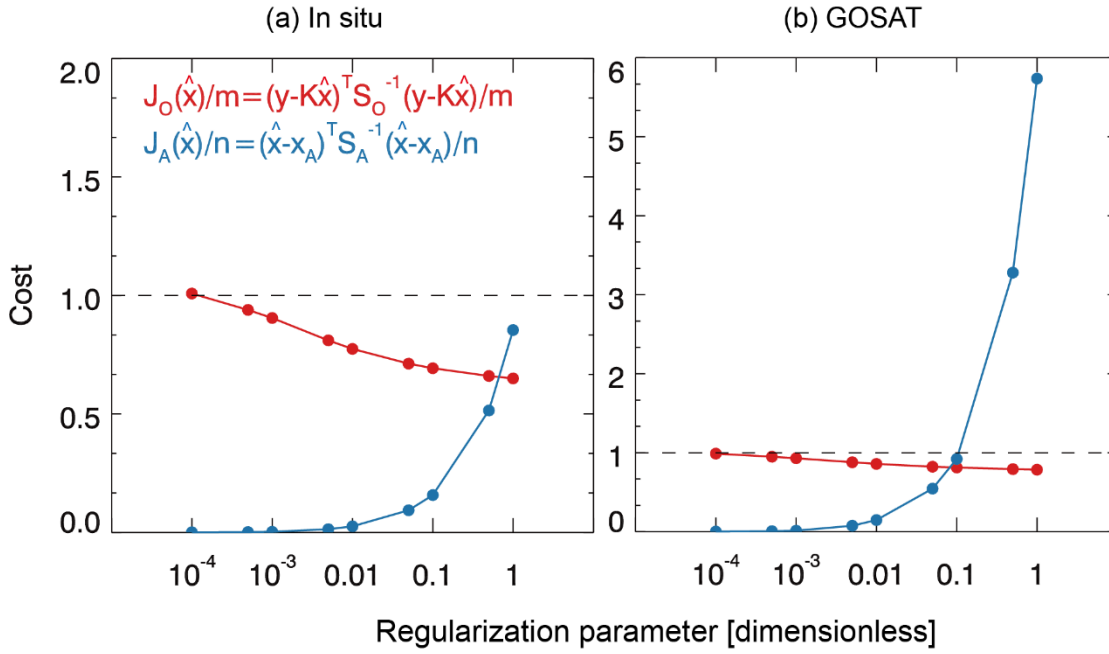
Figure.2 Mean 2010-2017 methane observations from the GLOBALVIEWplus ObsPack data product and from GOSAT. The GLOBALVIEWplus in situ data are local dry mixing ratios and are averaged over the $4^{\circ} \times 5^{\circ}$ model grid for visibility. The GOSAT data are dry column mixing ratios on a $1^{\circ} \times 1^{\circ}$ grid from the University of Leicester version 9 Proxy XCH₄ retrieval (Parker et al., 2020), excluding observations over oceans and poleward of 60°N. Note the difference in color scale between panels.



1064
 1065
 1066
 1067
 1068

Figure 3. Prior estimates of mean 2010-2017 methane emissions. The top panel shows the non-wetland emissions on the $4^\circ \times 5^\circ$ grid used for the inversion. The bottom panel shows the wetland emissions and the 14 subcontinental wetland regions used for the inversion following Bloom et al. (2017).

Optimization of regularization parameter gamma



1069
1070
1071
1072
1073
1074
1075

Figure 4. Optimization of the regularization parameter γ in the Bayesian cost function (Equation (1)). The figure shows the posterior observation component $J_o(\hat{\mathbf{x}}) = (\mathbf{y} - \mathbf{K}\hat{\mathbf{x}})^T \mathbf{S}_o^{-1} (\mathbf{y} - \mathbf{K}\hat{\mathbf{x}})$ and the posterior state component $J_A(\hat{\mathbf{x}}) = (\hat{\mathbf{x}} - \mathbf{x}_A)^T \mathbf{S}_A^{-1} (\hat{\mathbf{x}} - \mathbf{x}_A)$ for the in-situ-only and GOSAT-only inversions.

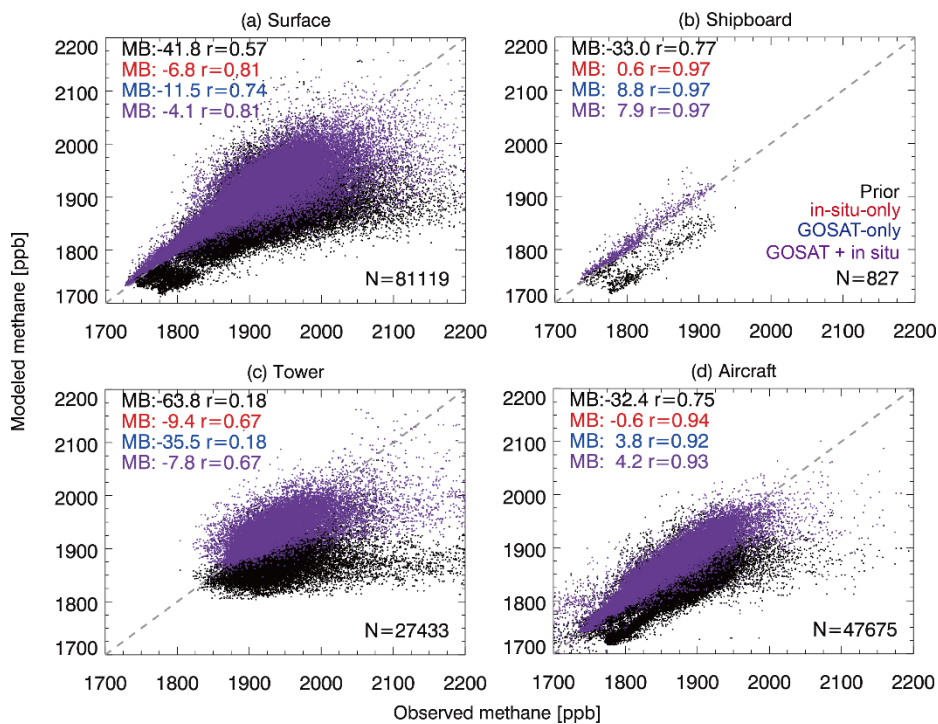
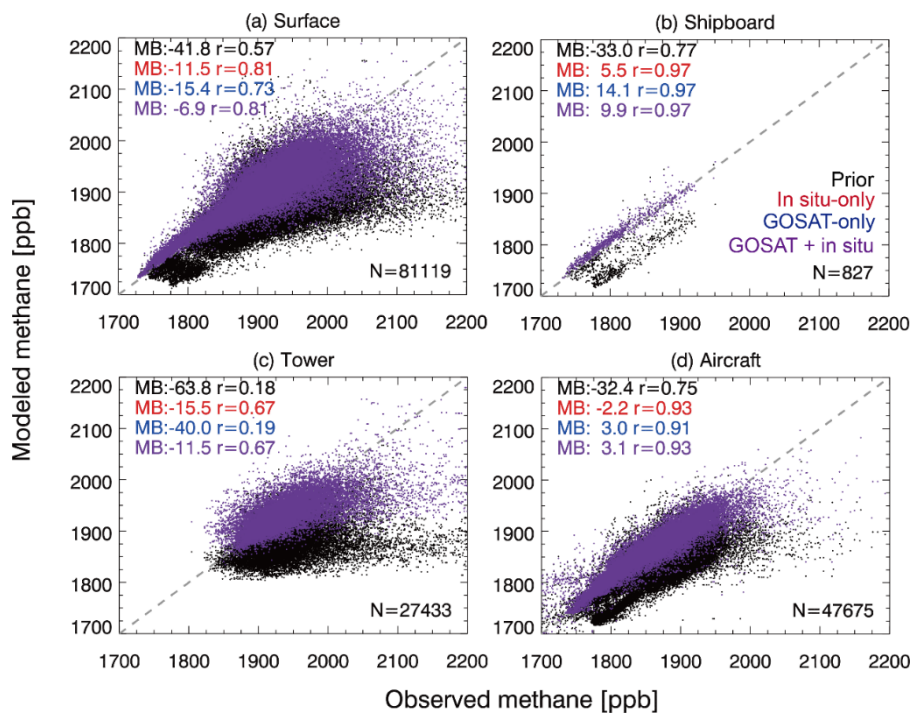


Figure 5. Ability of the inversions to fit the in situ methane observations. Panels (a)-(d) compare the surface, tower, shipboard, and aircraft observations in 2010-2017 to the GEOS-Chem simulation using the prior (black) and posterior estimates of methane emissions and OH concentrations from the in-situ-only inversion (red, dots not shown), GOSAT-only inversion (blue dots not shown), and GOSAT + in situ joint inversion (purple). The numbers (N) of observations from each platform, the mean bias (MB), and the correlation coefficients (r) between the observed and simulated values are shown inset.

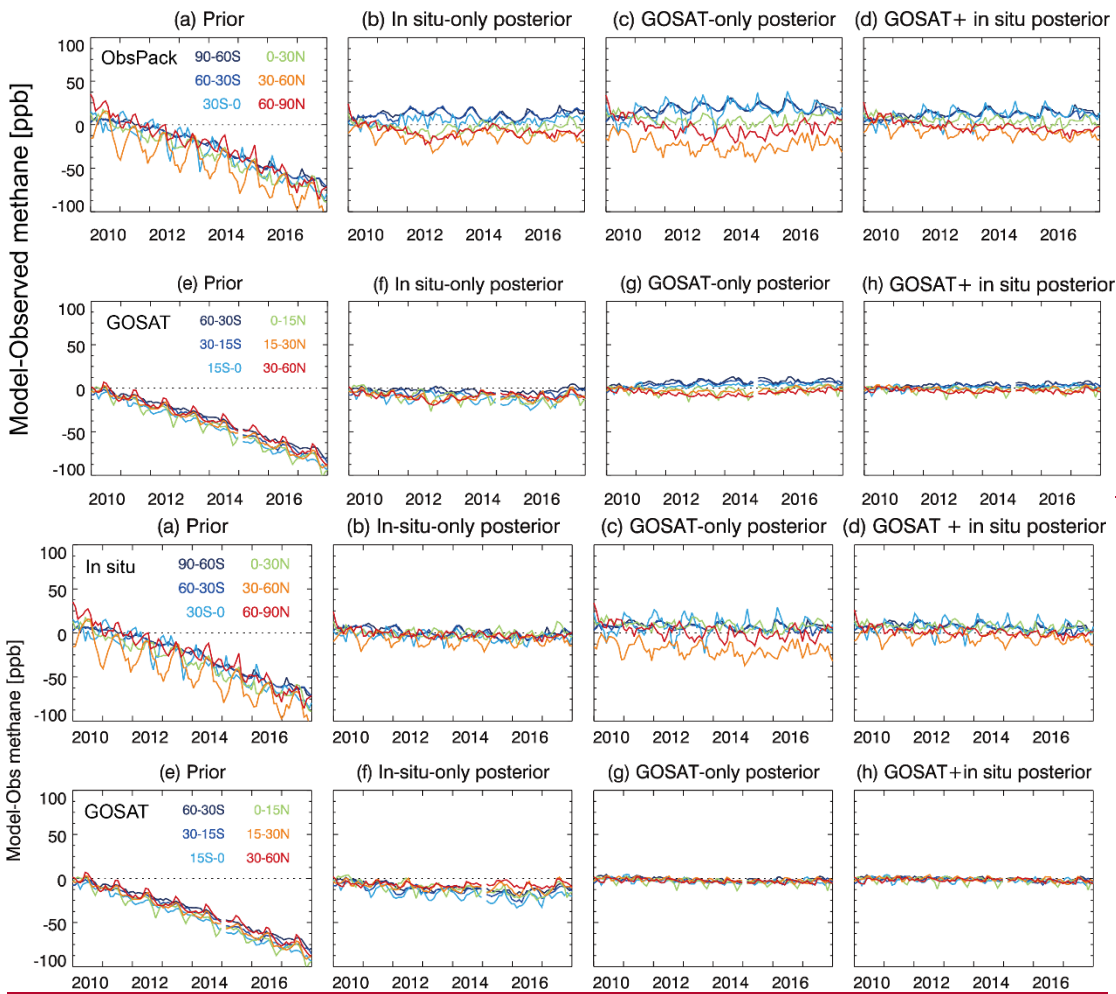


Figure 6. Ability of the inversions to fit the in situ methane observations and GOSAT satellite observations. Panels (a)-(d) show the monthly time series of the differences between observed and simulated in situ methane concentrations averaged over different latitude bands from 2010 to 2017. Panels (e)-(h) are the same as panels (a)-(d) but for GOSAT methane concentrations.

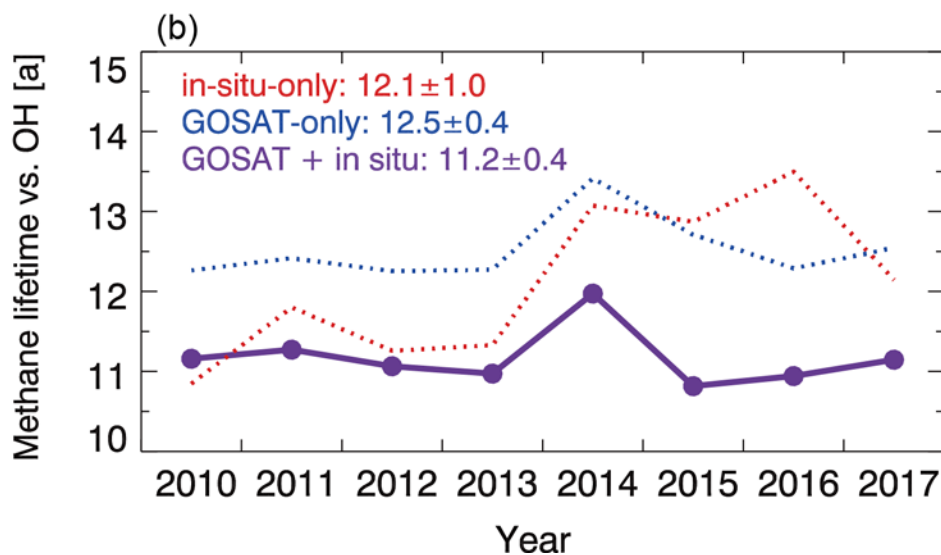
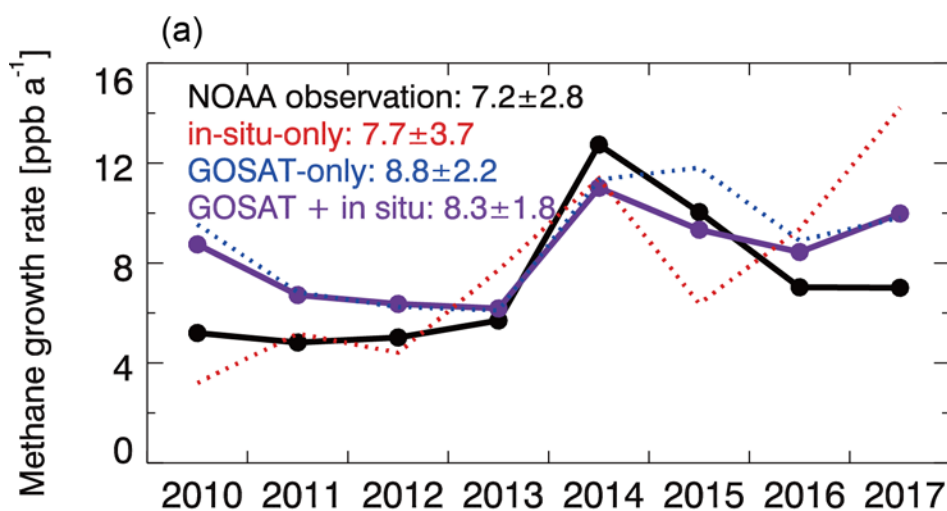
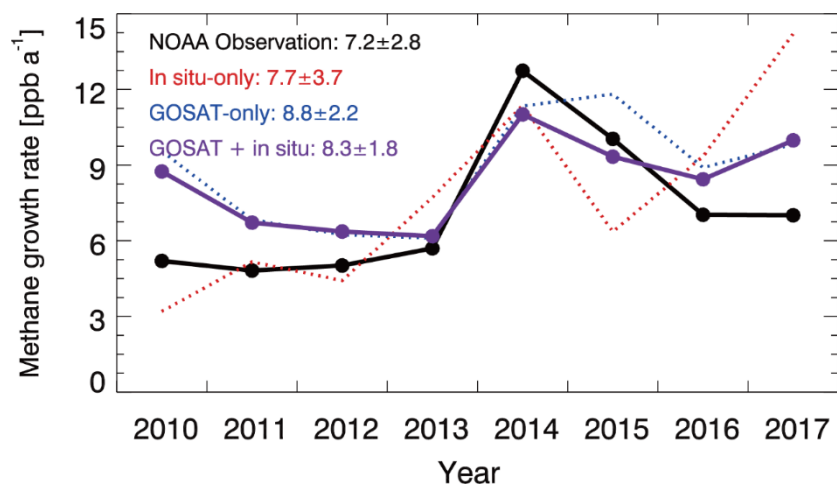
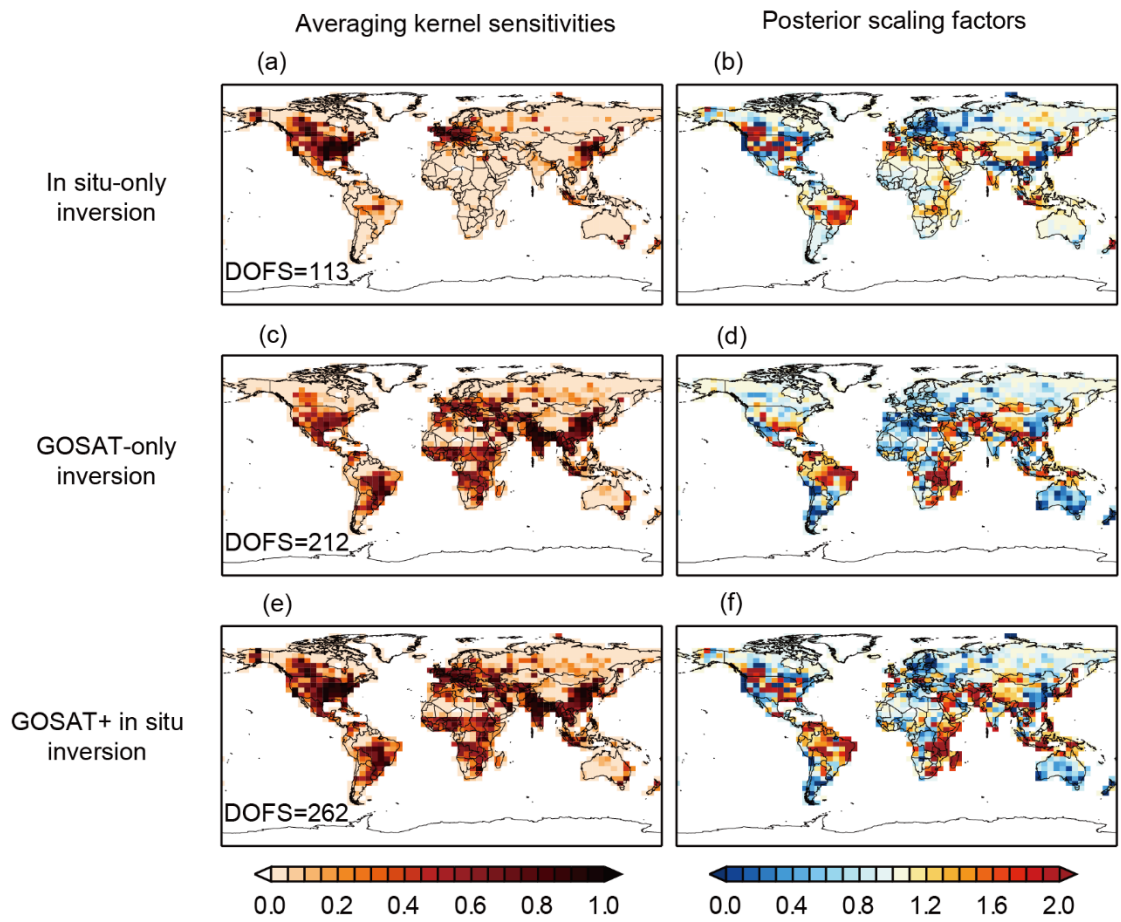


Figure 7. (a) Annual global growth rate of atmospheric methane, 2010-2017. Results from our three different inversions (in-situ-only, GOSAT-only, GOSAT + in situ) are compared to the observed growth rates inferred from the NOAA surface observational network (https://www.esrl.noaa.gov/gmd/ccgg/trends_ch4/, last access: 20 June, 2020). Mean annual growth rates and standard deviations from the different inversions are shown inset. (b) Methane lifetime against oxidation by tropospheric OH, 2010-2017, from the three different inversions. Mean lifetime and standard deviations are shown inset. The methane lifetime in the prior estimate is 10.6 years.



1106

1107

1108

1109

1110

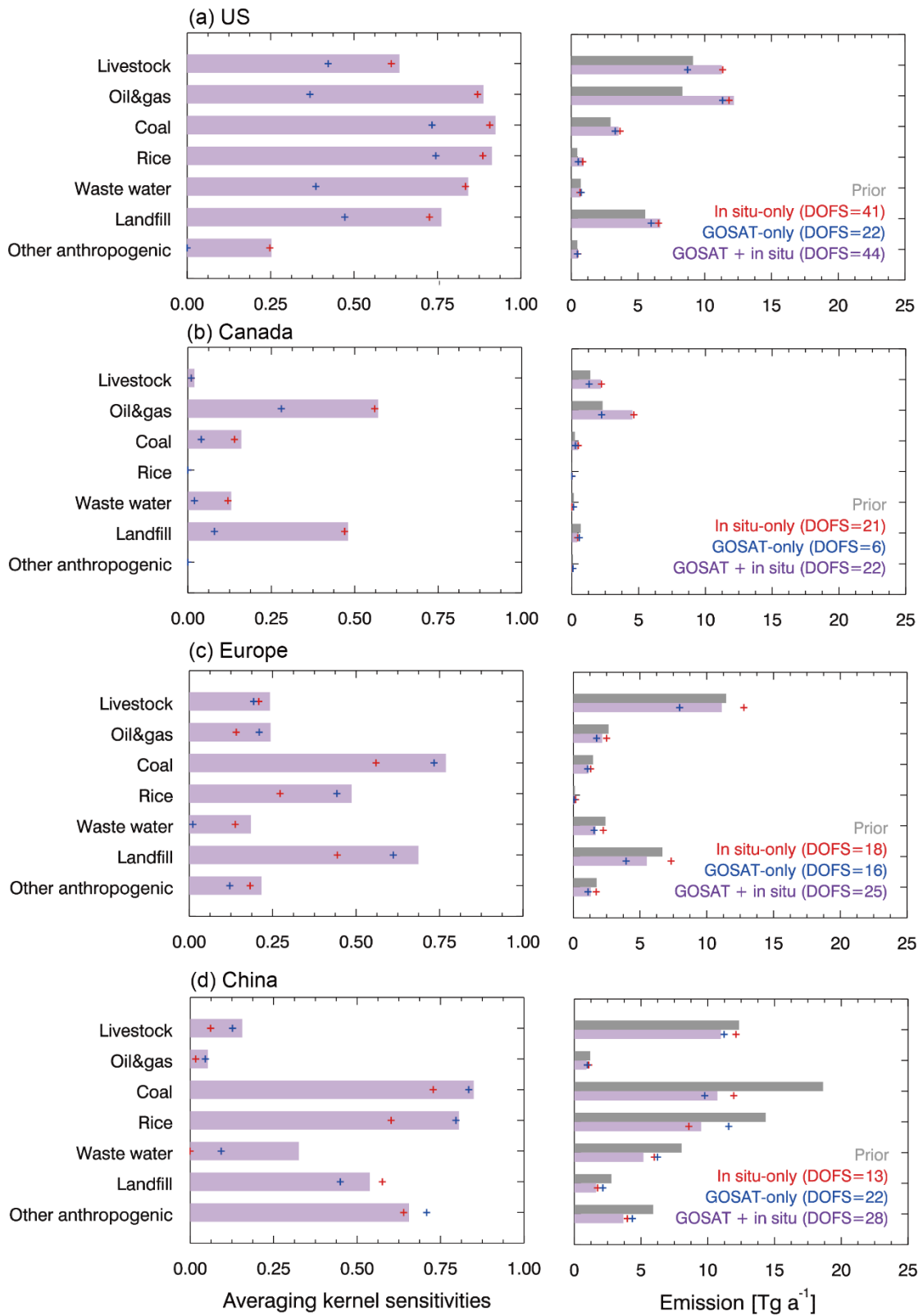
1111

1112

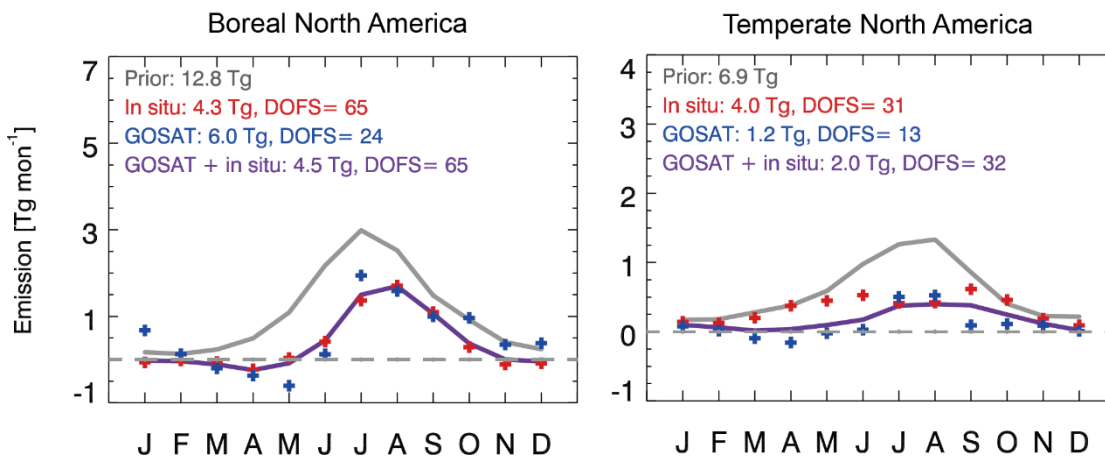
1113

1114

Figure 8. Optimization of mean 2010-2017 non-wetland (mainly anthropogenic) emissions. The *i*n-situ-only inversion uses in situ observations, the GOSAT-only inversion uses GOSAT satellite observations, and the GOSAT + in situ inversion uses both. The left panels show the averaging kernel sensitivities (diagonal elements of the averaging kernel matrix) for each inversion, with the degrees of freedom for signal (DOFS, defined as the trace of the averaging kernel matrix) given inset. The right panels show the correction factors to the prior emissions (Figure 3a). Wetland emissions are corrected separately (see text).

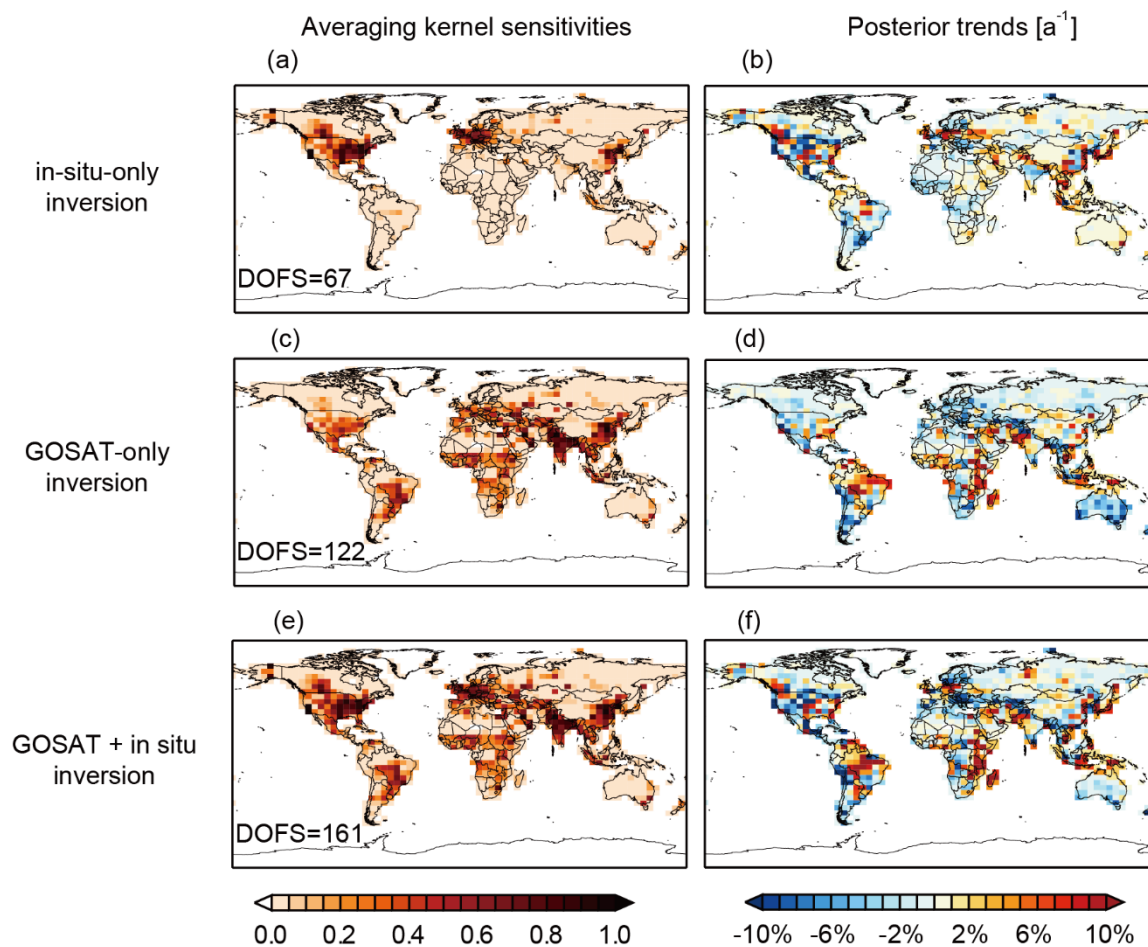


1115
 1116 **Figure 9.** Optimization of anthropogenic methane emissions by source sectors in the in-situ-only,
 1117 GOSAT-only, and GOSAT + in situ inversions. The left panel shows the averaging kernel sensitivities for
 1118 each emission sector (see text for description), the right panel shows the emissions. Europe is defined as
 1119 west of 30°E, which excludes Russia.
 1120



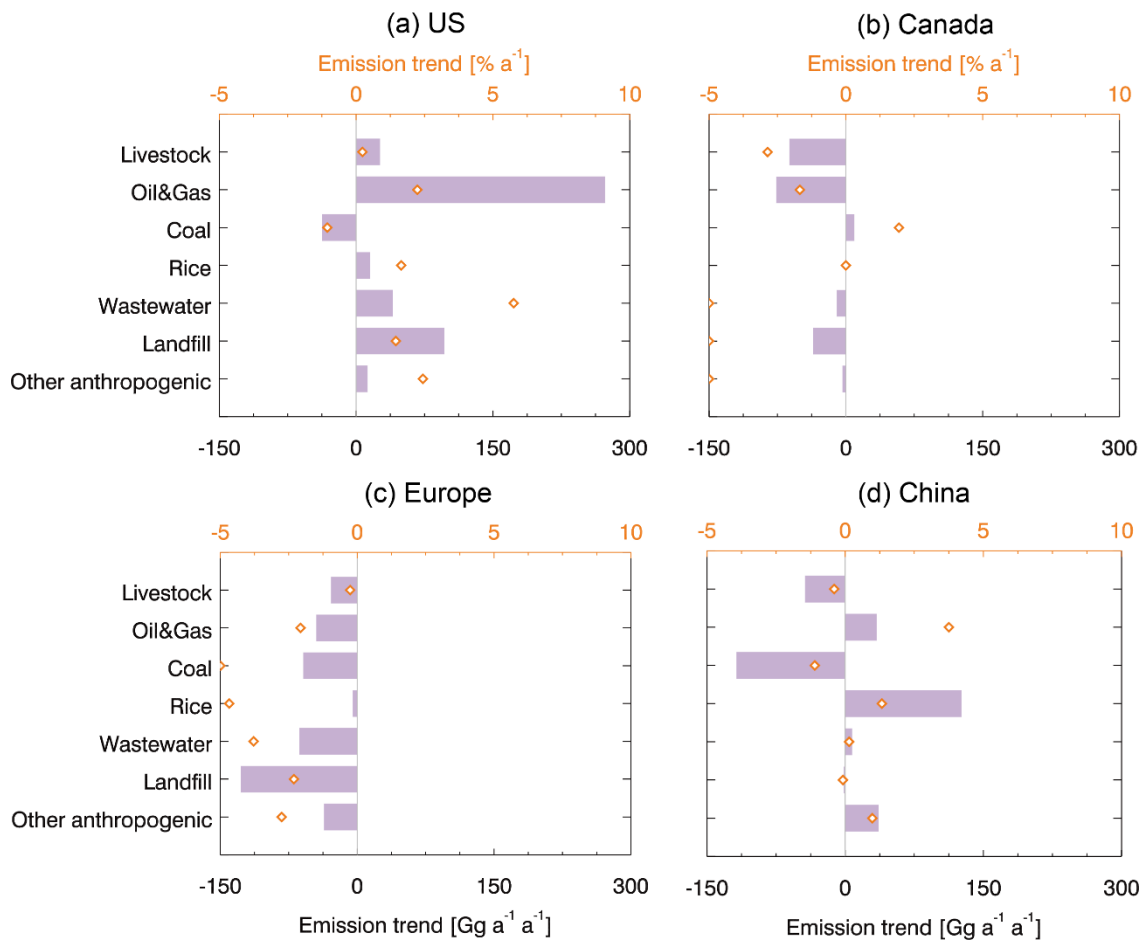
1121
 1122 **Figure 10.** Wetland emissions in boreal and temperate North America (regions 2 and 3 of Figure 3). Prior
 1123 and posterior estimates of the monthly mean wetland emissions averaged over 2010-2017 from different
 1124 inversions are shown. Annual mean emissions and the degree of freedom for signal (DOFS) for monthly
 1125 emissions in individual years are shown inset. Note differences in scale between panels. Negative
 1126 emissions are allowed statistically by the inversion but are likely not physical.
 1127

Anthropogenic methane emission trends in 2010-2017



1128
1129
1130
1131
1132

Figure 11. Same as Figure 8 but for optimization of non-wetland (mainly anthropogenic) emission trends ($\% \text{ a}^{-1}$) in 2010-2017.



1133

1134

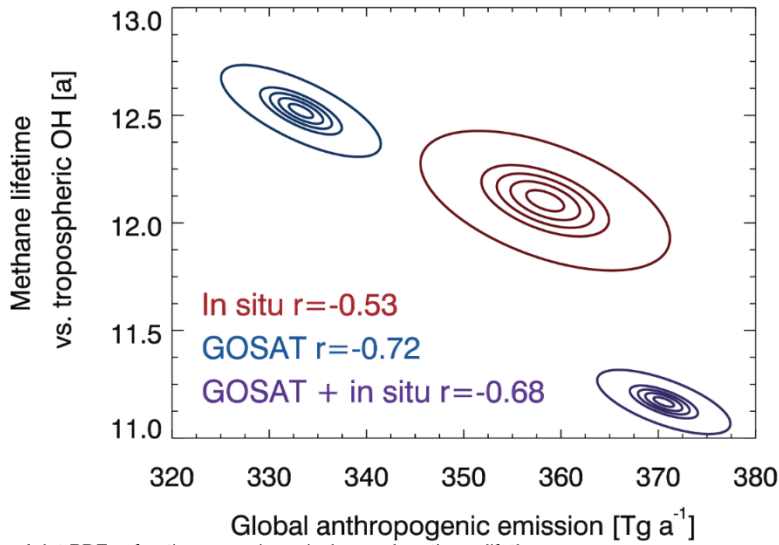
1135

1136

1137

Figure 12. Optimization by sector of regional anthropogenic methane emission trends in 2010-2017. Bars and diamonds represent trends in $\text{Gg a}^{-1} \text{a}^{-1}$ (bottom axis) and $\% \text{a}^{-1}$ (top axis) over the 2010-2017 period from the GOSAT + in situ joint inversion.

Joint PDFs of anthropogenic emission and methane lifetime



Joint PDFs of anthropogenic emission and methane lifetime

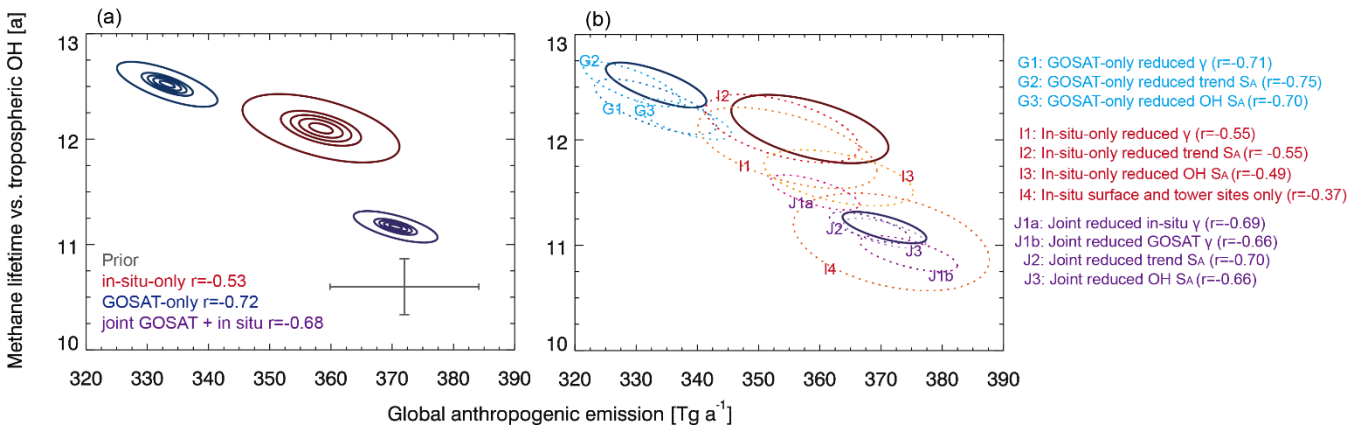


Figure 13. Joint probability density functions (PDFs) of global mean anthropogenic methane emission and methane lifetime against oxidation by tropospheric OH optimized by ~~the three different~~ inversions. Panel (a) shows the results from the prior and the three base inversions. The prior estimates are shown in grey with bars representing the prior error standard deviation. The thick contours show probabilities of 0.99 (outermost), 0.7, 0.5, 0.3, and 0.1 (innermost). from the three base inversions. The error correlation coefficients are given inset. Panel (b) shows the 0.99 probability contours from the three base inversions along with the same contours for ten additional sensitivity inversions using reduced values of the regularization parameter γ (0.05 instead of 0.1 for GOSAT, 0.5 instead of 1 for in situ); reduced errors for the methane emission trends on the $4^\circ \times 5^\circ$ grid (5% a^{-1} instead of 10% a^{-1}); reduced errors on annual hemispheric mean OH concentrations (5% instead of 10%); or surface and tower data only in the in-situ-only inversion.

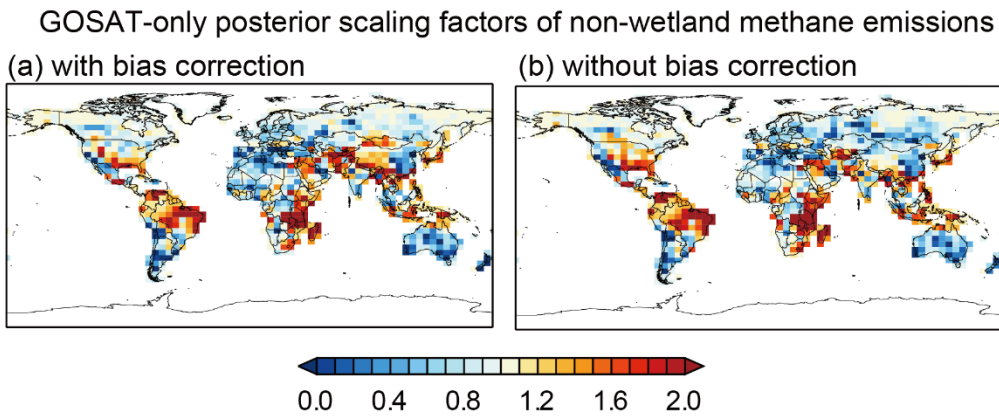


Figure S1. Posterior scaling factors of non-wetland methane emissions from GOSAT-only inversion (a) with GOSAT stratospheric bias corrections and (b) without GOSAT stratospheric bias corrections.

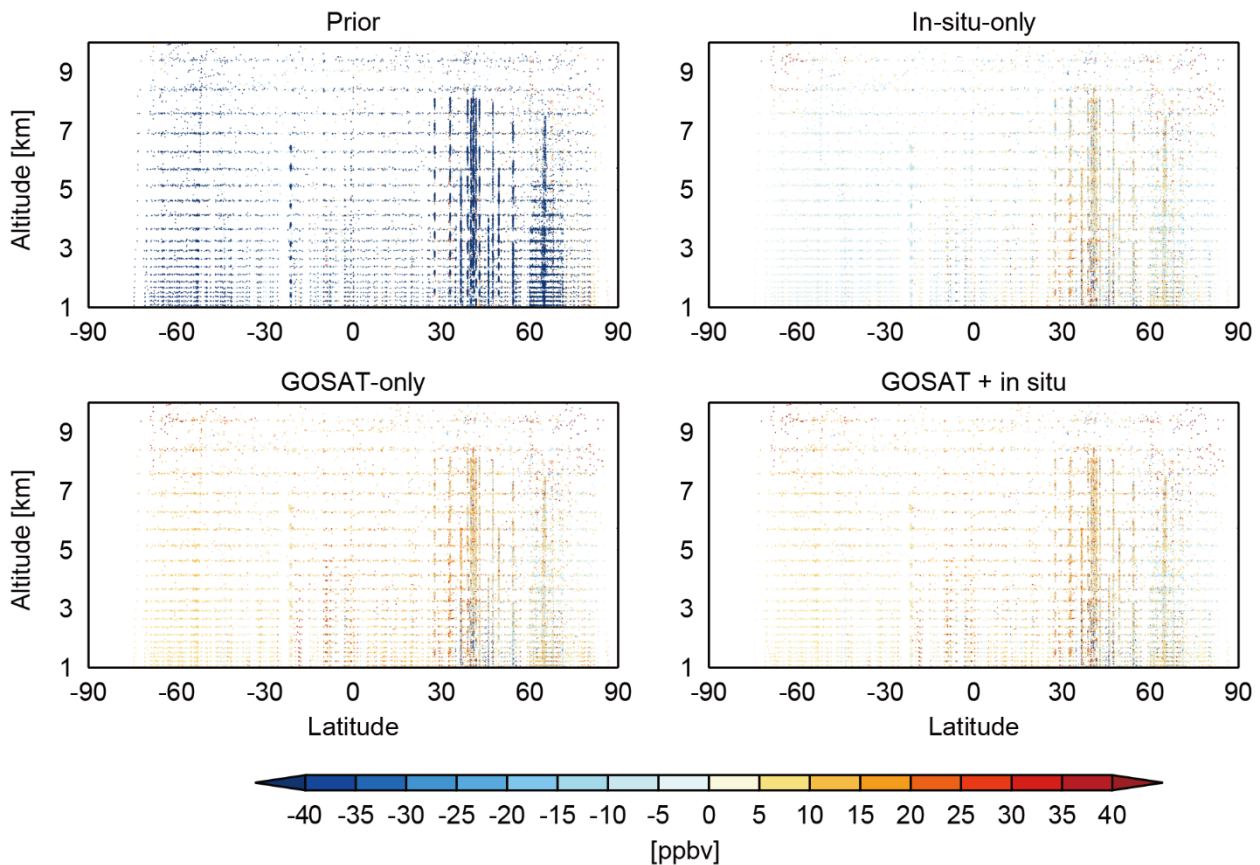
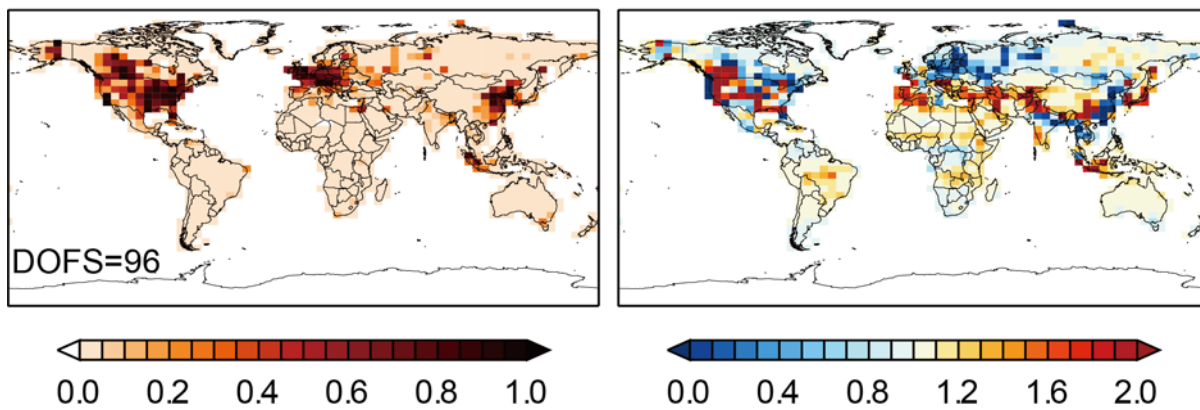


Figure S2. Differences between simulated and observed aircraft methane concentrations from the GLOBALVIEWplus ObsPack data product using GEOS-Chem with prior estimates and with posterior estimates from the in-situ-only, GOSAT-only, and GOSAT + in situ inversions.

(a) Averaging kernel sensitivities

(b) Posterior scaling factors



1164
1165 **Figure S3.** Same as Figure 8a and 8b but from a sensitivity inversion using only surface and tower
1166 methane observations.